

NEURAL REPRESENTATIONS OF APPETITIVE AND AVERSIVE LEARNING



Dissertation
zur Erlangung des Doktorgrades
der Humanwissenschaften
(Dr. sc. hum.)

der
Fakultät für Medizin
der Universität Regensburg

vorgelegt von
Aino-Lotta Ilona Alahäivälä
aus
Kemi, Finnland

im Jahr
2024

NEURAL REPRESENTATIONS OF APPETITIVE AND AVERSIVE LEARNING



Dissertation
zur Erlangung des Doktorgrades
der Humanwissenschaften
(Dr. sc. hum.)

der
Fakultät für Medizin
der Universität Regensburg

vorgelegt von
Aino-Lotta Ilona Alahäivälä
aus
Kemi, Finnland

im Jahr
2024

Dekan: Prof. Dr. Dirk Hellwig

Betreuer: Prof. Dr. Jens Schwarzbach

Tag der mündlichen Prüfung: 27.01.2025

TABLE OF CONTENTS

| | |
|---|-----------|
| ABSTRACT | 1 |
| ZUSAMMENFASSUNG | 3 |
| ABBREVIATIONS | 5 |
| 1. INTRODUCTION | 6 |
| 1.1 ABOUT REPRESENTATIONS: THIS IS NOT A PIPE..... | 6 |
| 1.1.1 <i>Information Representations in the Brain</i> | 7 |
| 1.1.2 <i>Approaches to Measuring Brain Representations</i> | 9 |
| 1.1.3 <i>Analyzing Neuroimaging Data</i> | 10 |
| 1.2 CLASSICAL CONDITIONING: BELL RINGS & SALIVA..... | 12 |
| 1.2.1 <i>Functional Neuroimaging of Learning Processes</i> | 12 |
| 1.3 FROM AN ODORANT TO PERCEPTION: WHAT'S THAT SMELL? | 15 |
| 1.3.1 <i>Anatomy of the Olfactory System</i> | 16 |
| 1.3.2 <i>Where is the Olfactory Cortex & Other Olfactory Processing Streams</i> | 18 |
| 1.3.3 <i>Trigeminal Nerve</i> | 24 |
| 1.3.4 <i>Olfactory Detection & Temporal Dynamics</i> | 25 |
| 1.3.5 <i>Olfactory Dysfunctions</i> | 27 |
| 1.3.6 <i>Olfaction & Emotion</i> | 28 |
| 1.3.7 <i>Odorants</i> | 29 |
| 1.3.8 <i>A Brief History of Olfaction Research</i> | 33 |
| 1.3.8.1 <i>Era of Olfactometry</i> | 36 |
| 1.3.8.2 <i>Imaging Olfaction</i> | 38 |
| 1.4 AIMS OF THIS THESIS | 41 |
| 1.4.1 <i>Research Questions & Hypotheses</i> | 41 |
| 2 MATERIALS & METHODS | 43 |
| 2.1 PARTICIPANTS | 43 |
| 2.2 APPARATUS | 43 |
| 2.2.1 <i>Olfactometer</i> | 43 |
| 2.2.2 <i>Visual Stimuli Presentation</i> | 44 |
| 2.2.3 <i>fMRI Data Acquisition</i> | 44 |
| 2.3 STIMULI..... | 45 |
| 2.3.1 <i>Odorants</i> | 45 |
| 2.3.2 <i>Visual Stimuli</i> | 46 |
| 2.4 PROCEDURE | 47 |
| 2.4.1 <i>Behavioral Experiment</i> | 47 |

| | | |
|-----------|---|----|
| 2.4.1.1 | Sniffin' Sticks: Odor Identification Test | 47 |
| 2.4.1.2 | Pleasantness Rating | 48 |
| 2.4.2 | <i>Neuroimaging Experiment</i> | 48 |
| 2.4.2.1 | Trial Protocol | 48 |
| 2.5 | DATA ANALYSIS | 50 |
| 2.5.1 | <i>Behavioral Data</i> | 50 |
| 2.5.1.1 | Sniffin' Sticks: Threshold for Normal Olfactory Function | 50 |
| 2.5.1.2 | Pleasantness Rating: Comparable Odor Sets | 50 |
| 2.5.2 | <i>Neuroimaging Data</i> | 51 |
| 2.5.2.1 | Preprocessing | 51 |
| 2.5.2.2 | Univariate Analysis | 52 |
| 2.5.2.2.1 | Brain Regions Which Distinguish Negative & Positive Odors | 52 |
| 2.5.2.2.2 | Brain Regions Activated by Conditioning | 53 |
| 2.5.2.3 | Multivariate Pattern Analysis | 54 |
| 2.5.2.3.1 | Classification Analysis | 55 |
| 2.5.2.3.2 | Representational Similarity Analysis | 59 |
| 3 | RESULTS | 64 |
| 3.1 | BEHAVIORAL EXPERIMENT | 64 |
| 3.1.1 | <i>Sniffin' Sticks</i> | 64 |
| 3.1.2 | <i>Odor Sets are Comparable in Terms of Their Valence Profiles</i> | 64 |
| 3.1.3 | <i>Participants Score Negative & Positive Odors Inconsistently Across Odor Sets</i> | 65 |
| 3.1.4 | <i>No Expected Differences for Neutral Odors Before & After Conditioning</i> | 68 |
| 3.2 | NEUROIMAGING EXPERIMENT | 69 |
| 3.2.1 | <i>Reaction Time</i> | 69 |
| 3.2.2 | <i>Univariate Analysis</i> | 70 |
| 3.2.2.1 | Brain Regions Which Distinguish Negative & Positive Odors | 70 |
| 3.2.2.2 | Brain Regions Activated by Conditioning | 72 |
| 3.2.3 | <i>Multivariate Pattern Analysis</i> | 73 |
| 3.2.3.1 | Classification Analysis | 73 |
| 3.2.3.2 | Representational Similarity Analysis | 78 |
| 3.2.3.2.1 | Multiple Model RDM Approach Using Minimal t-Conjunction | 78 |
| 3.2.3.2.2 | Single Model RDM Approach | 81 |
| 4 | DISCUSSION | 84 |
| 4.1 | INTERPRETATION OF FINDINGS | 85 |
| 4.1.1 | <i>Behavioral Findings</i> | 86 |
| 4.1.1.1 | Odor Sets are Comparable in Terms of Their Valence Profiles | 86 |
| 4.1.1.2 | Participants Score Negative & Positive Odors Inconsistently Across Odor Sets | 86 |
| 4.1.1.3 | No Expected Differences for Neutral Odors Before & After Conditioning | 87 |

| | | |
|---------|---|-----|
| 4.1.2 | <i>Neuroimaging Findings</i> | 88 |
| 4.1.2.1 | Reaction Time | 88 |
| 4.1.2.2 | Univariate Analysis..... | 88 |
| 4.1.2.3 | Multivariate Pattern Analysis | 90 |
| 4.2 | LIMITATIONS & METHODOLOGICAL CONSIDERATIONS | 92 |
| 4.2.1 | <i>Methodological Limitations</i> | 92 |
| 4.2.1.1 | Selected Odorants | 92 |
| 4.2.1.2 | Experimental Design | 93 |
| 4.2.1.3 | Conditioning | 94 |
| 4.2.1.4 | Searchlight | 94 |
| 4.2.1.5 | RSA..... | 95 |
| 4.2.2 | <i>Interpretational, Generalizability, & Conceptual Limitations</i> | 95 |
| 4.2.2.1 | Interpretational Limitations | 95 |
| 4.2.2.2 | Generalizability Limitations..... | 95 |
| 4.2.2.3 | Conceptual Limitations | 96 |
| 4.3 | FUTURE OUTLOOK..... | 96 |
| 4.3.1 | <i>Garbage In, Garbage Out</i> | 96 |
| 4.3.2 | <i>Particularities of Olfaction</i> | 98 |
| 4.3.3 | <i>Sampling the Odor Space</i> | 99 |
| 4.3.4 | <i>Synthesis & Perspectives: Asking Better Questions</i> | 100 |
| 5 | CONCLUSION | 103 |
| 6 | APPENDIX | 105 |
| A. | RIECH-O-MAT OLFACTOMETER | 105 |
| B. | DIVISION OF ODOR SETS AMONG PARTICIPANTS | 106 |
| C. | SNIFFIN' STICKS: 16-ITEM TEST FOR ODOR IDENTIFICATION..... | 108 |
| D. | fMRIPREP PREPROCESSING BOILERPLATE | 109 |
| E. | BEHAVIORAL RESULTS – ODOR RATING SCORES | 112 |
| F. | NEUROIMAGING EXPERIMENT– REACTION TIME..... | 117 |
| G. | NEUROIMAGING EXPERIMENT – RSA CLUSTERS | 118 |
| 7 | REFERENCES | 120 |
| | SELBSTÄNDIGKEITSERKLÄRUNG | 145 |

LIST OF FIGURES

| | |
|--|----|
| Figure 1. “This is not a pipe” – but rather, a representation of one. | 6 |
| Figure 2. Sparse and distributed encoding scheme for visual stimuli. | 8 |
| Figure 3. Model of the neural circuitry of appetitive conditioning. | 13 |
| Figure 4. Olfactory system structure in humans. | 17 |
| Figure 5. Cell types in the human olfactory system. | 18 |
| Figure 6. Olfactory pathways and projections. | 20 |
| Figure 7. The central olfactory system in humans. | 24 |
| Figure 8. Odorants with similar chemical compounds and perceived smells. | 31 |
| Figure 9. Odorants with dissimilar chemical structures and similarly perceived smells . | 32 |
| Figure 10. Illustration of the brain with olfactory bulbs highlighted. | 35 |
| Figure 11. Early illustrations of the olfactory epithelium, ORNs, and supporting cells. .. | 35 |
| Figure 12. Riech-O-Mat olfactometer | 37 |
| Figure 13. Hypotheses. | 42 |
| Figure 14. Experimental procedure and trial design. | 47 |
| Figure 15. A region of interest mask plotted on a glass brain. | 53 |
| Figure 16. A region of interest mask plotted on a glass brain. | 54 |
| Figure 17. Within subject leave-one-trial-out cross-validation scheme in the MVPA classification analysis. | 56 |
| Figure 18. The expected and the chance-level classification results from the conditioning run. | 58 |
| Figure 19. The expected and the chance-level classification results from the reference run. | 59 |
| Figure 20. Model RDMs for RSA using multiple models. | 62 |
| Figure 21. Model RDM for RSA using a single model approach. | 63 |
| Figure 22. Sniffin’ Sticks odor identification test results. | 64 |
| Figure 23. Valence scores (left panels) and their differences (right panels) for negative and positive odors for odor set A. | 65 |
| Figure 24. Valence scores (left panels) and their differences (right panels) for negative and positive odors for odor set B. | 66 |

| | |
|---|-----|
| Figure 25. Valence scores and their differences for negative and positive odors during the scan for all subjects. | 67 |
| Figure 26. Likert scores of CS+ aversive odor for both odor sets. | 68 |
| Figure 27. Likert scores of CS+ appetitive odor for both odor sets. | 68 |
| Figure 28. Likert scores of neutral odor without conditioning outcome for both odor sets. | 69 |
| Figure 29. Group-level averaged reaction times recorded during runs 1 and 3 in the odor valence rating task. | 70 |
| Figure 30. Whole-brain univariate analysis of unpleasantness negative-positive with a 95% percentile threshold (i.e., without multiple corrections). | 71 |
| Figure 31. ROI univariate analysis of unpleasantness (negative-positive) with a 95% percentile threshold (i.e., without multiple corrections). | 71 |
| Figure 32. Whole-brain analysis showed significant activation clusters in the visual regions during conditioning | 72 |
| Figure 33. ROI analysis showed significant activation clusters during the conditioning effect. | 73 |
| Figure 34. Region of interest. | 74 |
| Figure 35. Group mean confusion matrix from reference run. | 75 |
| Figure 36. Group mean confusion matrix from conditioning run. | 76 |
| Figure 37. Group mean confusion matrix from extinction run. | 77 |
| Figure 38. Results from MVPA RSA analysis of conditioning run. | 79 |
| Figure 39. Results from MVPA RSA analysis of extinction run. | 80 |
| Figure 40. Minimal t-conjunction t-map overlaid on a standard brain, adjusted for multiple corrections. | 81 |
| Figure 41. Results from MVPA RSA analysis using a single target matrix. | 82 |
| Figure 42. RSA searchlight t-map using a single model RDM approach overlaid on a standard brain, adjusted for multiple corrections. | 83 |
| Figure 43. Mosaic of RSA searchlight t-map using a single model RDM approach overlaid on a standard brain, adjusted for multiple corrections. | 83 |
| Figure 44. The interface of the Riech-O-Mat 2.0 computer program | 106 |

| | |
|---|-----|
| Figure 45. Valence results from the behavioral experiment involving negative odor rating. | 113 |
| Figure 46. Valence results from the behavioral experiment involving positive odor rating. | 114 |
| Figure 47. Valence results from the behavioral experiment involving CS+ appetitive odor rating. | 115 |
| Figure 48. Valence results from the behavioral experiment involving CS+ aversive odor rating. | 116 |
| Figure 49. Valence results from the behavioral experiment involving CS- odor rating (i.e., the neutral odor that was not conditioned)..... | 117 |
| Figure 50. Reaction times were collected during the first run (reference)..... | 118 |
| Figure 51. Reaction times were collected during the third run (extinction) | 118 |

LIST OF TABLES

| | |
|--|-----|
| Table 1. Brain regions commonly associated with olfaction and emotion information processing | 29 |
| Table 2. Olfactory stimuli used in the experiment. | 46 |
| Table 3. Metrics from the classification analysis of reference run..... | 75 |
| Table 4. Metrics from the classification analysis of conditioning run..... | 76 |
| Table 5. Metrics from the classification analysis of extinction run..... | 78 |
| Table 6. Example of a Riech-O-Mat punchcard file. | 106 |
| Table 7. Division of odor sets among participants. | 107 |
| Table 8. Sniffin' Sticks 16-item test for odor identification. | 108 |
| Table 9. Positive activations (one-tailed) identified through MVPA RSA | 119 |

ABSTRACT

Aversive and appetitive learning are vital processes for an organism to differentiate between harmful and beneficial stimuli in the environment. However, how neural representations of stimuli change following such learning processes remains largely unknown. While previous work in the visual domain has shown that fear-conditioning alters neural representations of stimuli (Dunsmoor et al., 2014; Levine et al., 2020; Visser et al., 2011), far less research has investigated conditioning processes in other sensory systems.

A recent olfactory study explored the classification algorithm's ability to decode neural representations of mint and citrus odors following appetitive conditioning (Howard et al., 2016). The authors found that reward-related brain regions, e.g., the ventromedial prefrontal cortex, are one such locus from which the reward aspect of appetitive-conditioned stimuli can be cross-decoded across different odor categories.

One interesting question that arises and is not discussed in the above study is how representations of conditioned and non-conditioned stimuli change relative to each other. Demonstrating that reward can be cross-decoded from different sensory categories does not demonstrate that such sensory categories have, for example, become more similar to one another. Thus, this doctoral project aims to apply aversive and appetitive conditioning to olfactory representations to determine whether aversive processes render olfactory stimuli more toward stereotypically "negative" and more stereotypically "positive", respectively.

Neuroimaging data were collected from 29 healthy individuals using an olfactometer to deliver odorants birhinally. Data preprocessing followed a standardized pipeline, and analysis comprised univariate and multivariate pattern analysis, with two approaches: classification analysis and representational similarity analysis.

Pertaining to the methodological limitations, particularly concerning stimuli quality, the findings of this thesis remained inconclusive. Nonetheless, this study contributes to our understanding of the challenges and complexities in olfactory neuroscience, especially regarding methodologies for studying olfactory representational spaces and conditioning

effects. Future research should prioritize robust stimulus selection, aligned with research questions, and ensure experimental paradigms' reliability. Leveraging multivariate pattern analysis methods may provide deeper insights into how conditioning influences neural representations of olfactory stimuli, advancing our understanding of sensory processing and associative learning in the olfactory domain.

ZUSAMMENFASSUNG

Aversives und appetitives Lernen sind vitale Prozesse für ein Organismus, um zwischen schädlichen und nützlichen Reizen in der Umwelt zu unterscheiden. Allerdings bleibt weitgehend unbekannt, wie sich neuronale Repräsentationen von Reizen nach solchen Lernprozessen verändern. Während frühere Arbeiten im visuellen Bereich gezeigt haben, dass Angstkonditionierung neuronale Repräsentationen von Reizen verändert (Dunsmoor et al., 2014; Levine et al., 2018; Visser et al., 2011), wurde weit weniger Forschung zu Konditionierungsprozessen in anderen sensorischen Systemen betrieben.

Eine kürzlich durchgeführte olfaktorische Studie untersuchte die Fähigkeit des Klassifizierungsalgorithmus, neuronale Repräsentationen von Minze- und Zitrusdüften nach appetitiver Konditionierung zu decodieren (Howard et al., 2016). Die Autoren stellten fest, dass belohnungsbezogene Hirnregionen, z. B. der ventromediale präfrontale Kortex, Orte sind, von denen aus der Belohnungsaspekt appetitiv konditionierter Reize über verschiedene Duftkategorien hinweg decodiert werden kann.

Eine interessante Frage, die sich stellt und in der oben genannten Studie nicht diskutiert wird, ist, wie sich Repräsentationen konditionierter und unkonditionierter Reize zueinander verändern. Der Nachweis, dass Belohnung aus verschiedenen sensorischen Kategorien decodiert werden kann, zeigt nicht zwangsläufig, dass solche sensorischen Kategorien beispielsweise einander ähnlicher geworden sind. Daher zielt dieses Doktorandenprojekt darauf ab, aversive und appetitive Konditionierung auf olfaktorische Repräsentationen anzuwenden, um festzustellen, ob aversive Prozesse olfaktorische Reize eher in Richtung stereotypisch "negativ" und appetitive Prozesse eher in Richtung stereotypisch "positiv" verschieben.

Neuroimaging-Daten wurden von 29 gesunden Personen unter Verwendung eines Olfaktometers zur binauralen Lieferung von Duftstoffen gesammelt. Die Datenverarbeitung folgte einem standardisierten Ablauf und die Analyse umfasste univariate und multivariate Musteranalyse mit zwei Ansätzen: Klassifikationsanalyse und repräsentative Ähnlichkeitsanalyse.

Hinsichtlich der methodischen Einschränkungen, insbesondere in Bezug auf die Qualität der Reize, blieben die Ergebnisse dieser Arbeit unklar. Dennoch trägt diese Studie zu unserem Verständnis der Herausforderungen und Komplexitäten in der olfaktorischen Neurowissenschaft bei, insbesondere in Bezug auf Methoden zur Untersuchung olfaktorischer Repräsentationsräume und Konditionierungseffekte. Zukünftige Forschung sollte eine robuste Stimulusauswahl priorisieren, die mit den Forschungsfragen übereinstimmt, um die Robustheit experimenteller Paradigmen sicherzustellen. Die Nutzung anspruchsvoller multivariater Musteranalysemethoden könnte tiefere Einblicke in die Art und Weise liefern, wie Konditionierung neuronale Repräsentationen olfaktorischer Reize beeinflusst und unser Verständnis der sensorischen Verarbeitung und assoziativen Lernens im olfaktorischen Bereich voranbringen.

ABBREVIATIONS

| | |
|------|---|
| CS | Conditioned stimulus |
| EEG | Electroencephalography |
| FDR | False discovery rate |
| fMRI | Functional magnetic resonance imaging |
| FN | False negative |
| FP | False positive |
| ISI | Interstimulus interval |
| ITI | Intertrial interval |
| MDS | Multidimensional scaling |
| MRI | Magnetic resonance imaging |
| MVPA | Multivariate (also multivoxel) pattern analysis |
| OB | Olfactory bulb |
| OFC | Orbitofrontal cortex |
| ORN | Olfactory receptor neuron |
| PC | Piriform cortex |
| PFC | Prefrontal cortex |
| RDM | Representational dissimilarity matrix |
| ROI | Region of interest |
| RSA | Representational similarity analysis |
| SVM | Support vector machine |
| TN | True negative |
| TP | True positive |
| UR | Unconditioned response |
| US | Unconditioned stimulus |
| VS | Ventral striatum |

1. INTRODUCTION

1.1 About Representations: This is Not a Pipe

Belgian surrealist René Magritte created a well-known painting depicting a pipe with a text underneath stating, “This is not a pipe” – rather, it is an illustration of one (1929; Figure 1). This piece serves as an apt metaphor for neural representations discussed in this dissertation. Similarly, the brain encodes information by sustaining a neural representation of it (such as a representation of a pipe) through specific patterns of neuronal activity (Vilarroya, 2017). Information – whether visual sensory information like the color blue or a cognitive map for a location in space (Keefe & Nadel, 1978) – is inherently represented by the neural architecture of the brain, either via local activation or distributed across regions.



Figure 1. “This is not a pipe” – but rather, a representation of one. René Magritte. (1929). *La Trahison des images (Ceci n'est pas une pipe)*. [Oil on canvas]. Los Angeles County Museum of Art, United States.

Using the analogy of neural representations as a starting point, the following sections will introduce the concept and its measurement in greater detail, particularly concerning the representation of sensory information through neuroimaging (1.1.1, 1.1.2.). We will then explore how these neural representations can be altered via learning, namely through aversive and appetitively conditioning (1.2.). Given the focus of this thesis on the olfactory system, the unique characteristics and brief history of this sensory system are summarized (1.3). Finally, the specific aims of this project are outlined (1.4).

1.1.1 Information Representations in the Brain

In short, neural representation is the brain's model for something in our external or internal environment, such as a table in front of you or an idea of you surfing in space, encoded as a particular neural pattern in your brain (Villarroya, 2017). This concept appears to have originated in neuroscience, derived from the psychological terms “mental” and “cognitive” representation. According to this approach, we can access the outside world via representations that reflect objects, concepts, and ideas. The roots of representations can be traced back to René Descartes's “Meditations on First Philosophy: Concerning the Nature of the Human Mind and the Fact that It Is Easier to Know than the Body” published in the 17th Century (2013). He speculates that we can only access our external world through *indirect* ideas, perceptions, memories, and beliefs. For example, O'Keefe and Dostrovsky (1971) discovered a cognitive representation of space in the hippocampal place cells, where certain cell activations reflected the relative position of a mouse on a tract.

Still, what does it exactly mean for the brain to represent something? According to Villarroya (2017), it involved understanding “...what it means for a nervous system *to represent* something, on *what* makes a neural activity a representation, and on *what* is represented” (italics in the original). In neuroscientific literature, “representation” has been extensively linked to two approaches: the single-cell approach and the context of neuron ensembles or populations of neurons.

A well-known example of a single neuron representing a highly complex but specific object is the “Grandmother cell”, an idea proposed by Jerry Lettvin in 1967 (Gross, 2002). According to this theory, one (and only one) neuron would selectively respond to a single object or a concept – such as an image of one's grandmother – through a process of converging input from other brain regions, like the occipital lobe. Similarly, neurons have been found to respond selectively to images of Jennifer Aniston and Halle Berry in the medial temporal lobe (Quiari Quiroga et al., 2005). However, researchers noted that given their limited sampling of stimulus space (faces of actors), they cannot claim that a single neuron would selectively code a discrete percept solely, nor that other percepts could not also activate it (Quiari Quiroga & Kreiman, 2010).

In contrast to the grandmother cell theory, where a single unit represents an intricate and complex concept, there is a model of distributed representation (Gross, 2002). In this model, a stimulus is encoded by a specific activation pattern across neuron ensembles, which may be extensively distributed in the brain. This distributed representation contrasts with the fairly simplistic notion of a grandmother cell idea, which is termed “sparseness” – a sparse activation pattern encoding a particular stimulus (Figure 2).

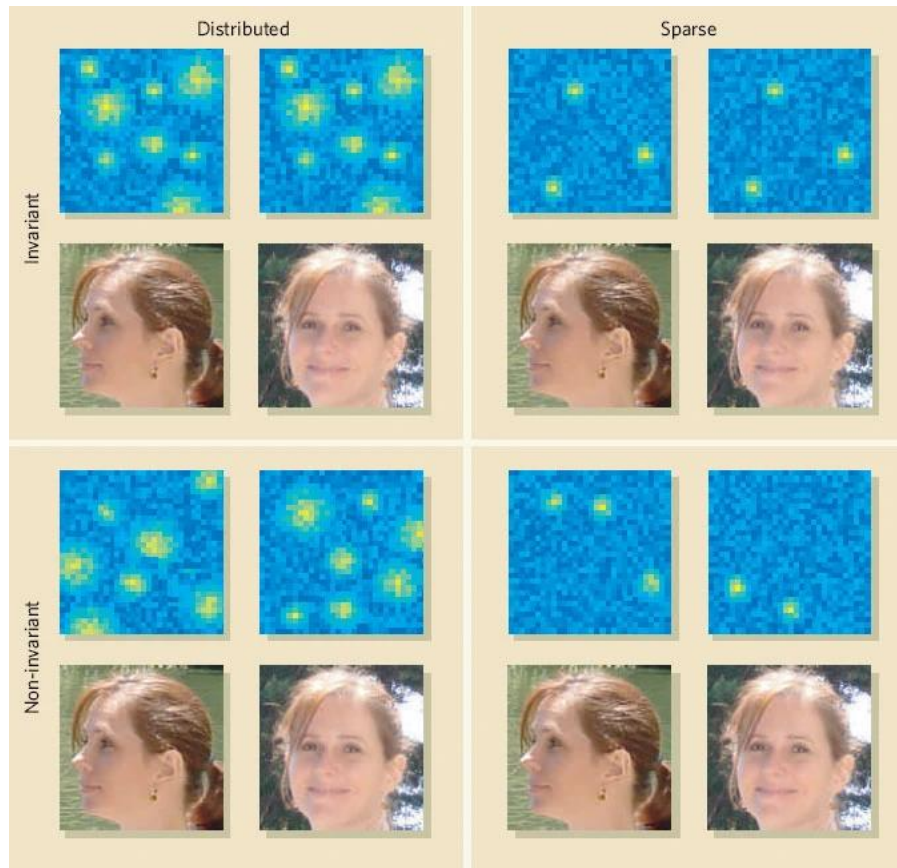


Figure 2. Sparse and distributed encoding scheme for visual stimuli. A Hypothetical population of neurons is depicted in blue (low activity) and yellow (high activity). According to a distributed encoding scheme, populations of neurons activate to represent a stimulus, whereas in the sparse encoding scheme, very few neurons activate. In an invariant encoding scheme, different profiles of the same stimulus elicit identical activations, whereas in a non-invariant scheme, the neural activation pattern varies according to the distinct profiles. The grandmother cell theory follows the sparse and invariant representation scheme. Adapted from Connor (2005).

Despite the literature often juxtaposing these views, both have biological plausibility and rather exist in a complementary matter. For instance, in the primary visual cortex, stimuli are first processed through their basic components (edges, motion, depth, color) in a distributed pattern across a population of neurons (Connor, 2005). As these features combine into a coherent visual percept, the representation becomes gradually more selective and sparser.

A study conducted by Handjaras and colleagues (2016) found that semantic knowledge is represented in the brain as a distributed, modality-independent network. The authors investigated the cortical organization of semantic information in sighted and congenitally blind individuals, finding that category-specific and modality-specific information is integrated on a regional level. This indicates that the brain organizes information representation in a flexible and integrative manner, allowing for semantic processing across sensory modalities.

1.1.2 Approaches to Measuring Brain Representations

Our understanding of how the human brain encodes information has advanced alongside scientific advancements and the progression of techniques over the past century (Doty, 2015, p. 279). Notably, our realizing of the nervous system has journeyed through varying levels of detail, from individual neurons to the collective activity patterns of neural ensembles.

The first mappings of single-neuron responses to various stimuli occurred through animal models (Purves et al., 2020, p. 17). This involved the placement of microelectrodes near or within specific brain regions to the activity of individual neurons. Single-unit recordings facilitated the capture of action potentials, enabling researchers to investigate the precise firing of individual neurons. These recordings laid the foundation for recognizing how the brain processes and represents information at the cellular level.

Early imaging techniques, including pen-and-ink, camera lucida, dry-plate photography, silver staining, and light microscopy, enabled the study of brain anatomy, rendering the previously unobservable aspects observable (Doty, 2015, p. 279). These methods evolved into clinical practices such as x-rays, pneumoencephalography, contemporary computerized tomography (CT scan) in the 70s, and magnetic resonance imaging (MRI) in the 80s. The advent of functional imaging marked a significant era, allowing the capture of small local changes in cerebral blood flow or metabolism (Purves et al., 2020, p. 18-20). Contemporary methodologies, such as positron emission tomography (PET), single photon emission computed tomography (SPECT), and functional magnetic resonance imaging (fMRI), offer further insights. Notably, fMRI presented some advances by exploiting intrinsic brain signals and allowing repeated observations within individuals.

Finally, magnetoencephalography (MEG) offered an unseen temporal resolution for pinpointing the functionality of the brain.

The inventions of PET, MRI, and electroencephalography (EEG) have played central roles in advancing our understanding of the functional aspects of the human brain, particularly how it represents and processes information (Doty, 2015, p. 279). These imaging techniques allowed researchers to non-invasively study brain activations for the first time. In experiments, the choice imaging method is intricately linked to the specific research question and availability of resources.

1.1.3 Analyzing Neuroimaging Data

Various methods have been developed to analysis the puzzles of fMRI data, from a local level (region of interest, ROI) to a whole-brain level. These methods can be broadly categorized into univariate and multivariate approaches (Hebart & Baker, 2018; Huettel et al., 2004).

As the name suggests, univariate involves the study of a single dependent variable, in this case, the blood-oxygen-level dependent (BOLD) signal, and its relationship with independent variables (experimental conditions or predictors) at the voxel level. Measurements in this context can be represented as one-dimensional vectors, where each number refers to a simple voxel sample (Oosterhof & Connolly, 2013).

In contrast, multivariate pattern analysis (MVPA), also known as multivoxel pattern analysis handles multiple dependent variables or features simultaneously. This method considers the interactions among multiple voxels, resulting in a two-dimensional matrix where each row represents a sample, and each column represents a feature. MVPA provides a more comprehensive analysis by considering the joint variability of multiple features.

The infamous dead salmon study (Bennett et al., 2009) highlighted the pitfalls of fMRI, particularly concerning the use of appropriate statistical thresholding. Spurious activations appeared in a dead salmon's brain, while it was "performing" social perspective-taking tasks. The key point of the study was not to critique fMRI per se but to draw attention to

the appropriate multiple comparison corrections essential in the statistical analysis of fMRI data (Lyon, 2017).

An excellent review by Kragel et al. (2018) outlines the progression from neurons to neuroimaging, illustrating how human neuroimaging has evolved from mapping local effects to predictive modeling of mental events through distributed information integration. A significant shift in the field has been the transition from brain maps to brain models: maps describe local information encoding, while models aim to specify the components of a neural system and how their collective activity predicts behavior and cognition.

Multivariate models have been developed for a wide range of mental events and states, including:

- ❖ Object recognition (Haxby et al., 2011)
- ❖ Wakefulness (Tagliazucchi & Laufs, 2014)
- ❖ Autonomic responses (Eisenbarth et al., 2016)
- ❖ Memory (Fullana et al., 2016; Polyn et al., 2005)
- ❖ Decision-making (Hampton & O'Doherty, 2007; Kahnt et al., 2011)
- ❖ Semantic concepts (Huth et al., 2016; Mitchell et al., 2008)
- ❖ Cognitive tasks (Poldrack et al., 2009)
- ❖ Emotion (Kragel & LaBar, 2015; Saarimäki et al., 2016)
- ❖ Neurological and mental disorders (Arbabshirani et al., 2017; Woo et al., 2017)

Despite the progress in predictive modeling and establishing brain-mind mappings, these models are only beginning to address the representations of mental constructs and processes (Kragel et al., 2018). Kragel and colleagues (2018) highlight that construct validation remains as key importance in cognitive neuroscience, with an emphasis on defining and validating mental constructs based on brain representations and empirical data.

1.2 Classical Conditioning: Bell Rings & Saliva

In the light of above-mentioned neural representations and their measurement, this section summarizes classical conditioning, its measurement in humans, and how it has been observed to alter neural representations.

In classical or Pavlovian learning (Pavlov, 1927), a neutral cue (conditioned stimulus, CS) is paired with a biologically salient event (unconditioned stimulus, US). This association can be established through aversive conditioning, such as a painful electric shock, or through appetitive conditioning, such as reward like food (Andreatta & Pauli, 2015). Once this pairing has been established, CS+ alone can elicit a response similar to the US (conditioned response, CR). Ivan Pavlov (1927) conducted his initial experiments at the end of the 19th century in dogs, using bell rings as the CS and food as the US, causing the animals to salivate (unconditioned response, UR).

1.2.1 Functional Neuroimaging of Learning Processes

The first studies utilizing neuroimaging with conditioning paradigms took place in the late 1990s, using classical fear conditioning (Büchel et al., 1998; LaBar et al., 1998). Unlike aversive conditioning, appetitive conditioning has been seldom studied in humans despite its clear relevance to normal and pathological behaviors such as addiction and obesity (Andreatta & Pauli, 2015; Austin & Duka, 2010; Delgado et al., 2011; Klucken et al., 2009, 2013; Levy & Glimcher, 2011). Although both types of conditioning hold evident significant for survival, human paradigms face the challenges of establishing an appropriate US that can elicit physiological responses similar to those of aversive stimuli (Martin-Soelch et al., 2007). Interestingly, monetary rewards have proven effective despite not being inherently rewarding items with intrinsic value, but rather, a conceptual reward. (Austin & Duka, 2010; Delgado et al., 2011; Haruno et al., 2004; Haruno & Kawato, 2006; Howard et al., 2016; Levy & Glimcher, 2011).

Gottfried et al. (2002) conducted one of the few studies combining appetitive and aversive conditioning in the same paradigm, using odor as a reinforcer. Neutral faces were linked to pleasant, neutral, and unpleasant odors. The study observed increased activation in the ventral striatum (VS) and orbitofrontal cortex (OFC) in response to appetitive CS+ compared to aversive CS+, determining OFC's role in processing odor value and

transferring affective value from olfactory (US) to visual (CS) system (Andreatta & Pauli, 2015). In addition to Gottfried, Metereau and Dreher (2013, 2015) conducted a neuroimaging study using both aversive and appetitive conditioning, employing rarely used gustatory US (juice and salt water), as well as aversive picture and monetary reward within the same paradigm.

In a review by Martin-Soelch and colleagues (2007), the authors found that appetitive conditioning involves a circuitry with the amygdala, anterior cingulate cortex (ACC), OFC, and striatum (Figure 3). The interconnectedness of these areas yields functional redundancy and specialization for various aspects of the learning process. Compared to animals, appetitive associative learning in humans shows discrepancies, particularly in subcortical structures.

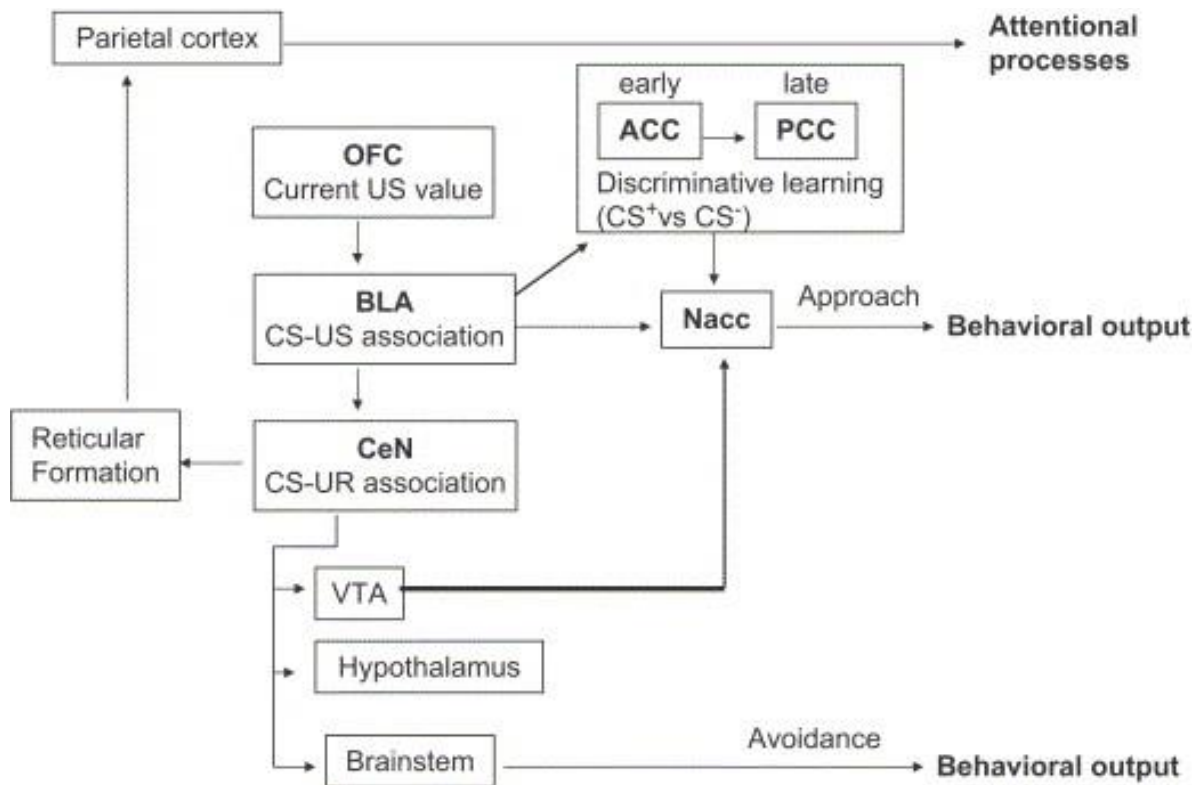


Figure 3. Model of the neural circuitry of appetitive conditioning. The model depicts the thoroughly studied and established neurocircuitry involved in appetitive conditioning based on findings from both animal and human studies. This model, adapted from Martin-Soelch et al., (2007), emphasizes the interconnected regions of the brain that play roles in processing and responding to rewarding stimuli.

A further review by Bissonette et al. (2014) compares animal and human studies on appetitive and aversive conditioning. They also highlight that most research considers

both types of learning in isolation: research that simultaneously incorporates both appetitive and aversive information to study the roles of various brain areas remains modest. Bissonette and colleagues emphasize that OFC holds a representation of value, while VS shows value and salience signals. The amygdala, in turn, acts as a stimulus intensity modulator, with signals modulated by the value or valence of the stimulus. The authors underscore the limitations of the current technologies, particularly the need for better temporal and spatial resolution to expand knowledge about the processes.

Numerous neuroimaging studies have found that CS evokes systematically increased or decreased BOLD signals compared to neutral control stimuli (Andreatta et al., 2012; Bach et al., 2011; Christian Büchel et al., 1998; Fullana et al., 2016; Gross & Canteras, 2012; Holland & Bouton, 1999; LaBar et al., 1998; Levine et al., 2018). Recent studies utilizing pattern-based analyses have finally allowed investigation into the representations of stimuli. Dunsmoor et al. (2014) showed that fear-conditioned stimuli within the same visual category became more similar to each other post-conditioning. Additionally, fear-conditioned stimuli tend to exhibit increased similarity to the US (Onat & Büchel, 2015). However, these studies often use concrete stimuli as reference or anchor points, leaving open the question of whether the found similarity pertains to the association with the stimulus or to the abstract properties of fear (Levine et al., 2018). To that end, Levine et al., (2018) investigated existing phobia compared to experimentally induced fear, finding shared neural representations for fear-inducing information, regardless of whether it was inherent (phobia) or conditioned.

1.3 From an Odorant to Perception: What's that Smell?

Our ability to smell is often overlooked, as it is not similarly essential as the sense of vision in allowing us to detect and differentiate objects or other people from the environment (Sarafoleanu et al., 2009). In addition to vision, our attentional spotlight in space is highly guided by audition (Sela & Sobel, 2010). Thus, the sense of smell maintains other functions beyond environmental exploration in humans, which are often social or emotional: assessment of the safety of inhaled air and food, social interactions, harm avoidance, reproduction, and feeding (Purves et al., 2018; Sarafoleanu et al., 2009; Zhou et al., 2019).

Notably, for most species besides humans, olfaction is one of the most vital senses for interaction with the environment. From an evolutionary perspective of Elsaesser and Paysan (2007), the olfactory area evolved smaller due to changes that occurred in primates achieving the bipedal position: the olfactory system rose from the ground level, thus lessening the odor mixing and contamination. The orbits became closer to one another, providing a stereoscopic view and hence taking space from the olfactory area. The authors state that this way the perception of odors became easier, and given the nasal cavities' air purification capacity, the sense of smell was not greatly diminished in the process.

Olfaction is one of the three chemical sensory systems, the others being the vomeronasal system for pheromone sensation and the gustatory system for taste perception (Purves et al., 2018). Accordingly, they all detect environmental chemicals – in the case of olfaction and vomeronasal system, airborne molecules. Vomeronasal system is in particular sensitive to odors relevant for potential mates, prey, and predator detection, and is notably missing in adult humans (although the organ can still be found in fetuses; Sarafoleanu et al., 2009).

Together with the vomeronasal system, olfaction is often viewed as the “most primitive” and “oldest” of senses from an evolutionary viewpoint, but still, it has received very little attention in research and remains the most poorly explored sensory modality (Purves et al., 2020, p. 323). Wilson et al. (2006, p. 4) argue the importance of olfaction further: the

1st cranial nerve in vertebrates indeed mediates olfaction, leading to the olfactory bulb, and chemosensory systems overall develop very early in an organism's ontogeny.

In the next part, let us consider the basic anatomy of the olfactory system (1.3.1), note the most common olfactory dysfunctions (1.3.5.), review the igniter for the sense of smell, the odorants (1.3.7.), and finally, take a brief look at the history of olfaction research (1.3.8).

1.3.1 Anatomy of the Olfactory System

In a nutshell, smell perception starts at the roof of the nasal cavity, where airborne odor molecules arrive through inhalation (orthonasal olfaction) or from the oral cavity through drinking or eating (retronasal olfaction). These molecules reach the nasal epithelium and bind with the olfactory receptor neuron's (ORN; aka olfactory sensory neurons) sensory endings (Figure 4; Purves et al., 2018, pp. 323-327). The olfactory epithelium is about 10 cm² large in adults (vs. in bloodhound dogs 150-170 cm²; Purves et al., 2018, p. 325), and encapsulates ~50 million ORNs (Elsaesser & Paysan, 2007). Each ORN has a single dendrite that expands through the epithelium, where about 8-20 sensory endings, referred to as olfactory cilia, emerge from the end of the dendrites. Cilia are protected by a thick layer of mucus in the nasal cavity (nasal mucosa; produced by Bowman's glands in the olfactory epithelium). When an odor binds to an odorant-specific receptor (G-protein-coupled-receptor) in the cilium, a second messenger-mediated signaling cascade is activated, resulting in membrane depolarization.

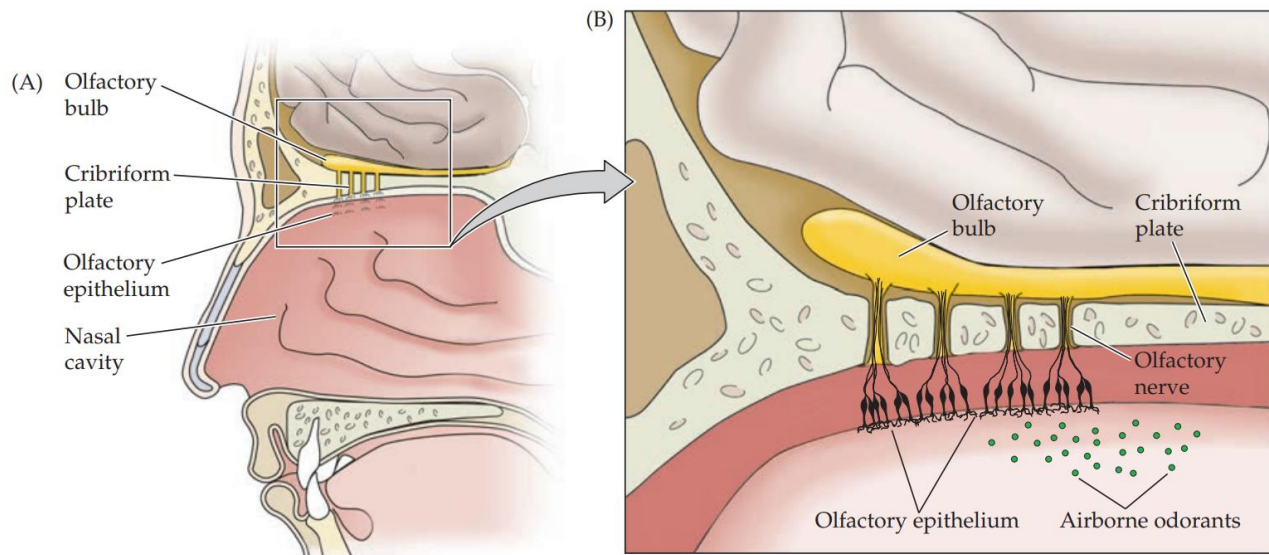


Figure 4. Olfactory system structure in humans. (A) The olfactory area is located at the roof of the nasal cavity. (B) Peripheral components of the olfactory pathway (olfactory epithelium and the olfactory receptor nerves) protrude through the cribriform plate into the central components of the pathway (olfactory bulb). Adapted from Purves et al., (2018, p. 324).

A single ORN expresses only one kind of protein receptor. Altogether, humans express about ~400 different receptor types, which are each odorant-specific, in comparison to 1000 types in dogs and 1200 in chimps (Malnic et al., 2004; Purves et al., 2018, p. 333). Many smells, for example, the smell of coffee, contain several different odor molecules that together create the recognizable smell – therefore also binding into several different receptor types. This combinatorial function enables us to recognize a vast number of smells, estimated to be about 10,000.

ORNs' axons project through the cribriform plate towards the olfactory bulb (OB) in bundles of 10-100 fibers (Figure 5; Sarafoleanu et al., 2009). There, they regroup according to their receptor cell types (although in the olfactory epithelium, different receptor types are distributed arbitrarily) and converge into synaptic arrangements called glomeruli. Lastly, in the synaptic structures of glomeruli, mitral cells are activated, relaying the signal to higher processing centers. This organization of regrouping and converging enhances the sensitivity of the olfactory system; from receptors to mitral cells, the converge ratio is 1000:1. OB, located bilaterally at the base of the skull, is considered a "relay station", through which olfactory information passes from the peripheral olfactory system to the central olfactory system structures within the CNS (Croy & Hummel, 2017).

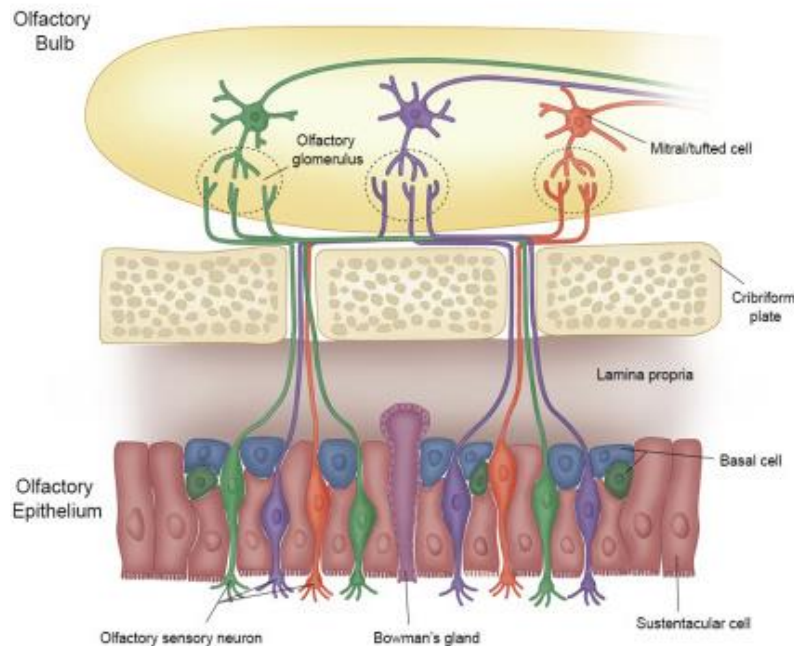


Figure 5. Cell types in the human olfactory system. The olfactory epithelium contains olfactory sensory neurons (transmit olfactory information), Bowman's glands (mucus secretion), sustentacular cells (maintain homeostasis), and basal cells (regeneration of ORN's). Adapted from Son et al. (2021).

Besides ORNs (and Bowman's glands), the nasal epithelium contains three other cell types: macrophages, sustentacular (supportive) cells, and basal cells (Purves et al., 2018). The first two are involved in immune defense, which is particularly crucial due to the uncommonly exposed location of the olfactory area to the external environment. Sustentacular cells catabolize organic chemicals and other harmful particles. Given the continuous susceptibility of the ORNs to external, possibly damaging substances, pollutants, micro-organisms, and allergens, the lifespan of matured ORNs is only about two-months. Hence, the basal cells maintain a constant cycle of degeneration and regeneration of ORNs from dividing stem cells.

1.3.2 Where is the Olfactory Cortex & Other Olfactory Processing Streams

As one of the sensory systems, olfaction has some curious characteristics. First, the olfactory information is mostly passed through unmyelinated axons (Croy & Hummel, 2017). The signaling pathways overall comprise (only) one to two synapses, one at the axonal terminals of ORNs in the glomeruli and the second at higher cortical olfactory centers. What is especially interesting, olfaction does not relay through the thalamus on

its processing path to the cortices as all other sensory systems do (Purves et al., 2018, p. 324). It is still unclear, which of the olfactory region(s) plays the “role of thalamus”, as a relay station that receives sensory signals and sends them further to appropriate cortical regions (mentioned by Martin Witt at the Smell & Taste 14 Conference in Dresden, 2022). Further, again in contrast to other sensory systems, regions involved in olfaction are mostly composed of 3-layered paleocortical structure, not 6-layered neocortex (Wilson et al., 2015, p.210). Olfaction has also been shown to evoke emotional and vivid memories, also from early life – events much earlier than those evoked by visual or verbal stimuli (Freiherr, 2017, p. 763; Larsson & Willander, 2009).

The current understanding of the olfactory cortex considers it as a structurally and functionally heterogeneous system (Wilson et al., 2015). As shown in Figure 6A and B, there number of areas involved in the processing of olfactory information, which receive direct input from the OB through the olfactory tract. **The piriform cortex** (PC; also pyriform cortex), **olfactory tubercle**, **amygdala**, and **entorhinal cortex** receive direct input from the OB through the olfactory track (Purves et al., 2018). All these regions further project to **OFC**, **thalamus**, and **hypothalamus**, whereas the entorhinal cortex has projections to **hippocampal formation**.

Below is a summary of the most relevant known olfactory functions of these regions (primary and secondary OB targets), despite the current understanding of the functionality of these regions being short at best (Zhou et al., 2019).

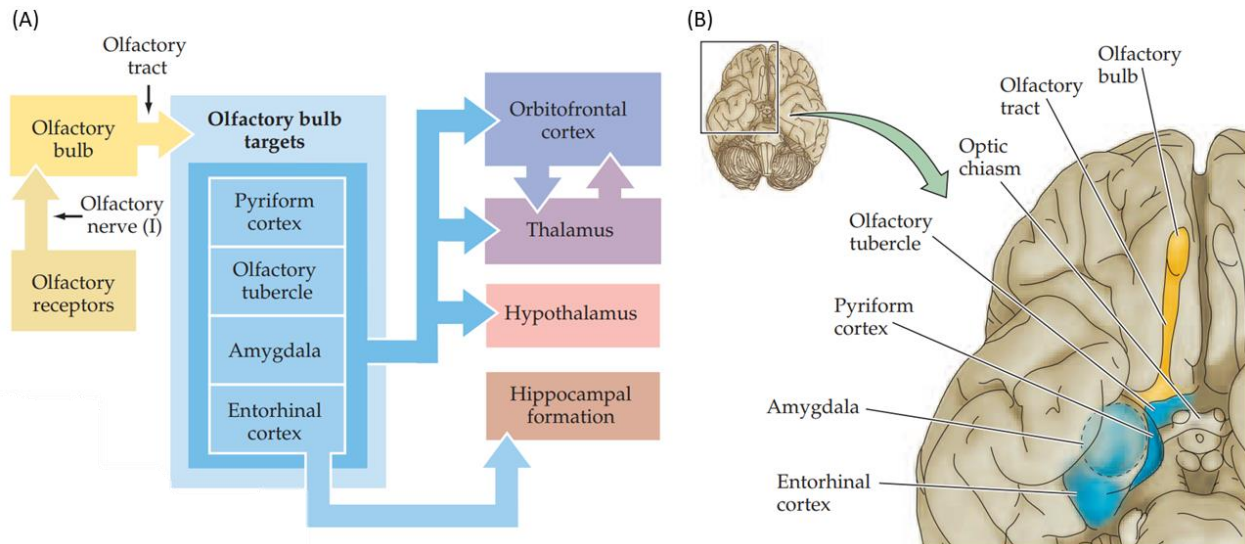


Figure 6. Olfactory pathways and projections. (A) The olfactory bulb has several target regions that process olfactory information, which can be divided into primary and secondary targets on the olfactory pathway. (B) The central components of the olfactory system, demonstrate the vicinity of the olfactory bulb to its target regions. Adapted from (Purves et al., 2004, p. 324).

Primary OB targets:

- ❖ **Piriform cortex:** PC receives the most projections from the OB, and it has hence been the center of olfactory research thus far (Zhou et al., 2019). The human PC can be separated into frontal (anterior) and temporal (posterior) divisions, but the functionality of these subdivisions is not yet fully defined (in contrast, rodent PC has other subdivisions that have been well studied). Anterior PC might be linked to odor identity and molecular feature decoding, whereas the posterior part may maintain an organization of odor categories with hedonic aspects (Freiherr, 2017, pp. 762-762; Wilson et al., 2015, p. 219). PC appears functionally heterogenous in neuroimaging studies and its exact role in olfaction information processing is still unclear (Bensafi, 2012; Fournel et al., 2016; Gottfried, Deichmann, et al., 2002; Howard et al., 2009; Seubert et al., 2013). Other sources have linked PC to short-term habituation and speculate its role in “pattern recognition of olfactory bulb odor-specific spatial-temporal output, with an experience-dependent synthesis of those feature-driven patterns into perceptual odor objects” (Wilson et al., 2015, p. 219). Howard et al. (2016) found that odor categories (e.g. citrus vs mint, irrelevant of the valence or intensity spectrum) are coded in PC, whereas Rolls et al. (2003) associated odor intensity coding to the region. PC exhibits synchronous activity

with sniffing and its responses to odors appear brief and quick to habituate (Zald & Pardo, 2000).

- ❖ **Olfactory tubercle:** Olfactory tubercle is involved in multi-sensory information processing based on its circuitry (Wilson et al., 2015, pp. 218-219). It may have a moderative role between odor perception and motivated behavior (i.e., odor-evoked attention)
- ❖ **Amygdala:** The amygdala is associated with odor intensity encoding and hedonic processing of odorants (Anderson et al., 2003; Zald & Pardo, 1997). In particular, it appears to preferentially respond to very aversive odors relative to pleasant and neutral ones (Zald & Pardo, 2000). These results can be considered together as olfactory intensity decoding taking place in the amygdala, but specifically for pleasant or unpleasant smells (Freiherr, 2017). The region has been found to be more active for unpleasant than pleasant odors (Royet et al., 2003). In other sources, the amygdala and periamygdaloid cortex are found to play a part in the cognitive evaluation of the olfactory input (Freiherr, 2017).
- ❖ **Entorhinal cortex:** Entorhinal cortex is considered a “gateway” for olfactory input towards the hippocampal formation, where it may play a role in memory association of odors; Kadohisa, 2013). The region is a “top-down modulator” of OB and other olfactory processing (Wilson et al., 2015, p. 219).

Secondary targets in the OB pathway:

- ❖ **Orbitofrontal cortex:** OFC is thought to be the center of cognitive olfactory processing (Freiherr, 2017, p. 763). OFC retains multiple olfactory relevant regions which respond differently according to the specific odor used or the specifics of the task (Zald & Pardo, 2000). PC projects to OFC for higher order processing, taking part in the conscious odor perception and affective coding (Freiherr, 2017, p. 763; Royet et al., 2003). Moreover, the region is also considered to have a role in olfaction memory, experience-dependent signal modulation, and in odor identification and discrimination (Freiherr, 2017, p. 763; Howard et al., 2016; Zald et al., 2002; Zald & Pardo, 1997). OFC appears to create a more integrative multi-sensory perception based on vision, olfaction, taste, and “mouth feel” (Freiherr,

2017, p. 763; Wilson et al., 2015). The region may be involved in decision-making following odor stimulation (Wilson et al., 2015, p. 219) and reward, especially regarding food odorants (Freiherr, 2017, p. 763). To put this together, OFC is not a primary processor of olfactory information, but rather involved in perceptual sensory integration, decision-making processes, and solving sensory ambiguity (Freiherr, 2017, p. 763).

- ❖ **Thalamus:** Thalamus is observed to give rise to awareness of the odor perception through its projections to OFC (Wilson et al., 2015, p. 219).
- ❖ **Hypothalamus:** Projections from the amygdala to the hypothalamus may relay olfactory influence to endocrine and autonomic systems, as has been found in rats and primates (Barbas et al., 2003; Gabbott et al., 2012; Kadohisa, 2013; Pitkänen et al., 2000)
- ❖ **Hippocampal formation:** The hippocampus receives projections from OB via the amygdala and entorhinal cortex (Kadohisa, 2013). Damage has been found to disrupt the temporal sequence of odor information memory formation (Kesner et al., 2002) and odor-place associative learning (Kesner & Rolls, 2015). The hippocampus may play a part in multisensory integration including olfaction (Freiherr, 2017, p. 763).

According to Freiherr (2017, p. 763), olfactory information is passed down through these secondary brain regions (in red), together with VT, cingulate cortex, cerebellum, and insula (not mentioned in Figure 6 and Purves et al., 2018), but do not actively take part in the basic olfactory information processing. Instead, they appear to have a role in the cognitive processes concerning smell perception. Below is a note on insula and its role in smell perception.

- ❖ **Insula:** Insula receives projections from OFC, amygdala, and PC (Freiherr, 2017, p. 763). The insula is known as the primary gustatory cortex since it represents the five gustatory categories (Purves et al., 2018, p. 325). Thus, it is speculated that it may further integrate chemosensations concerning food and flavor perception (Freiherr, 2017, p. 763). The anterior insula is associated with avoidance behavior evoking, which is shown to correlate with the processing of unpleasant olfactory

and multisensory stimuli. Royet and colleagues (2003) found lateralized activation in the insula as a function of handedness, where right-handers showed left ventral insula action and left-handers vice versa, for in particular unpleasant odors. The activation was higher for high-intensity odors, suggesting more intensity-based encoding, instead of valence.

Although the organization of other sensory systems has been well explored in the CNS (e.g. the auditory cortex is organized tonotopically; the insular taste cortex maintains a representation of the five main gustatory categories; visual and somatosensory cortices encode topographic maps relative to the receptor surface), the central representation of the olfactory perception remains unknown (Purves et al., 2018, p. 325). Several brain regions have been linked to processing olfactory information (Seubert et al., 2013; Zatorre et al., 1992), but such a single region deemed the “olfactory cortex” has yet not been exclusively recognized in humans. A study done on catfish was able to identify a spatial mapping of odorants, so-called odotopy, which was maintained not only in the OB (“glomerular odotopic map”) but also in the forebrain (Nikonov et al., 2005). Still, unluckily to us, the developmental steps of the catfish forebrain differ significantly from those in mammals, thus hampering the search for equivalent areas in our vertebrate class. A similar glomerular map of odorants has been found in rodents: as ORNs responding to similar odorant molecules group in glomeruli, those glomeruli that respond to similar molecular structures also tend to stay near each other (Johnson & Leon, 2009). Hence, this glomerular map represents a chemotopic organization of odors.

When comes to studies in humans, a few different views can be found in the literature. For instance, **PC** has been previously named as the “primary olfactory cortex”, due to its position as the largest area to receive direct OB input (Johnson et al., 2000). Still, other research has shown that the organization of PC differs essentially from those of the other sensory cortexes, weakening this assumption of its central role in olfaction (Purves et al., 2018).

According to another view reported, by Han et al. (2019), brain regions involved in the processing of olfactory information can be divided into primary and secondary olfactory cortexes (Figure 7). The former, hypothesized to receive direct OB input, would

encapsulate PC, subregions of the amygdala and entorhinal cortex. The latter would concern a number of subregions, to which the primary olfactory cortex projects: hypothalamus, mediodorsal thalamus, hippocampus, insula, striatum, amygdala, OFC, cingulate cortex, and parahippocampal gyrus.

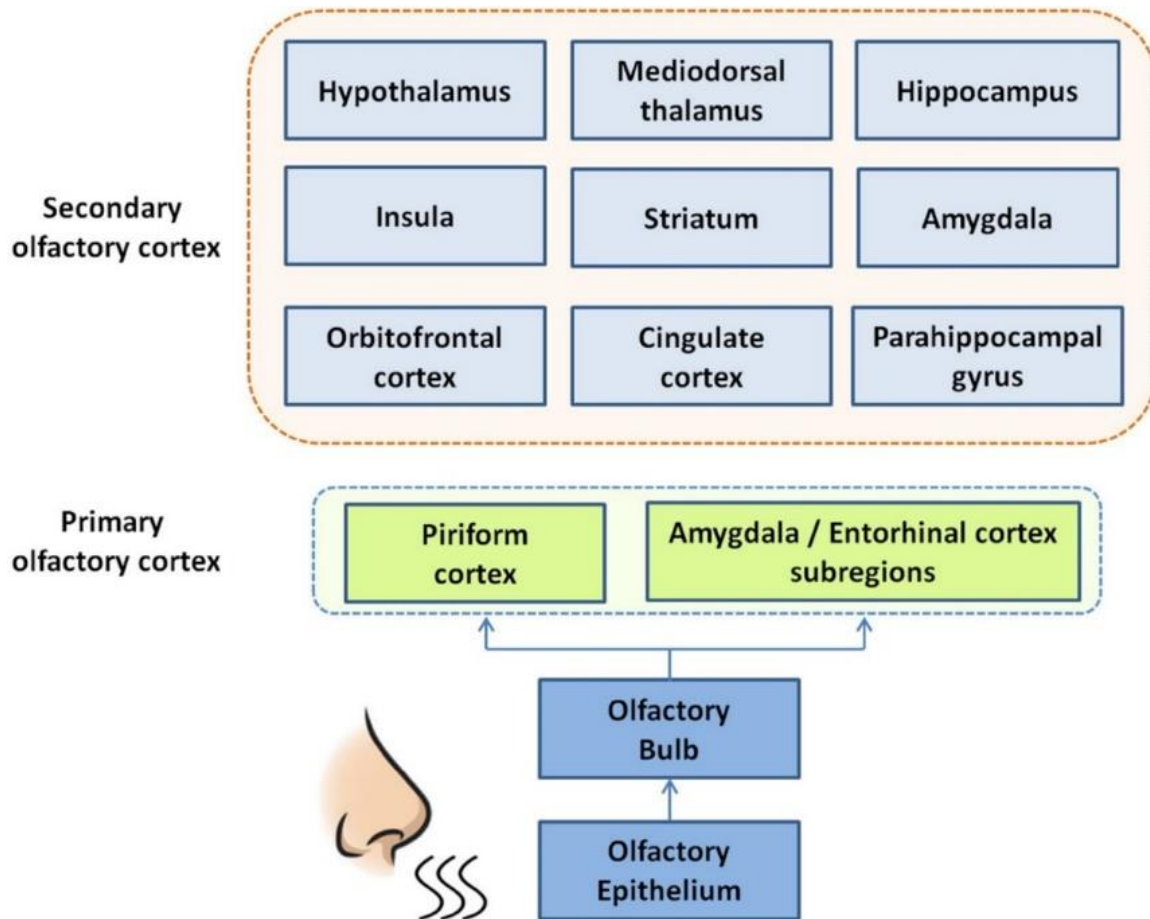


Figure 7. The central olfactory system in humans. Another view depicts the organization of the regions involved in olfactory processing into primary and secondary cortices. Both would involve more than one distinct brain region. Adapted from (Han et al., 2019).

Further views have been proposed on the organization of the central olfactory processing (see e.g. Croy & Hummel, 2017; Gottfried, 2006; Son et al., 2021). To conclude, the regions involved in olfaction may well have been recognized, but their distinct roles in the information processing are still unclear.

1.3.3 Trigeminal Nerve

When discussing olfaction, the trigeminal nerve must be at least briefly mentioned. The trigeminal nerve is the 5th cranial nerve, mainly responsible for the somatosensory and

motor functions of the face (Purves et al., 2018, p. 204). In addition to the olfactory system, most volatile compounds also activate the trigeminal nerve, where in particular the irritation perception of odors is assessed (Wysocki et al., 2003).

For example, the trigeminal thermosensitive nerve endings give rise to the feeling of cooling, often caused by menthol and eucalyptol (Viana, 2011). Assessment of trigeminal chemosensitivity – separately from olfaction – has proven to be a challenge in research (Wysocki et al., 2003). A way around this problem is to perform studies with anosmics, people with a lost sense of smell. One such study found that many odors, commonly used in research, also stimulated the trigeminal nerve at high concentrations (Doty et al., 1978). Later research has confirmed this finding and elaborated that while ORNs respond to relatively low odor concentrations, trigeminal nerve's free nerve endings respond to noxious and (possibly) damaging levels of chemostimulation (Keverne et al., 1986; Wysocki et al., 2003).

Given this mixed scheme of potentially compensating sensory interaction between olfaction and trigeminal nerve, further research is needed to fully understand the dynamic between these two systems (Frasnelli et al., 2007). In addition to the mentioned functions of chemo- and thermosensation, the trigeminal nerve is sensitive to mechanical stimulation. Increasing age, particularly in people above 60 years of age, decreases both olfactory detection and trigeminal sensitivity (Wysocki et al., 2003).

1.3.4 Olfactory Detection & Temporal Dynamics

Generally, the olfactory function is assessed in experimental or clinical settings by determining one's (subjective) odor detection and identification thresholds (Laska & Ringh, 2010). The odor detection threshold refers to the lowest concentration where odor can still be reliably perceived, while the recognition threshold is often a few folds higher, referring to the lowest concentration where the odor can be reliably identified. In addition to these threshold tests, odor discrimination (e.g., Sniffin' Sticks test; Hummel et al., 1997; Kobal et al., 1996), memory, perceived intensity, and hedonic assessments are often administered in experiments. Typically, olfaction tests requiring further cognitive processing (e.g., memory or valence estimation of odors) are temporally more demanding than simple odor detection tests.

Paradoxically, even though our threshold for smell detection is quite low, the concentration of the smell needs to be extremely high before we instinctively shift our attention toward it (Sela & Sobel, 2010). Humans have somewhat weak olfactory spatial abilities – for example, track sniffing is possible, but does not come as naturally as for other species (Purves et al., 2018, p. 326; Sela & Sobel, 2010). Neither is our attention selectively driven by different odorants in our immediate environment, but is mainly directed by our primary distal senses vision, and audition (Bregman, 1990; Sela & Sobel, 2010).

Besides this weak spatial processing, the temporal processing of odors differs from vision and audition (Sela & Sobel, 2010). The latter two are almost continuously sampling for sensory input, just occasional blinks are causing sampling breaks in vision (Caffier et al., 2003; Sela & Sobel, 2010). In contrast, olfaction processing happens in discreet sniffing events (typically 30 per minute, that is 0.5 Hz – vs. 30 Hz in vision; Croy et al., 2015; Galvin et al., 1976; Sela & Sobel, 2010), also depending on our breathing cycle (12 – 20 per minute; Flenady et al., 2017). As summarized by Sela and Sobel (2010), “olfactory information is made available to the brain during brief bursts followed by often prolonged periods of no input”.

First event-related potentials, as measured with EEG, peak about 250 – 450ms after olfactory stimulus onset (Croy et al., 2015; Hummel & Kobal, 2001; Lundström et al., 2006). Behavioral responses after such onset are usually reported to take place after 600-1200ms (vs. 100ms in vision; Posner & Cohen, 1984), given the information processing via unmyelinated (slow) axons and depending on the particular odor concentration (Cain, 1976; Schriever et al., 2015). More recent studies suggest that conscious olfactory perception takes place 600-900ms after stimulus onset (Walla, 2008; Walla et al., 2002). Typically, an interstimulus interval (ISI) of 20 – 30 seconds is used in olfactory studies to allow for the proper detection of the odor as well as a washout time between the stimuli (Croy et al., 2015). If odors are presented with ISI below 2 – 2.5 seconds, they tend to be perceived as a mix instead of two separate odorants (Croy et al., 2015; Schriever et al., 2015).

The temporal processing of odors appears to be also affected by the valence of the odors. Bensafi et al. (2003) investigated how differently pleasant, neutral, and unpleasant odors

are processed in the brain. Their results indicated that unpleasant odors are evaluated significantly faster than neutral and pleasant odors (as indicated by participants via a button press task), specifically during a pleasantness judgement task but not during detection, intensity, or familiarity judgement tasks. According to the authors, this is a common finding in studies particularly investigating affective evaluation, suggesting a differential processing of negative and positive odors. They further speculate that this more rapid assessment of unpleasant odors might occur due to evolutionarily reasons; possibly there is a subsystem, responsible for a rapid assessment of unpleasant odors leading to defensive and withdrawal behavior. Beyond the modality of olfaction, (Gagnon & Peretz, 2000) found a similar effect in hearing: unpleasant sounds were processed more rapidly than pleasant sounds (again, only during the affective judgement task vs. nonaffective judgement task). Boesveldt et al. (2010) confirmed these findings in an article descriptively named “Fish is bad”, where unpleasant food odors specifically were detected quicker and more precisely compared to odors from other categories. Given the central role of “good” and “bad” odor dissociation in our survival, the authors concluded this faster detection mechanism concerns ecologically relevant odors.

1.3.5 Olfactory Dysfunctions

Dysfunctions in other senses, particularly in vision and hearing, are easily noted, whereas dysfunction in olfaction can often go unnoticed (Hornuss et al., 2020). Although the latter does not have such an extreme impact on life quality as the other sensory dysfunctions do, curiously, olfactory disturbances influence a greater percentage of the population than other sensory disturbances (Han et al., 2019). Reduced ability to detect and smell odors is a sign of such olfactory loss (Han et al., 2019). Up to 5% of the population experience total olfaction loss (anosmia), whereas 15% suffer from partial loss of smell (hyposmia).

Temmel et al. (2002) have listed the common causes of olfactory loss – besides age-related olfactory function decline – in a sample of 278 hyposmics or anosmics (123 male, 155 female): upper respiratory tract infection (37%), sinonasal disease (22%), trauma (e.g. traumatic brain injury; 17%), congenital anosmia (3%) and other (3%), while for 18% of the patients the olfaction loss was idiopathic. Given the delicate projections of olfactory nerves through the cribriform plate (Figure 4 and 5), a trauma causing the brain to move

within the skull can simply rip the projections off – with no possibility of regrowing (see Figure 1 in Howell, Costanzo, and Reiter, 2018 for detailed depiction). Further, dysfunction in the sense of smell has been linked to numerous neurological disorders such as depression (Croy & Hummel, 2017), incipient schizophrenia (Moberg et al., 1999), Parkinson's disease (Hawkes et al., 1997), and Alzheimer's disease (Haehner et al., 2007; Ross et al., 2008). Normal, age-related olfaction loss has been described as a linearly decreasing ability to identify common odorants, with about a 10% decline in correct identification per decade (see Figure 15.5B in Purves et al., 2018, p. 328 for details).

1.3.6 Olfaction & Emotion

According to Soudry and colleagues (2011), a large collection of studies point to a close connection between emotion and olfaction information processing. As an odor is perceived, it is often quickly observed through its inherent valence, from positive (appetitive), neutral, to negative (aversive). Moreover, odors have been detected to induce emotional states (Seubert et al., 2009; Weber & Heuberger, 2008), and in turn, emotional stimulation can alter the following olfactory perception (Pollatos et al., 2007). This suggests an intertwined nature of emotional content or preference for odors, which has been speculated to be due to the anatomical and functional commonalities of emotion and olfactory processing (Gottfried, Deichmann, et al., 2002; Soudry et al., 2011).

Soudry and colleagues (2011) further highlight the relationship between odor and affect by the classical division of the central olfactory system into neocortical regions (which may enable conscious smell perception, e.g. OFC) and limbic regions (which may govern the affective feature of odors, e.g. amygdala and insula). Although this division is coarse, and functional imaging data is at least controversial, it may explain the interconnection of emotion and olfaction – assuming that the traditional idea of limbic regions giving rise to emotions holds true. The author provide a list of brain regions often associated with common emotional dysfunctions, specifically depression and schizophrenia, where olfactory dysfunctions are regularly diagnosed as comorbidities (Table 1; Pause et al., 2008; Schneider et al., 2007; Soudry et al., 2011).

Table 1. Brain regions commonly associated with olfaction and emotion information processing, with commonalities associated with depression and schizophrenia. Olfactory dysfunctions are regularly diagnosed as comorbidities of depression and schizophrenia. Adapted from Soudry et al. (2011).

| Brain Region | Olfaction | Emotion | Depression | Schizophrenia |
|---------------------------|-----------|---------|------------|---------------|
| Olfactory bulb | + | | + | + |
| Amygdala | + | + | + | + |
| Hippocampus | | + | + | + |
| Piriform cortex | + | | | |
| Entorhinal cortex | + | | + | |
| Anterior cingulate cortex | + | + | + | + |
| Insula | + | + | + | + |
| Orbitofrontal cortex | + | + | + | + |
| Central gray nuclei | | | + | + |
| Planum temporale | | | | + |
| Superior temporal lobe | | | + | + |
| Corpus callosum | | | + | + |
| Parietal cortex | | | | + |

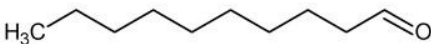
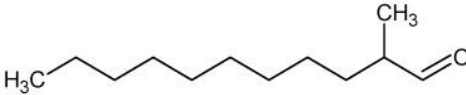
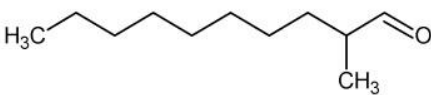
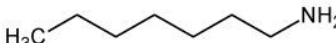
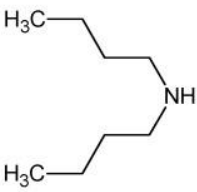
1.3.7 Odorants

Odor (also, odorant) is an airborne and volatile stimulant that activates the olfactory system by binding with the complementary ORN's receptors (Pickenhagen, 2017), i.e. a chemical stimulus causing physiological response (Genva et al., 2019). Odors can be either single-compound based, where they contain only one type of chemical compound (i.e. molecules), or perfume-based, where they contain a mix of several components (Pickenhagen, 2017). Odors used for experimental purposes to study the function of the olfactory system in the brain are products of modern perfumery; a composition of extracts from naturally odorous substances (Pickenhagen, 2017). These odors are most often oil or alcohol-based, where an aromatic extract is diluted with neutral oil or ethanol (carrier) to the desired concentration.

One of the earliest successfully isolated and identified odorants was cinnamaldehyde, cinnamon, in 1833 by scientists Dumas and Peligot (Pickenhagen, 2017). As the field evolved, odor extracts of naturally occurring substances were accompanied by non-natural odorants acquired by chemical syntheses (i.e. synthetic odors). Although both

organic and inorganic compounds may smell (e.g. ammonia NH_3 with a fishy scent), some odors humans cannot detect (e.g. CO_2 ; Genva et al., 2019)

Generally speaking, compounds with same functional groups (which humans can detect somewhat reliably; Nara et al., 2011) often smell alike; for example, esters tend to be floral or fruity, lactones are like apricot or coconut, thiols appear rotten (Dufossé et al., 1994), amines appear roasted or animalistic, aldehydes are like grass or nature (Goldstein, 2002), and volatile fatty acids appear sour or rancid (Figure 8; Genva et al., 2019).

| Functional related group | Odor-type and related compound | |
|--------------------------|--|---|
| Citrusy | | |
| Aldehydes |  decanal | Sweet, aldehydic, waxy, orange peel, citrus, floral |
| |  2-methylundecanal | Fresh, amber, aldehydic, moss, citrus, tuberose, metallic, waxy, coumarinic |
| |  2-methyldecenal | Fresh, dry, citrus, waxy, watery |
| Fishy | | |
| Amines |  heptan-1-amine | Fishy, amine-like |
| |  N-butylbutan-1-amine | Ammoniacal, fishy, musty |

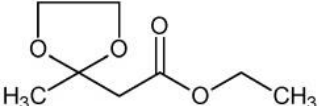
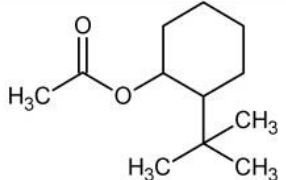
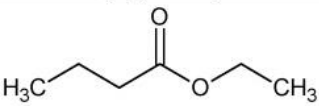
| | | |
|--------|--|--|
| Fruity | | |
| Esters |  ethyl (2-methyl-1,3-dioxolan-2-yl)acetate | Sweet, fruity, apple, green, tropical, plum, woody |
| |  2-tert-butylcyclohexyl acetate | Fruity, woody, green, apple, herbal |
| |  ethyl butanoate | Sweet, fruity, tutti-frutti, lifting, diffusive, apple |

Figure 8. Odorants with similar chemical compounds and perceived smells. Adapter from Genva et al. (2019).

Still, curiously, the smell of an odor can be predicted by its functional group only rarely (Genva et al., 2019). Some structurally different odors can result in similar perception (Figure 9a-d), while some perceptually dissimilar odors may have a largely similar chemical structural basis (Figure 9g-h). Slight structural variation may also affect the odor intensity (Figure 9e-f).

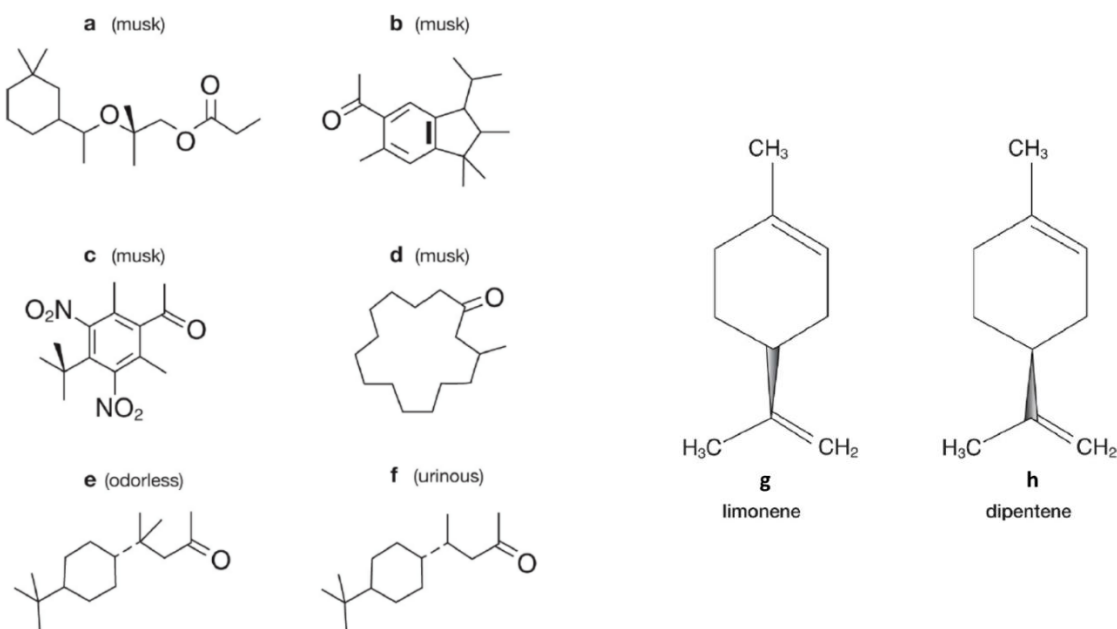


Figure 9. Odorants with dissimilar chemical structures and similarly perceived smells, and vice versa. (a-d) Musk is a well-recognized odorant, that can be evoked by vastly different chemical compounds, while odors (e) and (f) are structurally very similar but have varying perceived smell. (g-h) Limonene and its enantiomer (mirror-image) dipentene, smelling like lemons and oranges, respectively. Limonene is one of the easiest recognizable smells for humans (Purves et al., 2018, p. 326). Adapted from Asogwa (2019).

Besides the functional groups present in the molecular structure of the odorants, other attempts at the categorization of smells have been made (Auffarth, 2013). As mentioned above, given the unpredictable prediction of the odor smell by its functional group (Genva et al., 2019), such grouping is not very straightforward. Perhaps further challenging the creation of odorant categories is the mixed odors; e.g. 15 different functional groups have been identified in Arabica coffee, each group containing several different compounds (might also explain why is it so difficult to name how does coffee smell like; Yeretizian, 2017, pp. 111-113). Naturally, most simple categories are commonly made by odor sources (e.g. fruits and flowers), still used in perfumery (Pickenhagen, 2017). Odorants have a tight nomenclature with their originators – the name for the smell of citrus fruits is indeed “citronella”. With a more perceptual approach, most often in the research literature,

odors are ranked per their perceived valence profile (unpleasant to pleasant) and intensity (unnoticeable to intolerable) – although, this is highly subjective and thus unsuitable to be used as a systematic categorization method.

Similar to primary colors and main gustatory categories, a proposal for primary odors has been made (Auffarth, 2013). That is, some basic components that are independent of each other, upon which all other odors are built as mixtures. Although a common consensus has not been found as to what such primary odors are, Weiss and colleagues (2012) started the discussion on this compositionality principle by creating “olfactory white”. Just as “white” percept in vision or “white noise” in audition (in which components of equal intensity span across the stimulus space), the group discovered that mixtures of >30 odorants with equal intensity appear to smell alike without actually sharing any molecular components.

1.3.8 A Brief History of Olfaction Research

Much of the initial research on sensory systems was built upon histological findings (Zippel, 1993). Since the use of chemicals and fixating materials was still highly explorative and the technical research conditions were modest, the neuroscientific discoveries were an equal challenge. These obstacles impacted the understanding of the olfactory system, studies taking place in cadavers, where unfortunately the olfactory neurons were destroyed shortly after death. Figure 10 and 11 show illustrations from the father of anatomy Andreas Vesalius, a **16th-century** scientific revolutionist (Splavski et al., 2019). The published research of the 19th and 20th centuries, mostly printed in German, resulted in contradictory findings among scientists before a common consensus could be found.

In the **17th century**, it was still believed that the holes in cribriform plates allowed airborne odorants to reach the brain (not too far from the truth; Zippel, 1993). Schneider corrected this in 1655, stating that air cannot pass freely to the brain, and proposed that the olfaction takes place on the tender nasal mucosa in the nasal cavity (leading to another resilient dispute). Given the delicate architecture of the olfactory nerve and its somewhat humble projections in the nasal mucosa, it was not believed to be a crucial region for olfaction – in contrast, the nasal cavity is rich in trigeminal innervations. In 1856, Max Schultze noted

the “peculiar fiber cells” in olfactory epithelium, that were unique in the respiratory tract, and provided the first illustrations of the true olfactory cilia and receptor cells. His extensive work with humans and other vertebrates is still considered to be ahead of its time and did not leave much to be explored for the following years, given the limited technical resources of the time. Many of his observations, e.g. the nonuniform distribution of the ORN in olfactory epithelium, were later confirmed by other scientists (Figure 11). It still took another decade before the sensitive route from ORN to the olfactory nerve (OB) through the cribriform plate was recognized.

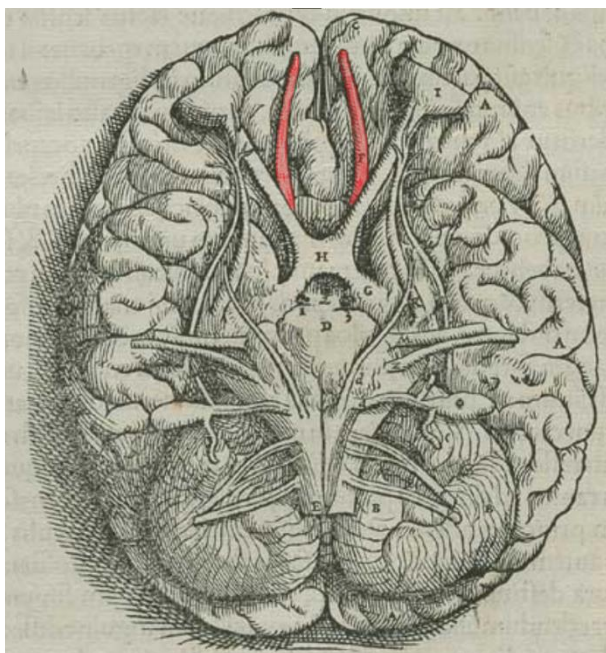


Figure 10. Illustration of the brain with olfactory bulbs highlighted. In comparison to other mammals, the human olfactory bulb is small relative to the overall brain size, which caused both Paul Broca and Sigmund Freud to believe that humans are “microsmatic” at the expense of a larger frontal lobe (McGann, 2017). Later it was found that the number of neurons in OB is in fact comparable in mammals alike. Andreas Vesalius. (1543). *De Humani Corporis Fabrica*. [Woodcut]. Retrieved and adapted from the National Institutes of Health’s Library of Medicine Digital Collection (public domain: https://www.nlm.nih.gov/exhibition/historicalanatomies/vesalius_home.html).



Figure 11. Early illustrations of the olfactory epithelium, ORNs, and supporting cells. Ecker’s (1857) depictions of the (1a, 2a) olfactory epithelium, (1b-c, 2b-c) respiratory epithelium, (4) ORN, and (6) supporting cells of a cadaver. Early investigations of the olfactory system were slow due to the limited technical resources, lack of fixatives and other chemicals, and the fast decay of the ORN following death. Reprinted from Zippel (1993).

As the anatomy of the olfactory regions was slowly starting to uncover, odors themselves also sparked interest. Carolus Linnaeus, a founder of present-day taxonomy, also suggested the first classification system for odors in the **18th century**: (1) camphoraceous, (2) musky, (3) floral, (4) pepperminty, (5) ethereal, (6) pungent and (7) putrid (Philpott et al., 2008). This classification has time and time again been revised by other scientists (e.g. Hans Henning’s 3-dimensional odor space in 1916), with new classification systems still suggested today; demonstrating not only the lack of standardized and universally agreed odor classification, but perhaps also the lack of understanding of the odor space within the neuronal architecture.

Finally, in the **19th century**, Golgi's silver staining technique under microscopy became available, allowing the detailed visualization of nervous tissue, and was followed by the exquisite work by Santiago Ramón y Cajal, illustrating the olfactory nerve pathway in its entirety (see: Levine & Marcillo, 2008; Zippel, 1993). Human lesion studies opened another door to the understanding of the olfactory percept. Mostly conducted in epileptic patients, Wiesmann et al. (2001) summarized the main findings in these studies to be, although limited, that (1) patients who underwent partial resection surgeries of the temporal lobe demonstrated unaffected odor detection thresholds (Eskenazi et al., 1983, 1986; Henkin, 1977; Jones-Gotman & Zatorre, 1988; Rausch & Serafetinides, 1975) (2) patients with temporal lobe lesions showed minor disruptions in odor discrimination when delivered to ipsilateral nostril (Eskenazi et al., 1983; Rausch et al., 1977; Zatorre & Jones-Gotman, 1991) and (3) patients with frontal lobe lesions had extreme deficits in odor identification and discrimination (Jones-Gotman & Zatorre, 1988, 1993; Zatorre & Jones-Gotman, 1991). Patients with either temporal or frontal lobe lesions show additional problems in odor memory.

1.3.8.1 Era of Olfactometry

Eugene Rimmel first filled a crowded and little ventilated room with vaporized odorants via the "Rimmel Vaporiser and Aromatic Perfume Disinfector" in the **mid-19th century** (Philpott et al., 2008). This was made to induce a positive mood amongst a crowd via olfactometry. Similarly, pleasant smells of flowers and plants were employed in schools to promote learning in the early 20th century (Anonymous, 1970; Philpott et al., 2008).

The olfactometer, as it is known today, was first invented by Dutch physiologist Hendrik Zwaardemaker in 1888, followed by other refined versions of the machine (Nicolas & Bensafi, 2021). Zwaardemaker's simple manually operated olfactometer comprised of a pipe, to be positioned in the nasal cavity, and a capsule containing a cylinder, where the angle of the pipe altered the odor intensity (Philpott et al., 2008). This invention made the controlled manipulation of the odor concentration and intensity possible, thus allowing a more systematic study of human olfaction (Nicolas & Bensafi, 2021). Figure 12 shows a simple customized, mobile, and computer-controlled olfactometer, as designed by Sommer and colleagues (2012; see further description in appendix A). When paired with

a stretch-sensitive breathing belt, researchers can precisely inquire about participants' stimulation periods, which is necessary given the inherently linked nature of olfaction processing and breathing. More advanced experimental setups allow e.g., respiration-triggered stimulus delivery (Wang et al., 2014; Sniff-O, CyNexo, Udine, Italy, <http://www.cynexo.com>).

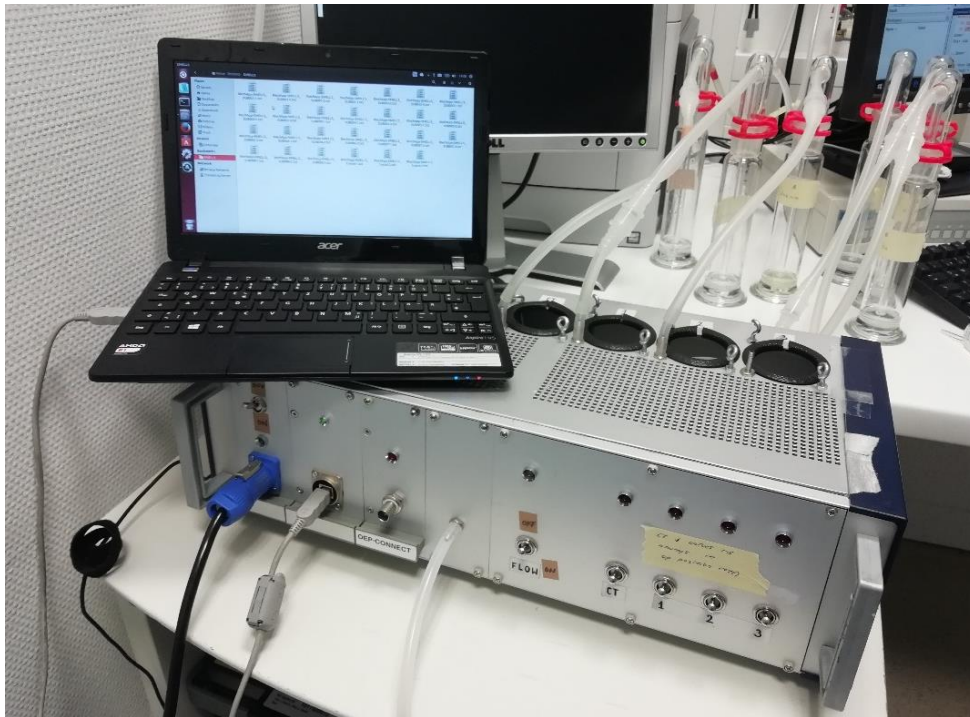


Figure 12. Riech-O-Mat olfactometer (version 1.12.1b; Sommer, 2012). The olfactometer is controlled via computer, which allows for different channels to open, one at a time, and pass air from the air source to designated valves. These valves are connected to glass vials containing liquid odorant. This causes clean air to be mixed with an odor, creating airborne odorant, that is then delivered via further tubing to the scanner room to the participant's noses. When the stimulation is off, clean air is passed through the machine. Photo by Aino-Lotta Alahäivälä.

The invention of olfactometry enabled the most important developments in the field to emerge: after the **1990s**, publications concerning olfaction finally started to increase, bearing in mind that most interest in the sensory systems generally focused on vision (Philpott et al., 2008). Standardized and easily implemented psychophysical tests became available, most notably the University of Pennsylvania Smell identification Test (“scratch and sniff”) by Richard Doty (1984), which is still the golden standard of today. Interestingly, the test does not have the same standing in Europe, as culture differences alter the familiarity of odors – the European equivalent is the Sniffin’ Sticks test from the Technical University of Dresden (Hummel et al., 1997; Kobal et al., 1996; Philpott et al.,

2008). Most likely the largest testing of olfactometry to date took place in the U.S. in 1987, where 1.5 million people took part in a National Geographic Society's psychophysics experiment (Philpott et al., 2008; Wysocki & Gilbert, 1989). The study with an impressive sample size found that although our olfactory abilities weaken with age, this decline is not uniform across participants, odorants (6 different odors were used), or response measures (detection, identification, intensity, and pleasantness tests were administered).

Perhaps the most notable discovery in olfaction was made by Linda Buck and Richard Axel in **2004**, who were awarded a Nobel prize for their discovery of a large odorant receptor gene family (Purves et al., 2018, p. 332). This family comprises ~1000 genes, resulting in a similar number of olfactory receptor types which are all specialized to detect only certain odor molecules (Philpott et al., 2008). This is still the largest currently known gene family in mammals, corresponding to 3-5% of the genome, although curiously, later studies show that about 60% of these genes are pseudogenes (nonfunctional genes; Purves et al., 2018, p. 333). It appears that the expressed odorant receptor amount correlates with the species' olfactory capacity.

1.3.8.2 Imaging Olfaction

Neuroimaging, as soon as it became applicable (e.g., Damadian et al., 1977), continued to further our understanding of the neural correlates of olfaction in humans and enabled more objective measures over psychophysics (which suffers from issues like response bias). First fMRI studies pinpointed the neuroanatomic regions relevant to olfactory processing in humans, e.g. Zatorre et al. already demonstrated piriform cortex activity in 1992. Subsequent studies became more refined and focused on olfactory brain function in terms of age and gender differences, odor-associated memories, semantic and hedonic processing (see e.g. Savic, 2002, 2005; Wiesmann et al., 2001). Two separate studies examined odor-memory-induced brain activity and found similar regions being activated by both imagined and real odors – although the regions reported in the two studies differed from each other (Kettenmann et al., 2000; Levy et al., 1999). The basic foundation for the methodological implementation of olfactory fMRI studies was set with the following: odor delivery can be unilateral or birhinal, odors selection and/or their concentration can be manipulated to selectively stimulate either olfactory nerve ending alone or with trigeminal

nerve endings (see more in Yousem et al., 1997), stimulus and ISI duration should be chosen to hinder habituation and adaptation, and constant air flow (ideally humidified if over 1L/min) is recommended to use instead of odorant pulses or blasts, that may unintentionally stimulate the tactile sensations of trigeminal nerve (Wiesmann et al., 2001). Another quite rudimentary consideration in these fMRI studies to ensure data quality was the participant instruction: participants tend to alter their respiration and attention toward odors, intentionally or not, thus exerting control over their exposure to stimuli (Zald & Pardo, 2000). Thus, the instructions need to be intentional for the study. Further, it is also still unclear to what level the neural correlates of olfaction can be altered by motivational factors (e.g., hunger, satiety) or cognitive factors (e.g., anticipation; Zald & Pardo, 2000).

The main challenge in these early fMRI studies concerning olfaction was the technical difficulties. Imaging of the ventral temporal and frontal regions often turned to be compromised by artifacts, especially in OFC, as the vicinity of air and bone produced magnetic field inhomogeneities, causing signal-distortions and dropouts (Wiesmann et al., 2001). Still, technical solutions were developed to overcome these challenges, namely post-processing and local shimming against field inhomogeneities (Morrell & Spielman, 1997) and image acquisition via spiral pulse sequences to reduce the effects of pulsatile motion artifacts (Glover & Lee, 1995).

Further, given that olfaction is inherently dependent on breathing, synchronization of breathing with stimulus delivery has been a challenge in olfaction fMRI. Traditionally, “boxcar” designs (e.g., 10s stimulus on, 10s stimulus off) were favored in all early fMRI studies due to their statistical power (Gottfried, 2015, p. 288), which also led to it being used in olfaction. This design, however, ignored the temporally variable breathing altogether, leading later “event-related” designs (different conditions presented rapidly within a block) to popularize. In event-related designs, participants were often cued with visual or auditory instructions to synchronize breathing with stimulus delivery (Gottfried, O’Doherty, et al., 2002; Howard et al., 2016). In the past decade, more sophisticated experimental designs are developed where fixed-timing stimulus delivery is replaced with a respiration-triggered event-related fMRI (Wang et al., 2014, 2017). This certainly

surpasses the previous attempts in the field but comes with the cost of requiring means for real-time respiratory data processing and stimulus delivery control.

Despite these discoveries and the insights they provide into the neural substrates of human olfaction, this sensory system remains poorly understood and the field continues to evolve. Fundamental questions continue to be debated, such as the interaction of olfaction with trigeminal nerve and vomeronasal organ in humans (Philpott et al., 2008). Further, locating the central representation of the olfactory percept or “smell map” (equivalent to the gustatory or auditory cortices; Carrie et al., 1999; Dawes et al., 2004) could be the next key finding in the field, allowing researchers to investigate the development, detrimental impact on, and recovery of olfaction in the brain.

1.4 Aims of This Thesis

This thesis aims to study how learning alters the neural and behavioral representations of odors. The primary question is whether appetitive (reward) and aversive (fear) conditioning renders the representations of neutral olfactory stimuli more stereotypically “positive” and “negative”, respectively.

As outlined earlier, the exact nature of human olfactory processing remains an open question in the scientific community. Examining the representational space of olfaction through conditioning could not only clarify the fundamentals of the olfactory cortex but also reveal the underlying neuronal mechanisms of aversive and appetitive learning.

The study is greatly influenced by the work of Howard and colleagues (2016), with the analysis pipeline based on the methodologies reported by Levine et al. (2018).

We hypothesized that there are certain parts of the brain in which the aversively conditioned neutral stimulus is similar to the negative stimulus and the appetitively conditioned stimulus is similar to the positive stimulus, with the non-conditioned neutral stimulus not showing a “preference” for each stereotypical valence class. Such brain regions would reflect the outcomes of these learning processes.

Since these brain regions may not be confined to or near olfactory brain areas, we will conduct a similarity analysis using the searchlight technique (Kriegeskorte, Goebel, & Bandettini, 2006). This approach allows us to examine the entire brain for the effects of interest in an unbiased manner, rather than restricting our analyses to predefined regions. Consequently, our experiment has the potential to provide novel insights beyond those presented by Howard and colleagues (2016). We will integrate both aversive and appetitive conditioning within the same paradigm and utilize multiband acceleration methods (Moeller et al., 2010; Seidel, Levine, Tahedl, & Schwarzbach, 2019) to acquire whole-brain functional images with the MR scanner. This enables a higher-resolution voxel size to image small structures relevant to olfaction.

1.4.1 Research Questions & Hypotheses

This study is motivated by two primary research questions:

Q1. Which brain areas can distinguish pleasant odors from unpleasant odors?

Q2. Does conditioning change the representation of neural odors?

This analysis tests three hypotheses, which can be evaluated using searchlight analysis.

We will investigate brain regions where:

1. For CS+aversive (aversively conditioned stimulus), the classifier will decode the respective activation patterns as those elicited by negative stimuli, while CS+ ap (appetively conditioned stimulus) and CS- (non-conditioned stimulus) will yield chance performance (Figure 13A).
2. For CS+ap, the classifier will decode the respective activation patterns as those elicited by positive stimuli, while CS+ av and CS- will yield chance performance (Figure 13B).
3. For both types of CS+, the classifier will decode the respective activation patterns as those elicited by the correspondingly-valenced stimuli, while CS- will still yield chance performance (Figure 13C).

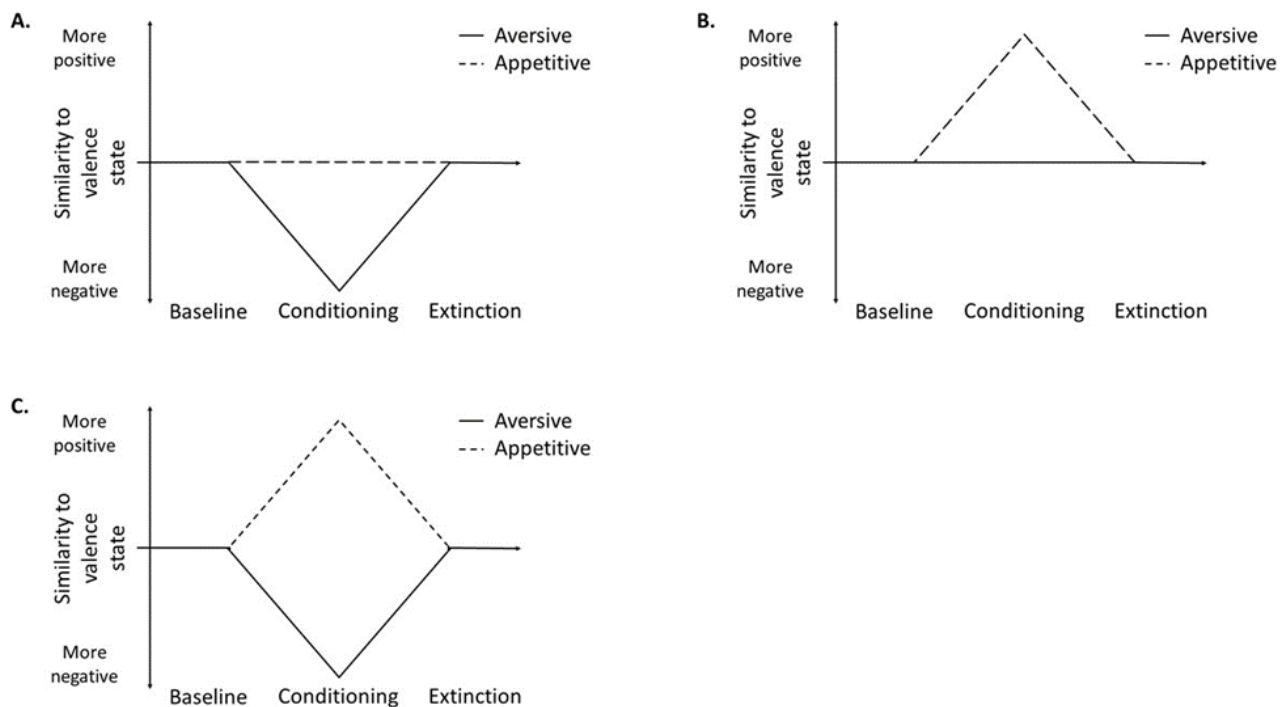


Figure 13. Hypotheses. A. When a neutrally-valenced stimulus is paired with an aversive stimulus, the cognitive representation of a neutral stimulus is hypothesized to shift toward a more negative-valence state. B. When a neutrally-valenced stimulus is paired with an appetitive stimulus, the cognitive representation of a neutral stimulus is hypothesized to shift towards a more positive-valence state. C. Brain areas that play a role in learning in general (i.e., regardless of the valence of the unconditioned stimulus) should be able to cross-decode both types of CS+ information.

2 MATERIALS & METHODS

2.1 Participants

Twenty-nine participants (18 females, 11 males; mean (\pm std) age = 27.21 (\pm 5.72) years) were recruited through advertisements from the local community. They were selected as healthy individuals with either normal vision or vision corrected to normalcy. Additionally, participants reported no prior or current diagnosis of neuropsychiatric disorders, no contraindications with MRI, and were not under the influence of psychotropic medication or other drugs known to affect cognitive function. With the exception of one left-handed participant, all others were right-handed. A further participant was not able to complete the experiment due to discomfort in the MRI scanner, and consequently, their corresponding partial dataset was excluded from the analysis.

All experimental procedures were approved by the Ethics Committee of the University of Regensburg (reference number 19-1644-101) and complied with the Declaration of Helsinki on human experimentation. Participants were required to provide signed informed consent before participating in the study, and they were explicitly informed of their right to withdraw from the study at any point without consequence. In appreciation for their involvement, participants were compensated with €15.00 for their time and contribution.

2.2 Apparatus

2.2.1 Olfactometer

A custom-built Riech-O-Mat olfactometer (version 1.12.1b; Sommer, 2012; Sommer et al., 2012) was employed to administer airborne odorants to participants during the fMRI data acquisition (see Figure 12 for a depiction of the setup). An ACER Aspire V5-123-3466 laptop operated specialized software to control the olfactometer (see Appendix A for technical specifications of the Riech-O-Mat's "punchcard file" that controls the device).

The olfactometer was located in a console room next to the MRI scanner. Teflon tubing (8 mm outer diameter; 6 mm inner diameter; 660 cm length) was connected to the device and pulled through an opening in the wall into the MRI scanner room. Within the scanner room, these tubes interfaced with custom-built Teflon nasal tubes positioned proximate to participants' nostrils.

The olfactometer provided a constant airflow averaging 2.3 L/min to participants' noses. Each glass vial contained about 10 ml of diluted liquid odorant. During the olfactory stimulation phase of each trial (see 1.4.2.1 Trial Protocol for details of the study paradigm), the olfactometer cycled through channels to present individual odors sequentially, directing airflow through the corresponding glass vial to vaporize the liquid odorant. When olfactory stimulation ceased, the constant airflow was directed through a vial containing tap water, generating odorless air. To ensure minimal odor crossover, each odor had a designated tubing reaching from the glass vial to the scanner. The tubing junction occurred only in close proximity to participants' nasal tubes, approximately 30 cm prior, to prevent odor mixing.

2.2.2 Visual Stimuli Presentation

Visual stimuli were presented to the participants during the neuroimaging experiment (2.4.2.), utilizing A Simple Framework (ASF; Schwarzbach, 2011) and Psychophysics Toolbox (Brainard, 1997) integrated within MATLAB R2015b (The Mathworks, Natick, MA, United States). Participants viewed the stimuli through a mirror attached to the scanner's head coil, enabling visualization of a semi-transparent screen that reflected an LCD video projector image (JVC DLA-G20; 60 Hz frame rate). This setup facilitated the presentation of visual stimuli in the MRI scanner environment.

2.2.3 fMRI Data Acquisition

The neuroimaging data were acquired using a 3-Tesla MRI scanner (Magnetom Prisma; Siemens, Erlangen, Germany), equipped with a 64-channel head coil, at the University of Regensburg, Germany. Functional images were obtained using a T2*-weighted echo planar imaging (EPI) sequence, with a multiband acceleration factor of 4 (Seidel et al., 2020; Setsompop et al., 2012). The acquisition parameters were as follows: 40 slices per volume, a field of view (FOV) = 192 x 192 mm², isotropic voxel resolution (VR) = 3 x 3 x 3 mm³, spacing between slices = 3 mm, repetition time (TR) = 900 ms, echo time (TE) = 30 ms, flip angle (FA) = 58°, slice thickness = 3 mm. Three functional scanning runs were conducted, with the number of volumes ranging from 482 to 505 for the first run and from 707 to 743 for the second and third runs, depending on the intertrial jitter (refer to section

1.4.2.1 Trial Protocol). To account for signal saturation, the first 10 volumes were discarded at the beginning of each functional run.

Following each functional run, a field map (B0-nonuniformity map) was acquired using a dual-echo (gradient-recall echo; GRE) sequence: (40 slices per volume, FOV = 192 x 192 mm², VR = 3 x 3 x 3 mm³, spacing between slices = 3 mm, TR = 715 ms, TE1 = 5.81 ms, TE2 = 8.27, FA = 40°, slice thickness = 3 mm) to correct for B0 inhomogeneities.

Between the second and third runs, after the field map scan, a high-resolution anatomical image was acquired for each participant to be used in co-registration of the functional images: 160 slices of T1-weighted scans using magnetization-prepared rapid gradient-echo (MPRAGE) sequence (FOV = 256 x 256 mm², VR = 1 x 0.98 x 0.98 mm³, TR = 1910 ms, TE = 3.67 ms, FA = 9°).

2.3 Stimuli

2.3.1 Odorants

Participants were presented with five perfume-based odors from Takasago Europe Perfumery Laboratory S.A.R.L. Unlike single-compound items, odorants with perfume-base contain multiple compounds. Among the stimuli, one stimulus was conventionally perceived as unpleasant, another as pleasant, and three were stereotypically perceived as neutral. To enhance the generalizability of findings beyond specific odors, two distinct odor sets (A and B) were created and randomly assigned to participants. Both sets contained the five aforementioned valence profiles, albeit with different specific odors. 15 participants received odor stimuli from odor set A, while 14 participants received stimuli from odor set B (see Appendix B).

Table 1 provides a comprehensive list of the odors utilized in the study, along with their odor sets, respective valence profiles, dilution ratios, and conditioning outcomes (see 2.4.2.1. Trial Protocol for details of the study paradigm). The odors were diluted with propylene glycol. All neutral odors had a dilution ratio of 1:5, all positive odors had a dilution ratio of 1:10, the fish sauce had a ratio of 1:10, and ammonium sulfate had a ratio of 1:100. This was done to ensure that all odors had similar perceived intensities regardless of their perceived valence. Additionally, the dilution ensured that the odors

could be presented repeatedly during fMRI scanning without becoming overwhelming for participants. The dilution process was overseen by Divesh Thaploo from the Smell and Taste Clinic at the Dresden University of Technology. Mr. Thaploo selected and prepared the odors and conducted a pilot study to confirm their similarly perceived intensity levels.

Table 2. Olfactory stimuli used in the experiment. Two odor sets were generated (A, B) to generalize the findings beyond the specific odors utilized in the study. Each set contained one stereotypically negatively perceived odor, one stereotypically positively perceived odor, and three conventionally neutral odors. All odors were perfume-based (Takasago Europe Perfumery Laboratory S.A.R.L) and were diluted with propylene glycol. During the fMRI scanning procedure, one neutral odor (from each odor set) was paired with an appetitive conditioning outcome (CS+ appetitive), one neutral odor was paired with an aversive conditioning outcome (CS+ aversive), while one neutral odor served as a control (CS-).

| Odor Set | Odor | Stereotypical valence | Dilution ratio | Conditioning Outcome |
|----------|-------------------------------------|-----------------------|----------------|----------------------|
| A | Fish Sauce (commercially available) | Negative | 1:10 | |
| | Orange (D-Limonene) | Positive | 1:10 | |
| | Musk | Neutral | 1:5 | CS+ appetitive |
| | Benzoyl | Neutral | 1:5 | CS+ aversive |
| | Basil | Neutral | 1:5 | CS- |
| B | Rotten Egg (Ammonium Sulphate) | Negative | 1:100 | |
| | Jasmin | Positive | 1:10 | |
| | Potato Chips | Neutral | 1:5 | CS+ appetitive |
| | Karmaflor | Neutral | 1:5 | CS+ aversive |
| | Vanillin | Neutral | 1:5 | CS- |

2.3.2 Visual Stimuli

During fMRI scanning, participants received visual instructions and were presented with images indicating monetary gain or loss. These stimuli were utilized to induce appetitive and aversive learning effects when paired with neutral odors. Figure 14B depicts the visual stimuli presented to the participants, including instructions regarding odor presentation (“sniffing”) and rating (refer to 2.4.2.1 Trial Protocol for details). Figure 14C describes the conditioning outcomes. An image of a one-euro coin used in the study was downloaded from Pixabay (pixabay.com).

2.4 Procedure

The study comprised both behavioral and fMRI experiments, as depicted in Figure 14A. The procedure commenced with the behavioral experiment, which encompassed odor set selection and the Sniffin' Sticks test to evaluate smell normality and odor rating. Subsequently, the fMRI experiment, included three phases (reference, conditioning, and extinction runs). The study concluded with another behavioral experiment involving odor rating. Additional information on each experiment is provided in sections 2.4.1 (Behavioral Experiment) and 2.4.2 (Neuroimaging Experiment).

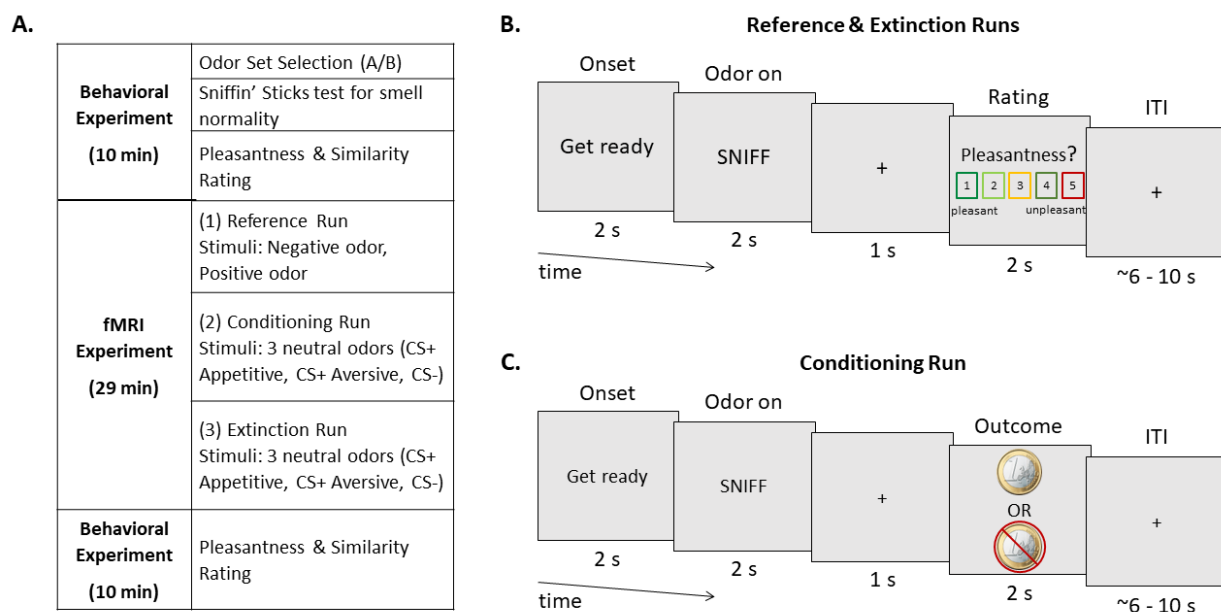


Figure 14. Experimental procedure and trial design. (A) The study comprised two behavioral and one fMRI experiment. (B) Trial design for the reference and extinction phase: Participants were cued for an upcoming odor presentation (“Get ready”), during which they were instructed to sniff (“SNIFF”), followed by an odor rating cue (5-point Likert scale indicating the odor valence from 1, pleasant, to 5, unpleasant). Responses were collected using an fMRI-compatible button box. The trial concluded with a temporally jittered intertrial interval. (C) Trial design of the conditioning phase: Participants were cued to prepare (“Get ready”) and sniff (“SNIFF”), while one of the neutral odors (CS+ appetitive, CS+ aversive, or CS-) was presented. Following a brief interlude (fixation cross), participants observed either a conditioning outcome (picture of a euro systematically linked for CS+ appetitive odor or crossed out euro systematically linked for CS+ aversive odor) or a fixation cross (depicting no conditioning outcome for CS- odor). The conditioning outcome was followed by temporally jittered ITI.

2.4.1 Behavioral Experiment

2.4.1.1 Sniffin' Sticks: Odor Identification Test

To assess participants' olfactory performance, a forced-choice olfactory test was conducted using the Sniffin' Sticks test kit “Identification Test 16, Blue” (Burghardt®,

Wedel, Germany; Hummel et al., 1997). The test comprises 16 common odors, each embedded in numbered markers (e.g., orange, shoe leather, turpentine; the complete list can be found in Appendix C). The participants were instructed to smell the markers in a birhinal manner and identify the correct odor from the four alternatives provided. A score below 10 indicates a diminished ability to identify odors, while a score above indicates normal olfactory function (MediSense®, 2019). To avoid olfactory desensitization, each marker was presented only once for a few seconds, followed by an interval of 20-30 seconds before the exposure to the next marker (Rumeau et al., 2016). All participants completed the test within two months after participating in the study (due to a delay in the test postal delivery).

2.4.1.2 Pleasantness Rating

Participants were tasked with evaluating the pleasantness of the five odors presented to them during scanning. This rating procedure was performed once before and once after the fMRI experiment outside of the scanner (Figure 14A). Odors were presented to the participants in random order and without odor-identifying labels in glass vials. Pleasantness was evaluated on a Likert scale from 0 (most disliked sensation imaginable) to 10 (most liked sensation imaginable). Each of the five odors was rated twice in each rating session, resulting in a total of 20 pleasantness ratings. The repeated rating was done to ensure consistent ratings within a subject.

2.4.2 Neuroimaging Experiment

2.4.2.1 Trial Protocol

In this study an event-related design was employed, resembling the approach described by Howard et al. (2016). The neuroimaging experiment comprised three distinct phases: reference, conditioning, and extinction.

Phase 1: Reference Run

During the reference phase, participants were presented with two odors: one with extremely positive valence and one with extremely negative valence. The purpose was to obtain neuronal reference points of the participants' states of "negativity" and "positivity". 14 trials were acquired with each stimulus. Each trial (Figure 14B) contained a 2-second

preparation cue (“Get ready” text displayed on the screen), a 2-second “SNIFF” cue (odor stimulation was turned on), a 1-second pause (a black fixation cross presented on the screen), and a 2-second rating cue. During the rating cue, the participants were asked to rate the odor valence using a five-point Likert scale. Responses to the odor rating were captured using an MR-compatible button box (Psychology Software Tools, Sharpsburg, PA, United States), attached to the participants’ right hands. Each trial lasted 7 seconds, followed by a temporally jittered intertrial interval (ITI) of 6–10 seconds, during which a fixation cross was displayed on the screen. All runs began with a 16-second fixation period to allow for T1 saturation, indicated by a fixation cross on the screen and concluded with a 1-second fixation period to accommodate the slow decrease of the hemodynamic response function. The exact duration of the run depended on the ITI periods, with the reference run averaging 7 minutes and 16 seconds.

Phase 2: Conditioning Run

During the conditioning phase, participants were presented with three neutral odors. The trial design mirrored the timing of the reference phase, providing 14 trials per odor and yielding an average run time of 10 minutes and 46 seconds. However, in the conditioning phase, the 2-second rating cue was omitted and replaced with an unconditioned stimulus (US): a picture of a one-euro coin or a crossed-out one-euro coin, depicting either a monetary gain or monetary loss, respectively (Figure 14C). One of the neutral odors was systematically paired with a monetary gain (conditioned stimulus; CS+ appetitive), another with monetary loss (CS+ aversive), while the third neutral odor had no pairing with the US (CS-). The USs were paired with a partial reinforcement rate of 50% (Lonsdorf et al., 2017), and in their absence, a fixation cross was shown instead. Participants were instructed to pay attention to the pairing of monetary gain and loss with the odors, as the monetary outcomes might be systematically linked to certain odors. They were also motivated by the knowledge that they would earn each Euro and lose each crossed-out Euro they saw. The conditioning phase aimed to alter the odor similarity, ensuring that post-conditioning, two conditioned (neutral) odors would be distinguishable from each other, as well as from the neutral control (CS-).

Phase 3: Extinction Run

During the extinction phase, the trial design was identical to that of the reference phase (Figure 14B), wherein participants rated the valence of the odors during the rating cue. However, the stimuli used in the extinction phase differed. In this phase, the three neutral odors, two of which had undergone conditioning, were employed (providing 14 trials per odor and yielding an average run time of 10 minutes and 46 seconds). The total duration of the neuroimaging experiment was approximately 29 minutes, encompassing anatomical and field map scans. Between reference and conditioning runs, a brief pause in the scanning occurred due to the change of odor stimuli and their respective tubing.

2.5 Data Analysis

2.5.1 Behavioral Data

2.5.1.1 Sniffin' Sticks: Threshold for Normal Olfactory Function

Among the 16 odors included in the Sniffin' Sticks test for normal olfactory function ("Identification Test 16, Blue"; Burghardt®, Wedel, Germany; Hummel et al., 1997), a correct identification score ranging from 10 to 16 signifies normal olfactory function (normosmia). Scores between 6 to 10 indicate a diminished ability to identify odors (hyposmia), while a score below 6 suggests either a complete or partial loss of ability to smell (anosmia; MediSense®, 2019). All participants recruited in the current study reached the normal criteria.

2.5.1.2 Pleasantness Rating: Comparable Odor Sets

To ensure the comparability of the two odor sets (A and B; see Table 2), we conducted an independent-sample t-test to compare the mean valence ratings of the negative, positive, and neutral odors in each odor set. The null hypothesis stated that there was no significant difference between the mean valence ratings of the two odor sets. Conversely, the alternative hypothesis described a significant difference between the mean valence ratings of the two sets.

2.5.2 Neuroimaging Data

2.5.2.1 Preprocessing

The neuroimaging data were organized according to the Brain Imaging Data Structure (BIDS; Gorgolewski et al., 2016) and were standardly preprocessed using fMRIPrep 20.2.1 (Esteban et al., 2019) software package based on the Nipype 1.5.1. framework (Gorgolewski et al., 2011). An automatically generated comprehensive summary of fMRIPrep's processing steps can be found in Appendix D.

The structural preprocessing performed by fMRIPrep included intensity non-uniformity correction (ANTs 2.3.3 N4BiasFieldCorrection algorithm), skull-stripping (Nipype's antsBrainExtraction workflow), brain tissue segmentation of cerebrospinal fluid (CSF), white-matter (WM) and gray matter (GM) (FSL 5.0.9 fsl_fast), brain surface reconstruction (FreeSurfer 6.0.1 recall), and spatial normalization (nonlinear alignment to ICBM 152 Nonlinear Asymmetrical template version 2009c; ANTs 2.3.3 antsRegistration).

The functional data were preprocessed using fMRIPrep, which accounted for susceptibility distortion correction using field maps acquired after each run (SDCFlows workflow, FSL fugue), co-registration (Freesurfer bbregister; boundary-based registration with six degrees of freedom), motion correction (transformation matrices, six rotation, and translation head-motion parameters; FLS mcflirt), and slice-timing correction (AFNI 20160207 3dTshift). BOLD time-series were resampled to native space and further to standard space (Montreal Neurological Institute; MNI152NLin2009cAsym) in a single interpolation step with all pertinent transformations, including volumetric resampling (ANTs antsApplyTransforms) and surface resampling (FreeSurfer's mri_vol2surf). The data underwent high-pass filtering using a discrete cosine filter with 128s cut-off, and a confound signal estimation was performed (using CSF, WM, and GM mean series and a set of principal component analysis-derived CompCor physiological regressors for component-based noise correction). No spatial smoothing was applied.

For each run, a general linear model (GLM) analysis was applied to the time-course data of each voxel, including predictors for all olfactory conditions and trials, as well as 24 motion correction parameters within each run (NLTools version 0.4.2). These motion

covariates included the standard three rotations, three translations, and their quadratic, derivative, and square of derivative versions. This approach accounts for the potential nonlinear relationship between motion and signal intensity. Additional regressors were incorporated to capture these nonlinear changes resulting from motion (Chang, 2021). To obtain beta values for each olfactory condition, all predictors with a double gamma hemodynamic response function were convoluted for each voxel and each participant.

2.5.2.2 Univariate Analysis

As a “sanity test” and to ensure data quality for subsequent multivariate analyses, two whole-brain massive univariate analyses were conducted. Firstly, the aim was to identify brain regions capable of negative odors from positive odors (2.5.2.2.1.). Secondly, an investigation was conducted to determine whether brain regions previously linked to conditioning (e.g., ventromedial prefrontal cortex, cingulate cortex, insula, amygdala, OFC, supplementary motor area, VS; Bissonette et al., 2014; Hayes et al., 2014; Pessiglione & Delgado, 2015) appeared in our data (2.5.2.2.2.). The univariate analyses were performed using a two-stage summary statistic approach. First-level models were estimated for each participant separately, and the resulting beta values were combined at the second level.

2.5.2.2.1 Brain Regions Which Distinguish Negative & Positive Odors

To investigate which regions can distinguish negative odors from positive odors, we performed a first-level analysis separately for each participant using GLM (NLTools toolbox version 0.4.2. on Python) with a design matrix that included two regressors of interest: negative odors and positive odors. Each odor condition was modeled as an event with a duration of 2 seconds. To address nuisance variables, six head motion parameters were included as regressors of no interest, as well as their quadratic, derivative, and square of derivative versions. The data were high-pass filtered (128 seconds) to remove low-frequency noise. Additionally, an intercept term was included to account for effects that were unrelated to specific odors being presented. The data were smoothed with a 6mm 3-D Gaussian kernel with a full-width half maximum (FWHM).

At the second level, a contrast of interest between negative odors and positive odors [1,1] was created. One-sample t-test was performed on the contrast to identify brain regions

that consistently exhibit differences in response to odors across participants at the group level. False Discovery Rate (FDR) correction ($q < 0.05$) was used to control for multiple comparisons and to determine significant activations. The statistical parameter map was overlaid on the Montreal Neurological Institute (MNI152NLin2009cAsym template) standard brain template.

The analysis was repeated separately for each odor set given the potential for different performance between sets. Additionally, we conducted the analysis in a ROI, to increase power by restricting the sample space into regions most likely to respond to valence differences. The ROI mask was generated from NeuroSynth with the term “valence” (Figure 15; Yarkoni et al., 2011). NeuroSynth employs a vast database of published neuroimaging studies to perform meta-analyses and identify commonly activated regions associated with specific terms. The mask generated with the term “valence” included data from 361 studies.

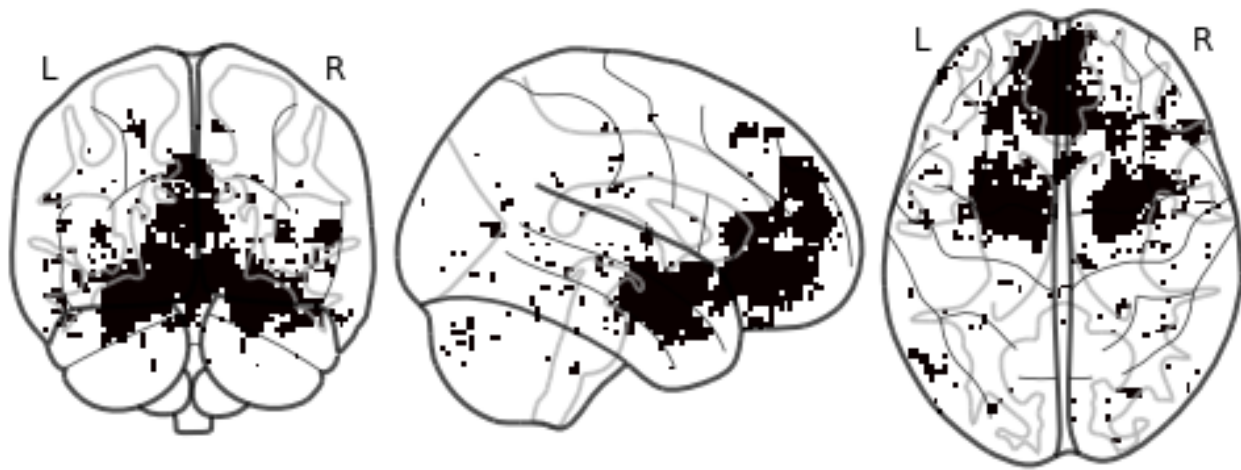


Figure 15. A region of interest mask plotted on a glass brain. The ROI mask was generated using data published in NeuroSynth (Yarkoni et al., 2011) with brain regions commonly associated with the term “valence”. The mask was used to define ROIs in a massive univariate analysis, aimed at identifying brain regions that consistently exhibit differences in response to negative and positive odors.

2.5.2.2.2 Brain Regions Activated by Conditioning

With the second whole-brain univariate analysis, the effect of conditioning on the data was investigated. For each participant, a GLM was used, incorporating regressors of interest (CS+ appetitive, CS+ aversive, and CS-) and nuisance regressors to account for motion and other sources of noise. The resulting beta values for each odor condition were passed

to second-level analysis. A contrast was constructed contrasting CS+ appetitive and CS+ aversive against unconditioned neutral odor CS- $[-0.5, -0.5, 1]$. A one-sample t-test was subsequently conducted on the contrast to identify brain regions consistently active in response to conditioning across participants. FDR correction was applied to control for multiple comparisons. The statistical parameter map was overlaid on the standard brain template (MNI152NLin2009cAsym template).

We repeated the analysis within a ROI, using a mask generated from NeuroSynth with the term “conditioning” (Figure 16; Yarkoni et al., 2011). This mask generated with the term included data from 160 studies.

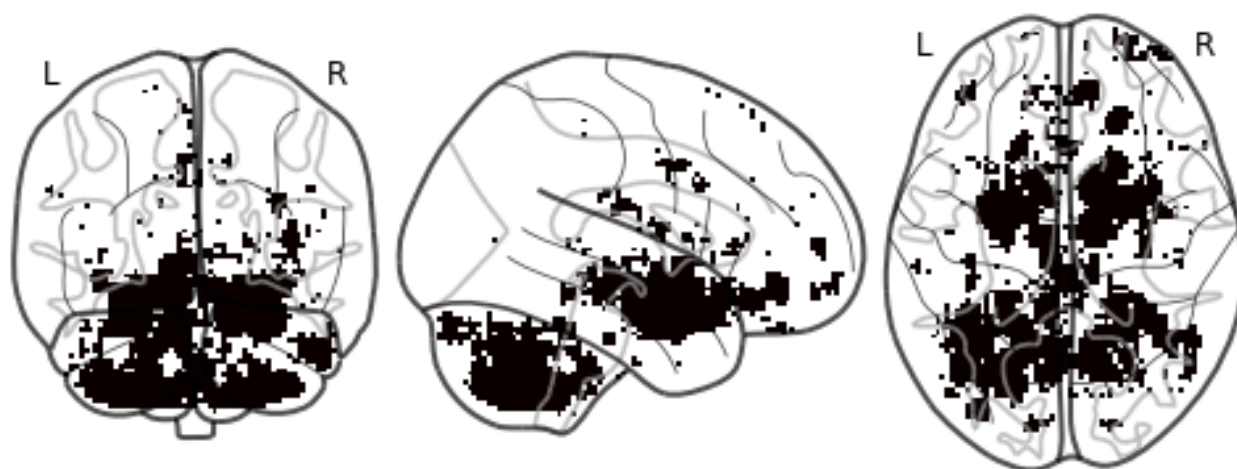


Figure 16. A region of interest mask plotted on a glass brain. The ROI mask was created using data published in NeuroSynth (Yarkoni et al., 2011), which identified brain regions commonly associated with the term “conditioning”. The mask was used to define ROIs in a massive univariate analysis, aimed at identifying brain regions that consistently exhibit differences in response to conditioning.

2.5.2.3 Multivariate Pattern Analysis

A more sophisticated data analysis was conducted using MVPA (Haxby et al., 2001) via whole-brain searchlight analysis (Kriegeskorte et al., 2006) in CoSMoMVPA toolbox (Oosterhof et al., 2016) for MATLAB (R2019b; The Mathworks, MA, United States). Specifically, two main flavors of MVPA were utilized: a classification scheme with machine learning (2.5.2.3.1.) and a correlation scheme using representational similarity analysis (RSA; 2.5.2.3.2.; Kriegeskorte, 2008). Unless mentioned otherwise, the following analysis steps were performed using CoSMoMVPA.

2.5.2.3.1 *Classification Analysis*

The classification analysis followed the cross-decoding scheme described by Levine et al. (2018). Briefly, this analysis aimed to train a support vector machine (SVM) classification algorithm to distinguish the neural representations of negative and positive odors. Subsequently, the classifier was tested on the representations of the three neutral odors (CS+ appetitive, CS+ aversive, CS-) to see if the representations of the conditioned odors became more similar to those of the stereotypically negative and positive stimuli. Thus, classification analysis aims to predict (or classify) which categories or conditions correspond to which observations (Weaverdyck et al., 2020). In comparison to the conventional univariate analyses, where $P(\text{brain}|\text{condition})$, the direction of inference is reversed in decoding analyses, $P(\text{condition}|\text{brain})$. The steps of this analysis are described in more detail below.

Data Requirements

Within the first-level analysis, we generated unsmoothed (FWHM = 0) single-trial estimates (t-maps) for each subject using GLM (NLTools toolbox version 0.4.2 on Python), yielding one map per participant per condition (odor). Each map contained data from 14 trials. The conditions were (1) negative odor (reference run), (2) positive odor (reference run), (3) CS+ appetitive odor (conditioning run), (4) CS+ aversive odor (conditioning run), (5) CS- odor (conditioning run), (6) CS+ appetitive odor (extinction run), (7) CS+ aversive odor (extinction run), and (8) CS- odor (extinction run; Figure 14A).

Step 1: Within-Subject Cross-Validation

Individually for each participant and utilizing t-maps from the reference run, a searchlight-based SVM classifier (spherical searchlight with a radius of 1 voxel; 9 mm; Weaverdyck, 2020) was trained to identify regions in the brain where representations of negative and positive odors could be distinguished. This process entailed leave-one-trial-out cross-validation within the subject; the classifier was trained to discriminate between 13 negative and 13 positive trials and was tested on the remaining 14th trial in each category (Figure 17A). This procedure was repeated so that each trial acted once as a testing sample. The resulting accuracy values were averaged across all folds for a given voxel (center voxel of the searchlight sphere), indicating the likelihood that the SVM classified the test sample

correctly. Finally, these within-subject results (classification accuracy maps) were aggregated and combined into group data for further statistical analysis (Figure 17B).

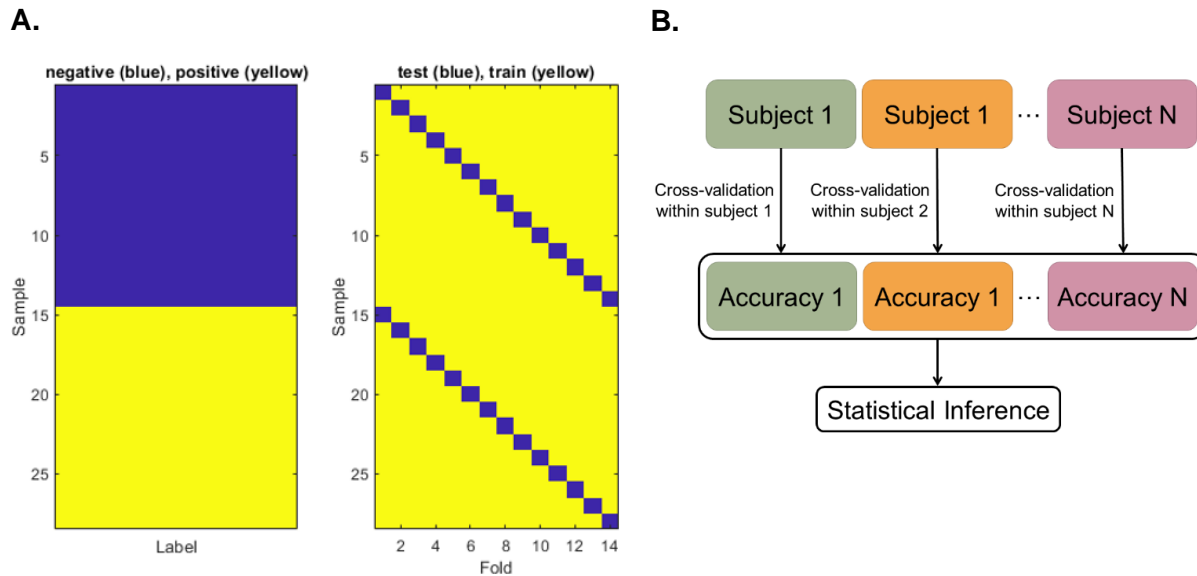


Figure 17. Within subject leave-one-trial-out cross-validation scheme in the MVPA classification analysis. (A) Right: The data submitted into the SVM classification analysis contained 14 samples (i.e., trials) for each label (i.e., odor condition: negative (blue) and positive odors (yellow)) for each participant. Left: For a given participant, the data was divided into training (yellow) and testing (blue) sets. The classifier was then trained to discriminate between 13 negative trials and 13 positive trials and was subsequently tested on the remaining 14th trial in each category. (B) Illustration of the hierarchical group-level multivariate classification. Cross-validation is performed within subjects, where a classifier was trained using the training data, and its ability to generalize into new data is evaluated on the test set by measuring classification accuracy. These accuracy maps were stacked across subjects to generate group-level data, which was then subjected to statistical inference. Adapted from Wang et al. (2020).

Step 2: Group Analysis to Generate an ROI

To evaluate regions demonstrating significant classification performance, group-level accuracy maps underwent a Monte Carlo permutation test, as implemented in the CoSMoMVPA toolbox (using default parameters: $dh = 0.1$, 10 000 iterations; Poldrack et al., 2011, p. 172). This procedure entailed a one-sample t-test against chance (i.e., 0.5, given that there were two conditions) and multiple comparisons correction using the Threshold-Free Cluster Enhancement method (TFCE; Smith & Nichols, 2009). The resulting statistical map was adjusted to a corrected cluster threshold of $p = 0.05$. Voxels surpassing the corresponding z-score of 1.64 (one-tailed, as we are only interested in positive values) were then masked as an ROI, indicating the regions where the representations of negative and positive odors could be differentiated. The ROI was subsequently utilized in the third step of the analysis, cross-decoding.

Step 3: Cross-Decoding Neutral Odors in an ROI

In the final step, the SVM classifier was retrained to differentiate between the neural patterns associated with positive and negative odors within the ROI generated in step two. Subsequently, it was examined whether the classifier would label the t-maps from the conditioning run (CS+ aversive odor, CS+ appetitive odor, and CS- odor) as “negative” or “positive”, indicating a shift in the similarity of neural representation.

Afterward, the data was split into training (negative and positive odors) and testing sets (three neutral odors from the conditioning run). If conditioning changes, or generalizes, the neural representation of neutral odors to become more similar to those of negative and positive valence, the analysis should yield results as shown in the confusion matrix in Figure 18 left. The confusion matrix provides a summary of the performance of a classification algorithm by illustrating the relationship between the actual true values of the data and the values predicted by the classifier.

Step 4: Statistical Inference

A chi-squared (χ^2) goodness-of-fit statistical test was utilized to evaluate the significance of the classification results – i.e., how the actual observed data compared to a chance-level performance (Figure 18 right; Johnson & Bhattacharyya, 2019, pp. 555-556). The goodness-of-fit test compared the observed frequencies of the predicted labels with the expected frequencies under the null hypothesis of chance-level classification.

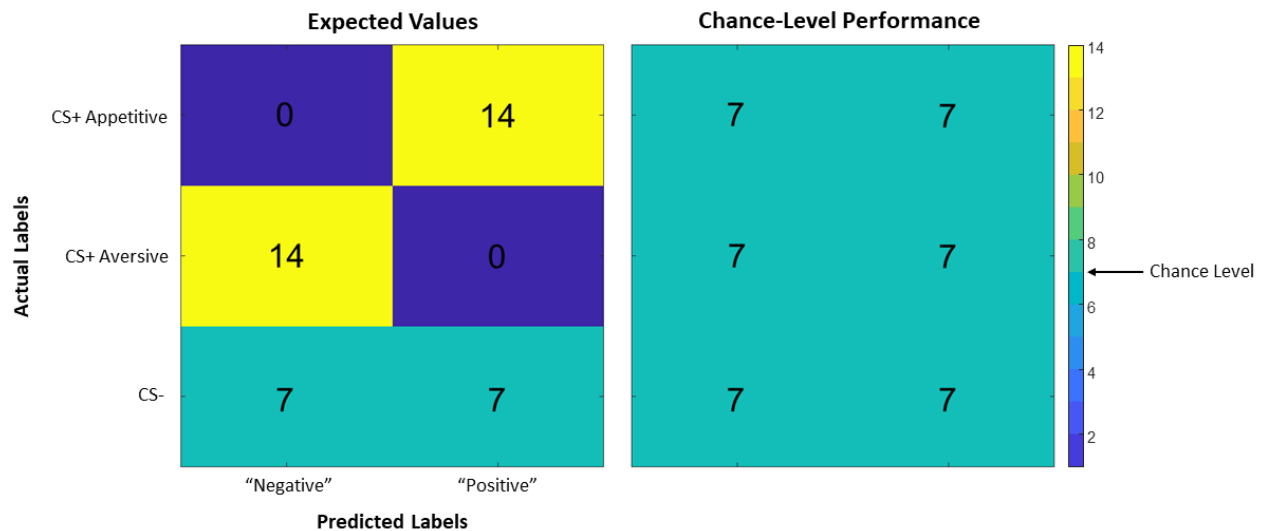


Figure 18. The expected and the chance-level classification results from the conditioning run. Left: The expected classification results shown as a confusion matrix when a classifier was trained on the reference run data (negative odor vs positive odor) and tested on the conditioning run data (CS+ appetitive odor, CS+ aversive odor, and CS- odor) in an ROI. The actual labels of the data are shown on the left, and the predicted labels are shown at the bottom. Since there were 14 trials per odor condition, the chance-level is at 7. Assuming that conditioning alters, or generalizes, the neural representation of neutral odors to become more similar to those of negative and positive valence, we would expect the CS+ appetitive odor to be classified as “positive” (with 14 trials vs 0 trials classified as “negative”), CS+ aversive odor to be classified as “negative”, and CS- odor to be classified at chance level. Right: If the classifier performs at chance level, the confusion matrix would comprise 7/7 values throughout.

A chi-square statistic was calculated by summing the squared differences between the observed and expected (Figure 18 left) values, divided by the expected values, cell-by-cell of the confusion matrix ($\chi^2 = \sum (\text{observed} - \text{expected})^2 / \text{expected}$). Degrees of freedom were calculated as the number of categories minus one. In this case, only CS+ appetitive and CS+ aversive were included in the calculations (omitting CS-, which was expected to perform at chance level), so the degrees of freedom were one. If the p -value was less than the significance level (0.05), the null hypothesis was rejected and a significant difference between the observed and expected (chance-level) values concluded. A significant chi-square value indicated that the classification accuracy was higher than chance.

Proof-of-Concept

Besides the conditioning run, the classification performance was further assessed using the data from the reference and extinction runs as a proof-of-concept. In the ROI, the classifier was trained and tested on the reference run data, with the expected classification results shown as a confusion matrix on the left of Figure 19. The observed values were

subjected to a chi-squared goodness-of-fit test as described above, comparing them to chance-level performance (Figure 19 right). For the extinction run, the classifier was trained on the data from the reference run and tested on the data from the extinction run. The results were expected to be at a chance-level (Figure 18 right), assuming that the effect of conditioning had ceased.

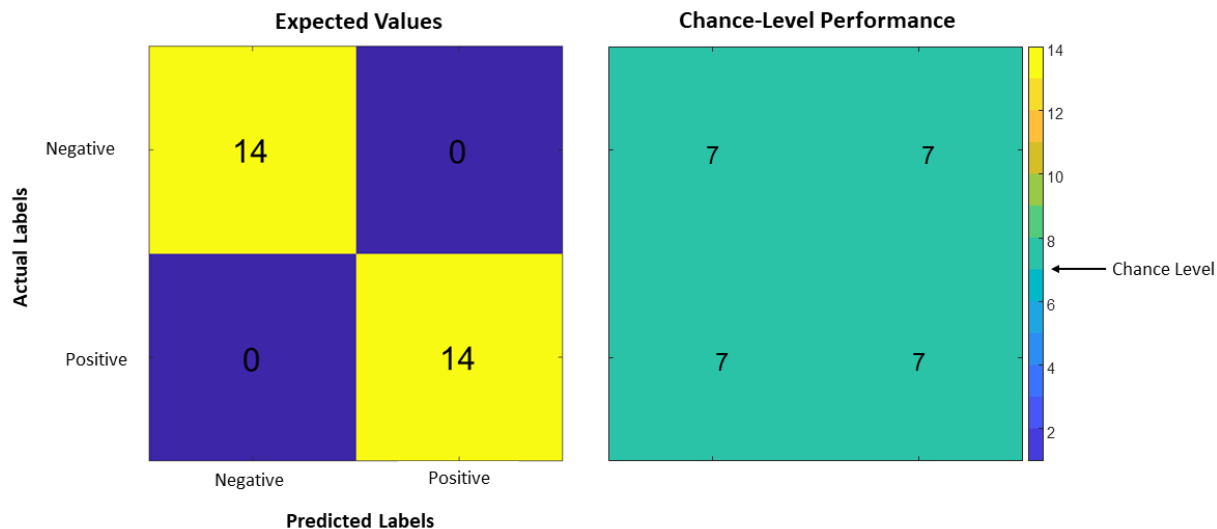


Figure 19. The expected and the chance-level classification results from the reference run. Left: The expected classification results shown as a confusion matrix when a classifier was trained and tested on the reference run data (negative odor vs positive odor) in an ROI. The actual labels of the data are shown on the left, and the predicted labels are shown at the bottom. Since there were 14 trials per odor condition, the chance-level is at 7. Assuming that the data is classified perfectly, all 14 trials of negative and positive odors would be classified correctly as negative and positive, respectively. Right: If the classifier performs at chance-level, the confusion matrix would yield 7/7 values throughout.

2.5.2.3.2 Representational Similarity Analysis

Compared to classification-based MVPA, RSA (Kriegeskorte, 2008) aims to examine the relative similarity structure of neural response patterns across stimulus categories or brain regions, rather than directly decoding the different stimulus categories from the patterns (Weaverdyck et al., 2020). These spatial activity patterns can be compared across conditions in terms of similarity (e.g., via Pearson’s correlation coefficient, r) or dissimilarity (via correlation distance metric, $1 - r$). To accomplish this, a whole-brain RSA searchlight analysis was conducted for each participant by correlating their neural data with a theoretically driven model. Analysis steps are outlined below.

Data Requirements

In the first-level analysis, we generated unsmoothed (FWHM = 0) single-trial estimates (beta-maps) for each subject using GLM (NLTools toolbox version 0.4.2 on Python).

14 trials for a given participant, run, and condition (odor) were acquired, which corresponded to 14 beta values per voxel. To increase the power of the data, these beta values were averaged across trials (Popal et al., 2019), resulting in one sample per condition for each participant. The conditions were (1) negative odor (reference run), (2) positive odor (reference run), (3) CS+ appetitive odor (conditioning run), (4) CS+ aversive odor (conditioning run), (5) CS- odor (conditioning run), (6) CS+ appetitive odor (extinction run), (7) CS+ aversive odor (extinction run), and (8) CS- odor (extinction run; Figure 20). Additionally, the beta values from CS- odor across the condition and extinction runs were averaged together.

Using beta values in RSA, in contrast to t-maps in the classification analysis, provides a direct measure of the relationship between experimental conditions and the neural response patterns (% signal change; Misaki et al., 2010). This measure is more suitable for the examination of the similarity structures of patterns themselves. Conversely, t-maps, which are produced by dividing the beta estimate by its standard error estimate for each voxel, are found to be advantageous in classification (i.e., decoding) tasks as they reflect the statistical significance of a particular activation and can identify regions significantly activated by a given condition.

Step 1: Constructing Representational Dissimilarity Matrices

For a given searchlight sphere (containing 100 voxels on average), we obtained the mean beta values for each odor condition to capture its local multivariate activation pattern. These beta values were demeaned by subtracting the mean beta value from each individual voxel to remove the common activity pattern and bring its overall mean to zero (Diedrichsen & Kriegeskorte, 2017). To produce a representational dissimilarity matrix (RDM) for each searchlight sphere and participant, the patterns from each odor condition were further correlated with each other, resulting in a symmetrical matrix along its diagonal (Figure 20; Popal et al., 2019). The RDM captured the dissimilarity between multivoxel activation patterns in response to different stimuli and was used to compare neural representations across conditions.

Step 2: Comparing the RDMs

To explore whether aversive and appetitive conditioning can alter the representation of neutral odors to align more closely with stereotypically negative and positive valence, respectively, RSA offers two methodological approaches: multiple model RDMs or a single model RDM. Each approach is explained in detail below (steps 2A and 2B).

With the first approach, we aimed to identify common brain regions where the effect of conditioning and extinction on neutral odors occurs by correlating the participants' neural RDMs with model RDMs of conditioning (Figure 20A) and extinction (Figure 20B). These results, comprising two correlation maps per participant, are then summarized using minimal t-conjunction. Alternatively, the second approach involves constructing a single model RDM that includes all conditions and encapsulates the hypothesized effect of both conditioning and extinction on neutral odors (Figure 21).

The main difference between these two approaches lies in the level of statistical threshold. The multiple model RDM approach employs minimal t-conjunction of the two correlation maps, allowing only those regions that show significant effects in both correlation maps to surpass the threshold. Consequently, this represents a more conservative approach necessitating the effects in both models. In contrast, the single model RDM approach employs a single correlation map per participant and may be a less strict technique.

Step 2A: Multiple Model RDM Approach

Each participant's neural RDM was separately correlated (using Spearman's rank correlation, ρ) with the model RDMs for conditioning and extinction (Figures 20A and 20B). The resulting correlation coefficients were centered for the central voxel of the searchlight sphere. The process was repeated for all voxels for a given participant. The resulting coefficient maps were normalized using Fisher's z-transformation. Next, for minimal t-conjunction, each voxel for a given participant was looped through and the smaller value from the two z-maps (conditioning and extinction) was selected. The resulting map was submitted to the second-level group analysis (step 3).

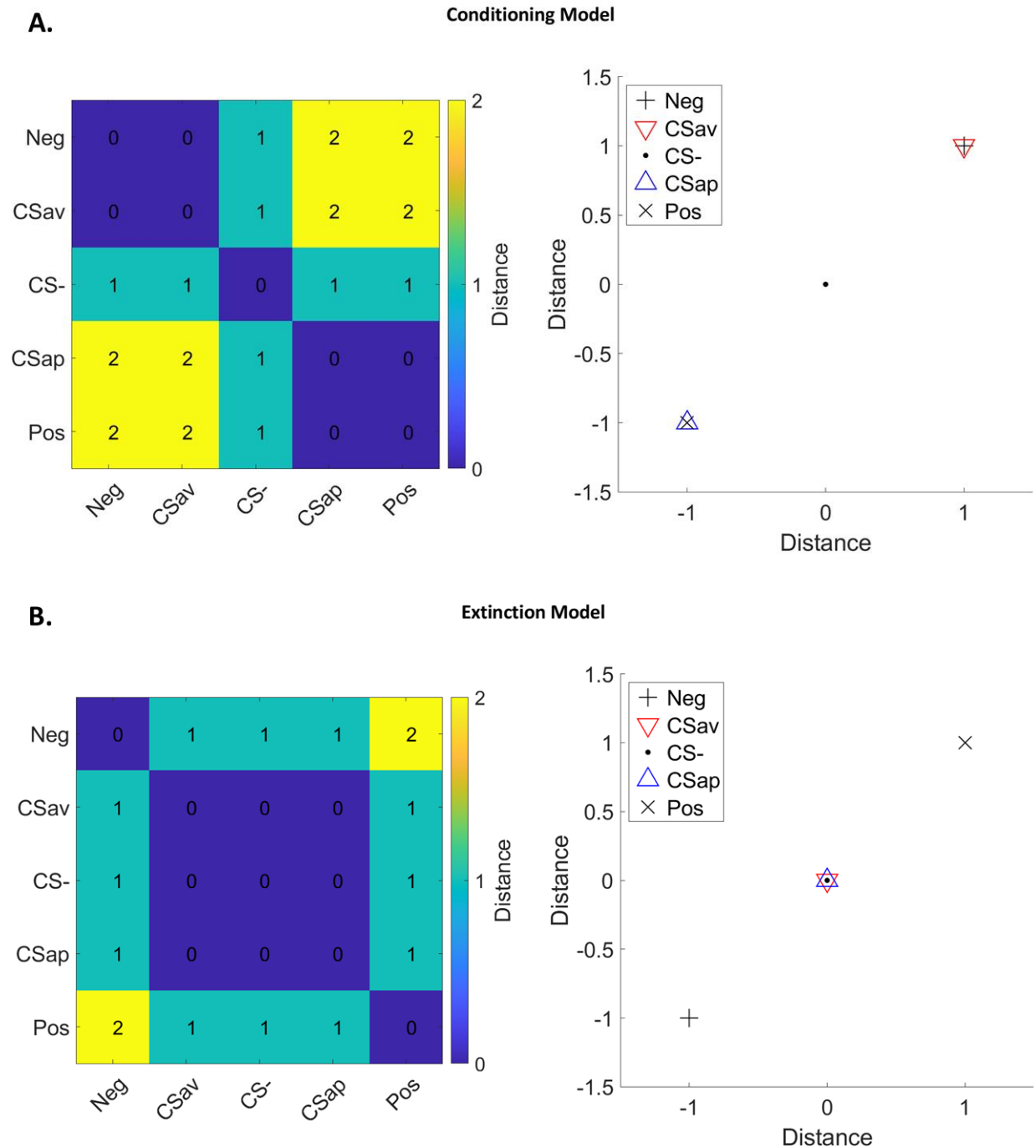


Figure 20. Model RDMs for RSA using multiple models. The RDM has a diagonal of zeros, expressing that a stimulus is identical when compared to itself (in contrast to a similarity matrix, which has a diagonal of ones). The RDM captures the dissimilarity between multivoxel activation patterns in response to different stimuli and is used to compare neural representations across conditions. (A) During a conditioning phase, it was hypothesized that the distance between negative and CS+ aversive (CSav in the figure), and positive and CS+ appetitive (CSap in the figure) is zero. Meanwhile, there is a large dissimilarity between these pairs of conditions. CS- holds a moderate dissimilarity to all other conditions. The RDM is visualized via multidimensional scaling on the right, where the x- and y-axes have arbitrary units. (B) During the extinction phase, it was hypothesized that the conditioning effect on the neutral odors (CSav, CS-, and CSap) has shifted and the distance between them is zero. Negative and positive odors have a high dissimilarity between each other and a moderate dissimilarity with neutral odors. The RDM is visualized via multidimensional scaling on the right, where the x- and y-axes have arbitrary units.

Step 2B: Single Model RDM Approach

For each participant, their neural RDM was correlated with the single model RDM using Spearman's rank correlation (ρ ; Figure 21). The correlation coefficient was centered for the central voxel of the searchlight sphere and the process was repeated for all voxels. The resulting coefficient map was normalized using Fisher's z-transformation before statistical testing (step 3).

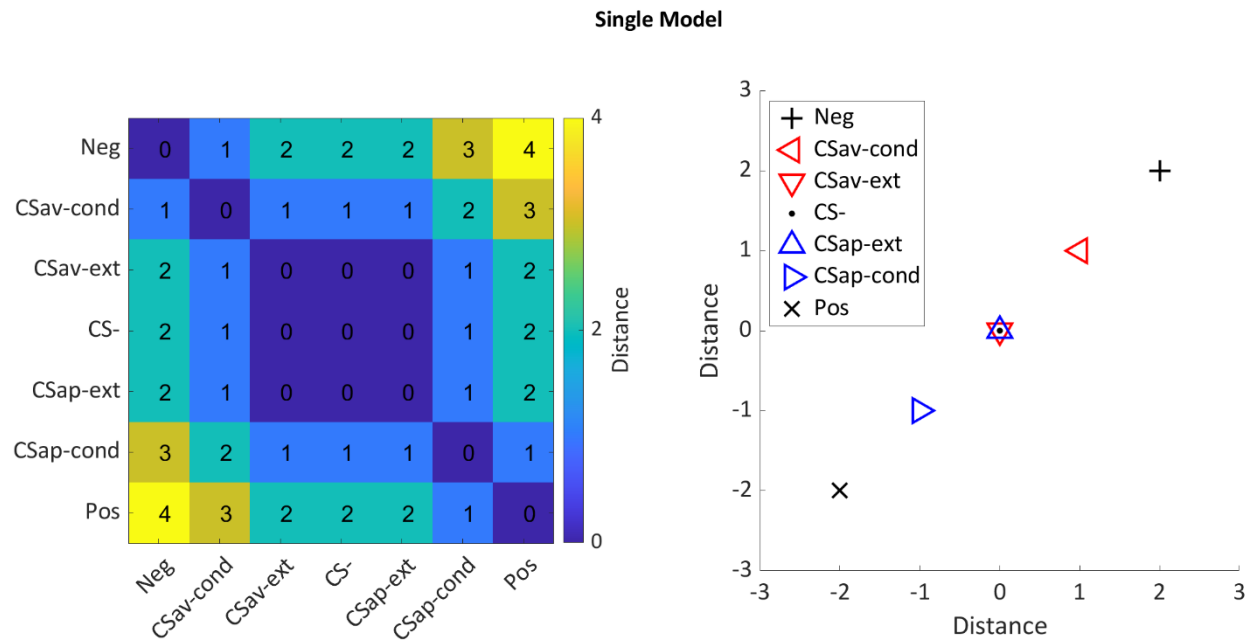


Figure 21. Model RDM for RSA using a single model approach. The RDM includes all experimental conditions and their hypothesized respective representational distances. The three neutral odors are similar to each other in extinction (CS+ aversive, labeled CSav-ext in the figure; CS-; and CS+ appetitive, labeled CSap-ext in the figure). During conditioning, the respective distances of the conditioned neural odors grew and approached negative and positive odors according to their conditioning schema (labeled CSav-cond and CSap-cond in the figure). Negative and positive odors hold the greatest distance. The RDM is visualized via multidimensional scaling on the right, where the x- and y-axes have arbitrary units.

Step 3: Statistical Inference at Group Level

The z-maps from all participants were stacked for a group level and entered into a one-sample t-test. The statistical maps were corrected for multiple comparisons with TFCE (Smith & Nichols, 2009) and a total of 10'000 Monte Carlo iterations were used with a corrected cluster threshold of $p = 0.05$. A grey matter mask was applied to restrict the results to relevant regions only.

3 RESULTS

3.1 Behavioral Experiment

3.1.1 Sniffin' Sticks

All participants scored above the threshold for diminished ability to identify odors (10 out of 16 smells), indicating a normal olfactory function (mean score (\pm std) = 13.4 (\pm 1.2); Figure 22; MediSense®, 2019).

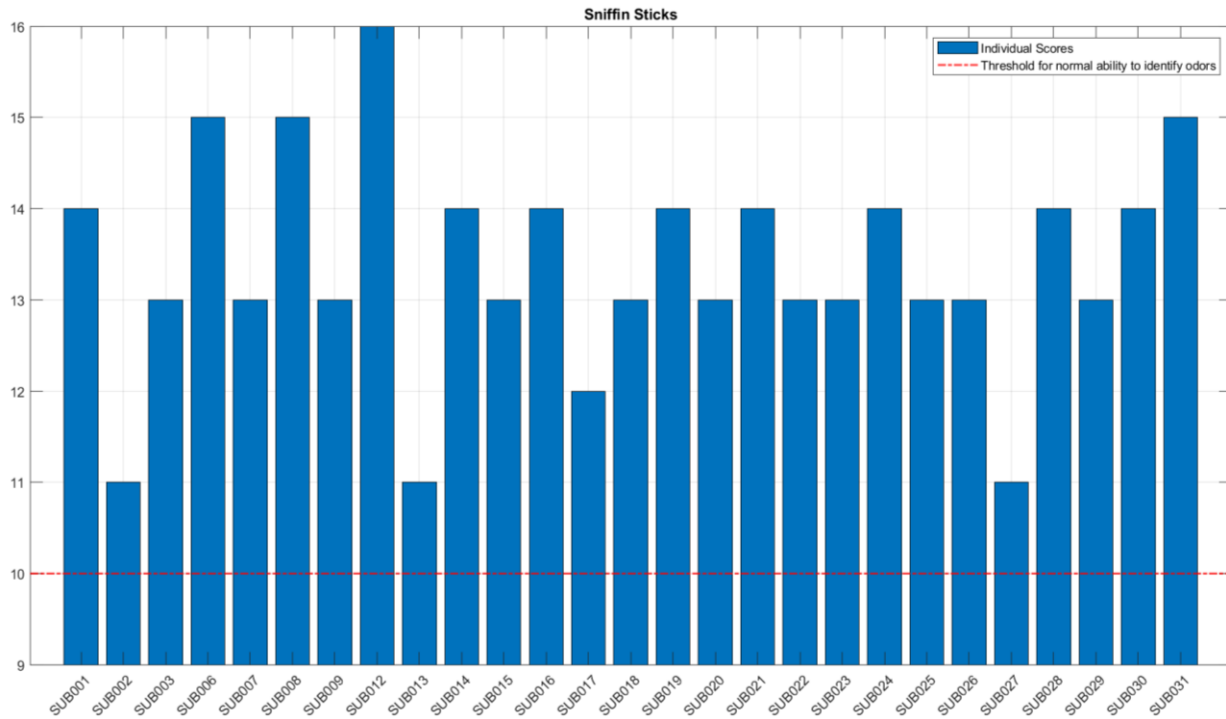


Figure 22. Sniffin' Sticks odor identification test results. All participants demonstrated normal olfactory function, scoring above the threshold for diminished odor identification ability (10 out of 16 odors; mean score (\pm std) = 13.4 (\pm 1.2)).

3.1.2 Odor Sets are Comparable in Terms of Their Valence Profiles

As a proof-of-concept for our decision to use two odor sets (A and B), we assessed their comparability (between odor sets) in terms of eliciting similar valence ratings (see scores in Appendix E). Valence ratings, acquired before and after the neuroimaging experiment (2.4.1.2. Pleasantness Rating), were submitted to an unpaired (independent) t-test. The results indicated no significant difference in the mean valence ratings between the two

odor sets ($t(288) = -0.03$, $p = 0.9726$). Thus, we concluded that the two stimuli sets were comparable for the purposes of this experiment.

3.1.3 Participants Score Negative & Positive Odors Inconsistently Across Odor Sets

When assessing scoring within each set, participants showed differences between negative and positive odors both *before and after* scanning in odor set A (Figure 23). Negative odor was rated with lower Likert scores, as expected, compared to positive odor (Figure 23 left panels).

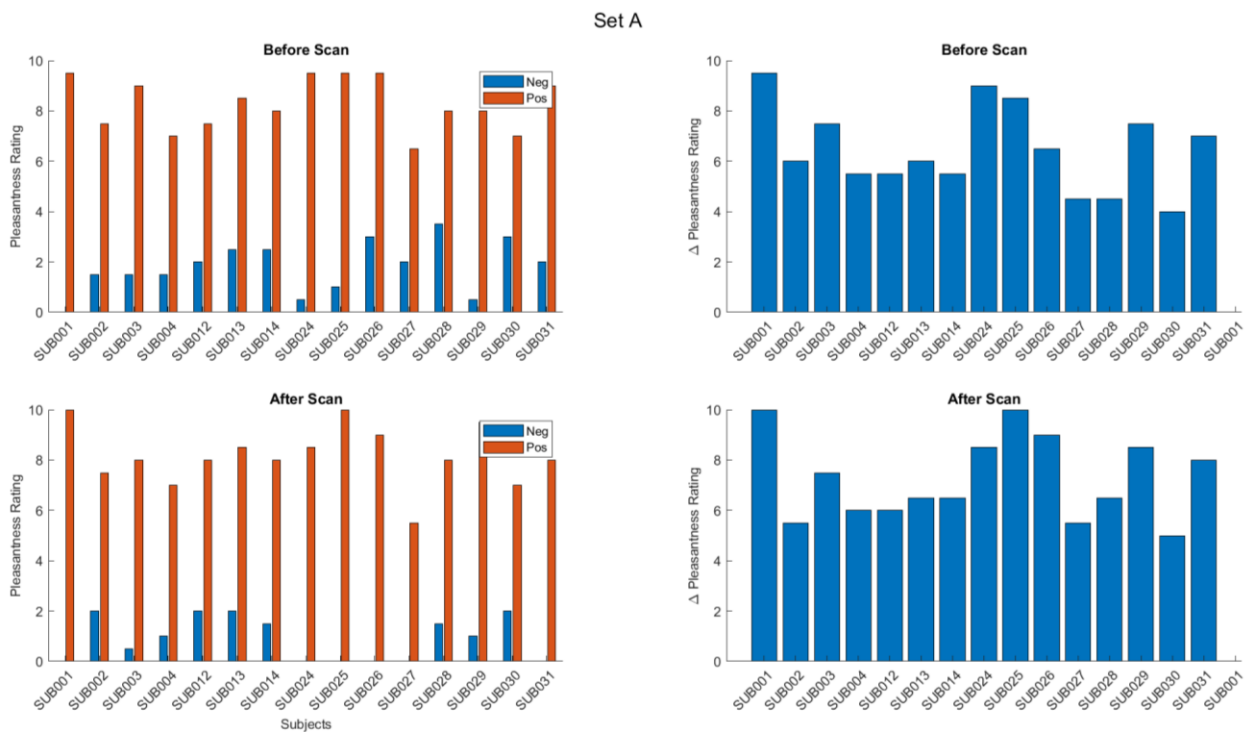


Figure 23. Valence scores (left panels) and their differences (right panels) for negative and positive odors for odor set A. Participants display differences between the valence scores, both before (top) and after (bottom) the scan, as indicated by the high deltas on the left panels.

However, this association was not observed in odor set B. Participants did not consistently display differences between the scores, neither before nor after the scan, as indicated by the inconsistent deltas in the right panels of Figure 24. Considering the high valence rating of the negative odor in set B compared to set A, it appears that the participants did not perceive the odor as negative as intended in the study design.

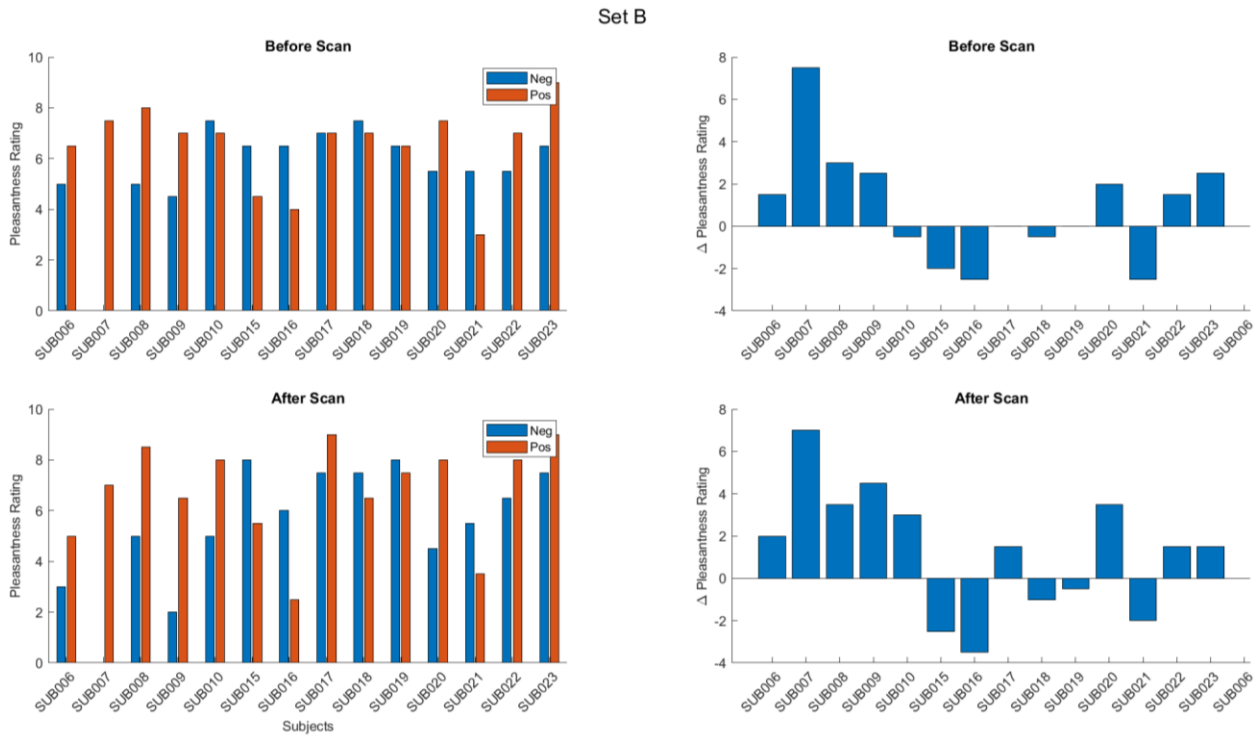


Figure 24. Valence scores (left panels) and their differences (right panels) for negative and positive odors for odor set B. Participants do not show consistent differences between the valence scores, neither before (top) nor after (bottom) the scan, indicated by the inconsistent deltas on the left panels.

Lastly, participants of set A tended to exhibit valence differences between negative and positive odors also *during the scan*, unlike those in set B, as indicated by the lower panel in Figure 25.

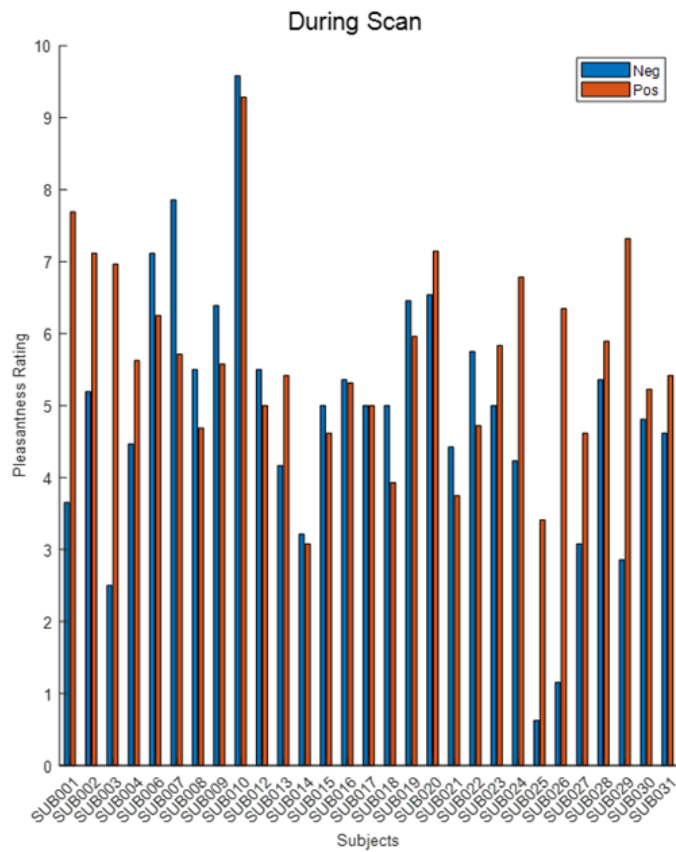
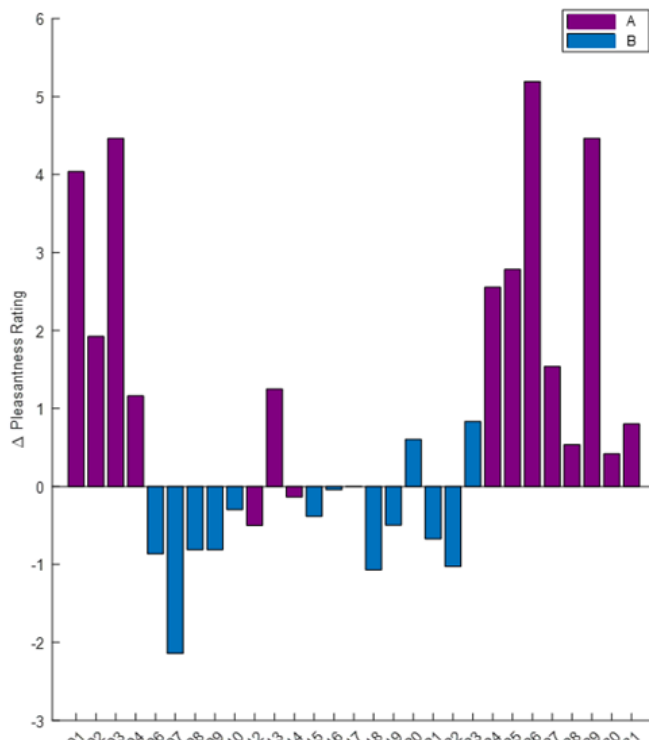


Figure 25. Valence scores and their differences for negative and positive odors during the scan for all subjects. The right panel indicates that subjects, who were presented with odor set A, tend to show differences in perceived pleasantness between the two odors, while subjects, presented with odor set B, do not.



3.1.4 No Expected Differences for Neutral Odors Before & After Conditioning

Neutral odors, conditioned as CS+ aversive and CS+ appetitive, do not exhibit the anticipated systematic differences *before* and *after* conditioning in either odor set (Figures 26-28). Specifically, the scores collected after the scanning would have been expected to decrease for CS+ aversive and increase for CS+ appetitive, compared to the neutral odor with no anticipated rating changes.

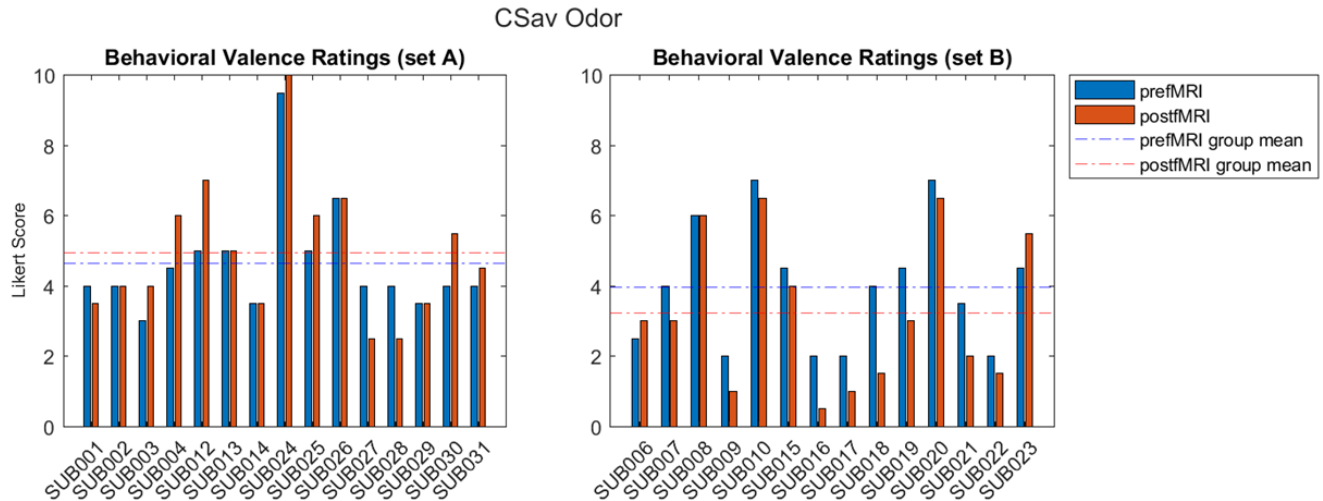


Figure 26. Likert scores of CS+ aversive odor for both odor sets. Behavioral scores collected before (blue) and after (red) scanning do not show directionally-expected systematic differences – i.e., after scanning, the scores would have been expected to decrease, due to conditioning with aversive pairing.

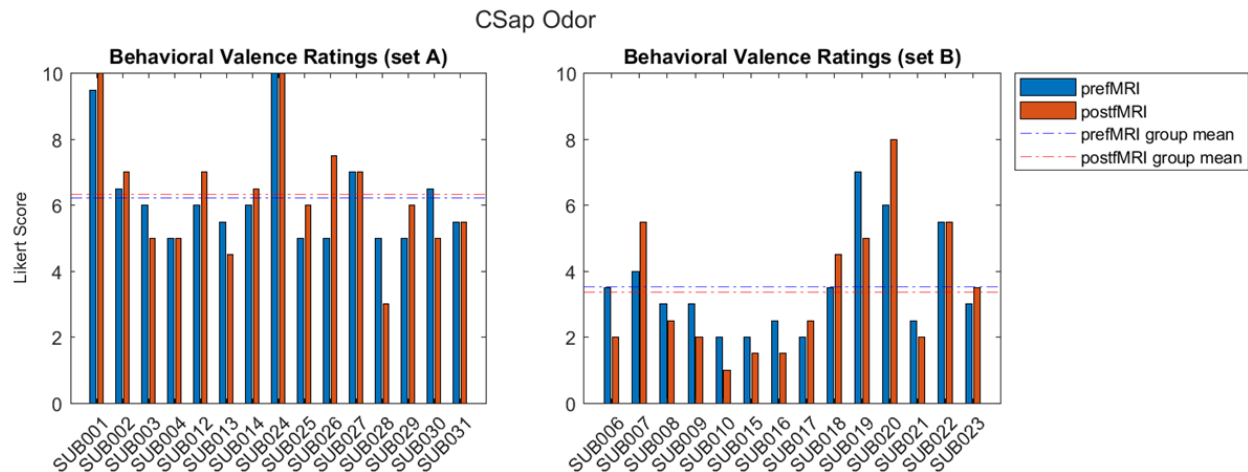


Figure 27. Likert scores of CS+ appetitive odor for both odor sets. Behavioral scores collected before (blue) and after (red) scanning do not show directionally-expected systematic differences – i.e., after scanning, the scores would have been expected to increase, due to conditioning with appetitive pairing.

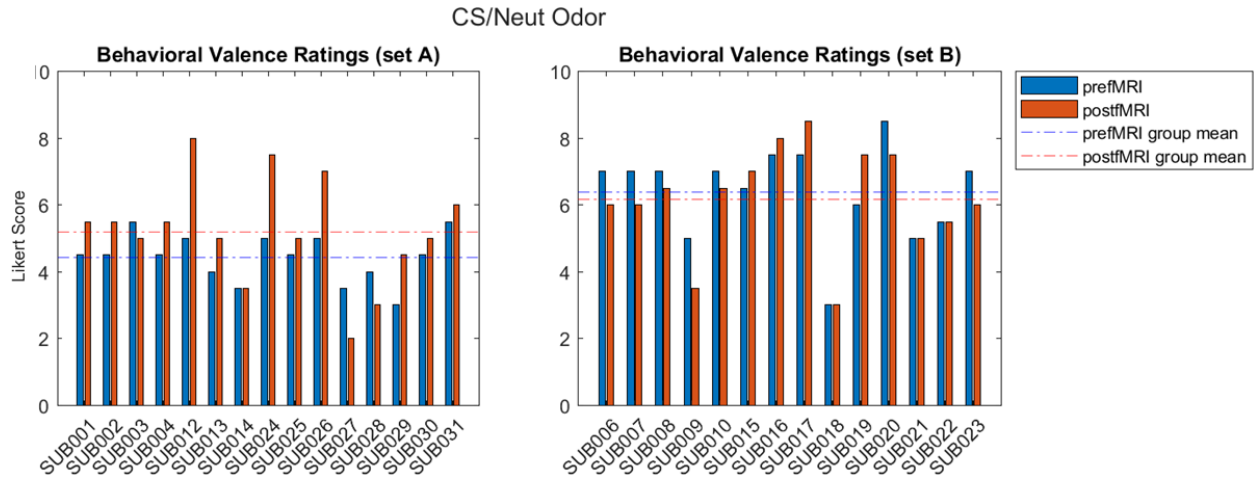


Figure 28. Likert scores of neutral odor without conditioning outcome for both odor sets. Behavioral scores collected before (blue) and after (red) scanning do not show directionally expected systematic differences, as expected.

3.2 Neuroimaging Experiment

3.2.1 Reaction Time

During runs 1 (reference) and 3 (extinction) of the neuroimaging experiment, participants rated the valence of each odor, and their reaction times were recorded using a bottom box. These times were averaged across the 14 trials per odor. To assess potential variations in reaction times between the odors, repeated measures ANOVA was applied to the averaged subject-wise times. The results indicated no statistically significant differences among negative, positive, and three neutral odors (F-statistic: 0.5020, p-value: 0.7342). This suggests consistent processing speed, irrespective of the valence or conditioning paradigm associated with the odor. Group-level averaged reaction times are shown in Figure 29, as an illustration of the overall pattern, with the individual subject-wise times available in Appendix F.

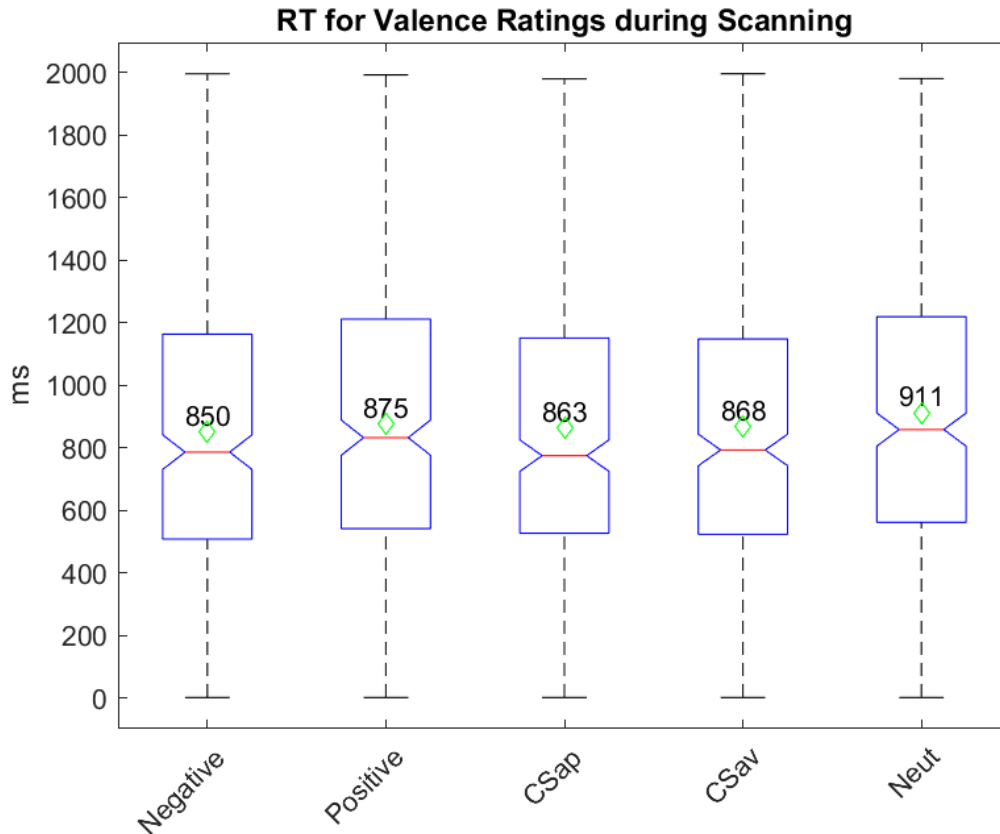


Figure 29. Group-level averaged reaction times recorded during runs 1 and 3 in the odor valence rating task. Participants maintained consistent reaction times across different odors as they rated valence during scanning. The boxplot includes a green diamond representing the median, with the mean value displayed numerically.

3.2.2 Univariate Analysis

As a preliminary validation for the MVPA analysis (3.2.3.), two univariate analyses were conducted to identify the brain regions responsible for odor valence – specifically distinguishing negative and positive odors from one another (3.2.2.1). Secondly, we aimed to showcase the regions responsible specifically for conditioning, irrelevant whether appetitive or aversive (3.2.2.2.).

3.2.2.1 Brain Regions Which Distinguish Negative & Positive Odors

To find brain regions distinguishing negative from positive odors, a univariate analysis was conducted at a whole-brain level and using an ROI. At the whole-brain level, no voxels surpassed the FDR correction at a significance level of 0.05. The results were further evaluated without multiple corrections, using a 95% threshold (equivalent to a significance level of $p < 0.05$), where scattered negative brain activations were evident, with a positive

cluster at bilateral olfactory regions (coordinates 2, 10, -8), left superior temporal lobe (-44, 4, -8), right superior temporal pole (50, 10, -8), and brain stem (Figure 30; regions identified with MRIcroGL 1.2.20210317 Automated Anatomical Labelling (AAL) Atlas; Tzourio-Mazoyer et al., 2002).

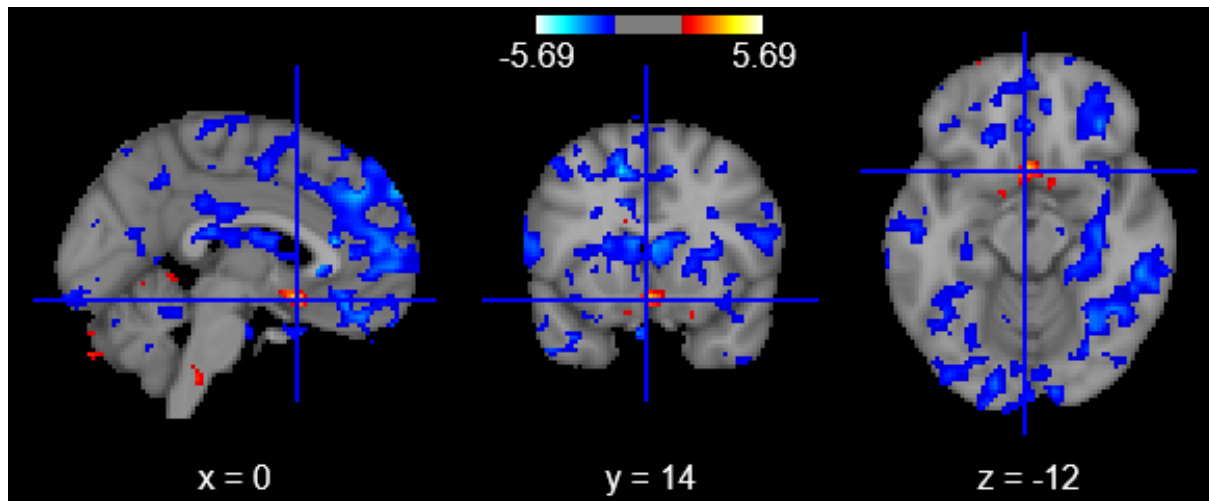


Figure 30. Whole-brain univariate analysis of unpleasantness negative-positive with a 95% percentile threshold (i.e., without multiple corrections). Scattered negative activations are evident throughout, with a positive cluster at bilateral olfactory regions, left superior temporal lobe, right superior temporal pole, and brain stem.

Using a ROI (mask generated via Neurosynth for term “valence”; see methods 1.5.2.2.1.), no voxels surpassed FDR 0.05. With a 95% threshold, positive activations were found in the bilateral olfactory regions (2, 12, -8), left parahippocampal gyrus (-12, 0, -18), and left amygdala (-26, 2, -18; AAL atlas; Figure 31).

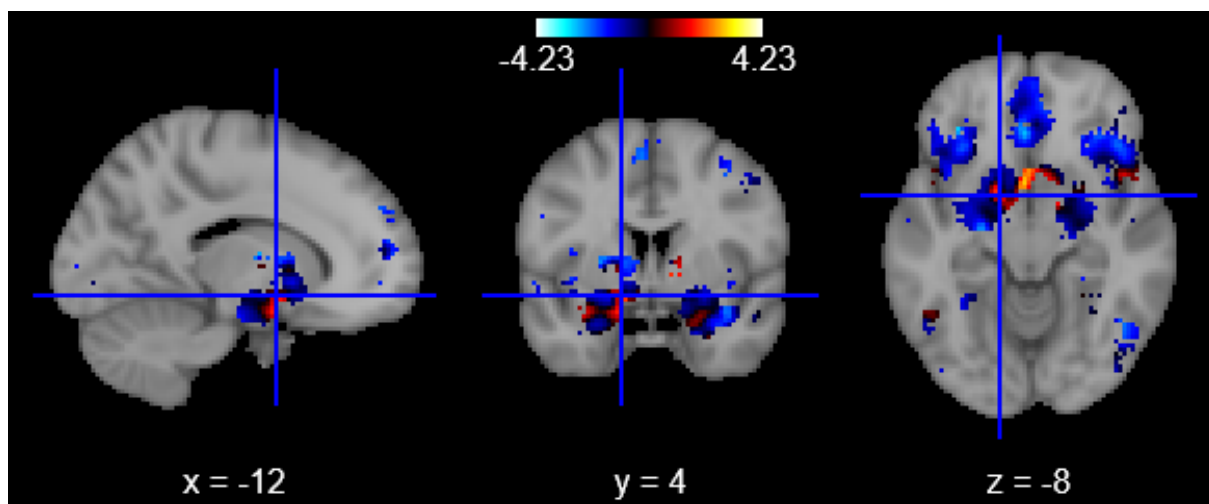


Figure 31. ROI univariate analysis of unpleasantness (negative-positive) with a 95% percentile threshold (i.e., without multiple corrections). Scattered negative activations are found throughout the masked regions, with a positive cluster at bilateral olfactory regions, left parahippocampal gyrus, and left amygdala.

3.2.2.2 Brain Regions Activated by Conditioning

Whole-brain analysis revealed significant activation clusters during the conditioning effect (**Figure 32**). Left inferior occipital area (-28, -80, -10), right middle occipital gyrus (30, -90, 12), and bilateral fusiform (30, -79, -10; -40, -62, -10), as well as in the white matter near the left inferior parietal lobule (-24, -48, 42).

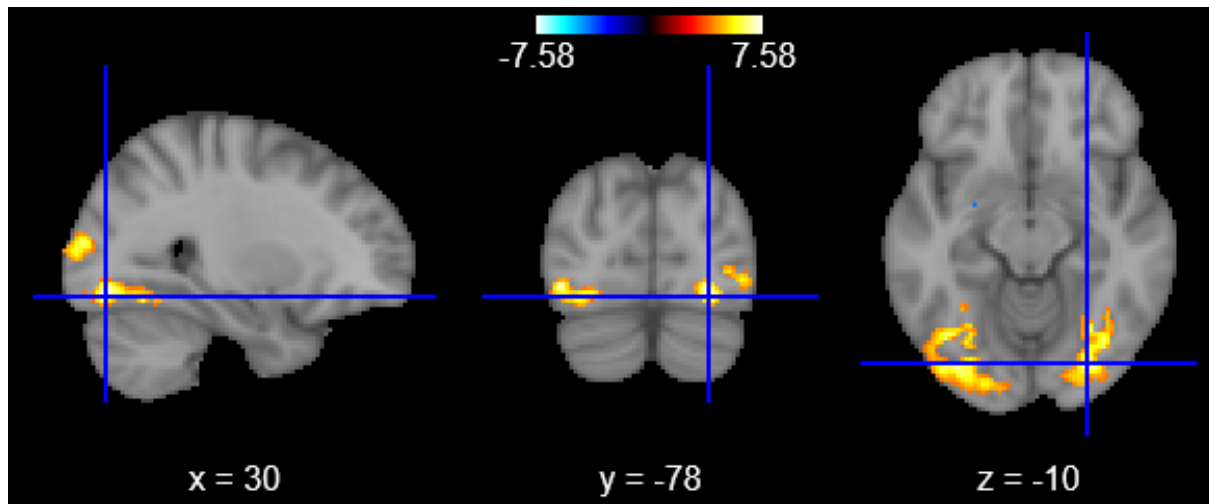


Figure 32. Whole-brain analysis showed significant activation clusters in the visual regions during conditioning (left inferior occipital area, right middle occipital gyrus, bilateral fusiform, and in the white matter near the left inferior parietal lobule). The mean of CS+ appetitive and CS+ aversive was contrasted against CS-. Results were FRD corrected with 0.05.

ROI analysis (mask generated via Neurosynth for term “conditioning”; see methods 1.5.2.2.1.) showed significant activations with FDR 0.05 during the conditioning effect (Figure 33). Positive activations were found in the bilateral insula (36, 24, 6; -28, 26, 6), left caudate (-6, 8, -2), right inferior orbital frontal gyrus (26, 34, -14), and right amygdala (18, 2, -12).

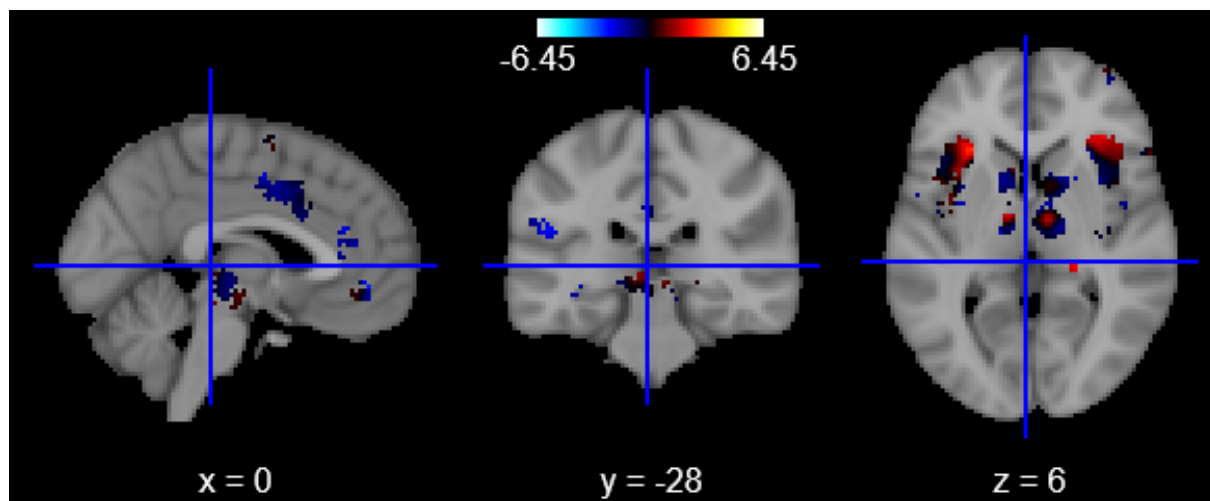


Figure 33. ROI analysis showed significant activation clusters during the conditioning effect. The mean of CS+ appetitive and CS+ aversive was contrasted against CS-. Results were FDR corrected with 0.05. Activations were present in the bilateral insula, left caudate, right inferior orbital frontal gyrus, and right amygdala.

3.2.3 Multivariate Pattern Analysis

3.2.3.1 Classification Analysis

Generated Region of Interest

As the initial phase of MVPA classification analysis, an algorithm was trained to differentiate between negative and positive odors. The regions where representations of negative and positive odors could be distinguished were masked as ROI for later use. To that end, the group-level accuracy maps were submitted into TFCE correction, where the surviving voxels (825 voxels) were masked, although none surpassed the z-score of 1.64 (Figure 34). The ROI exhibited somewhat distributed clustering but demonstrated notable activations in the insula, as well as in the pre- and post-central regions.

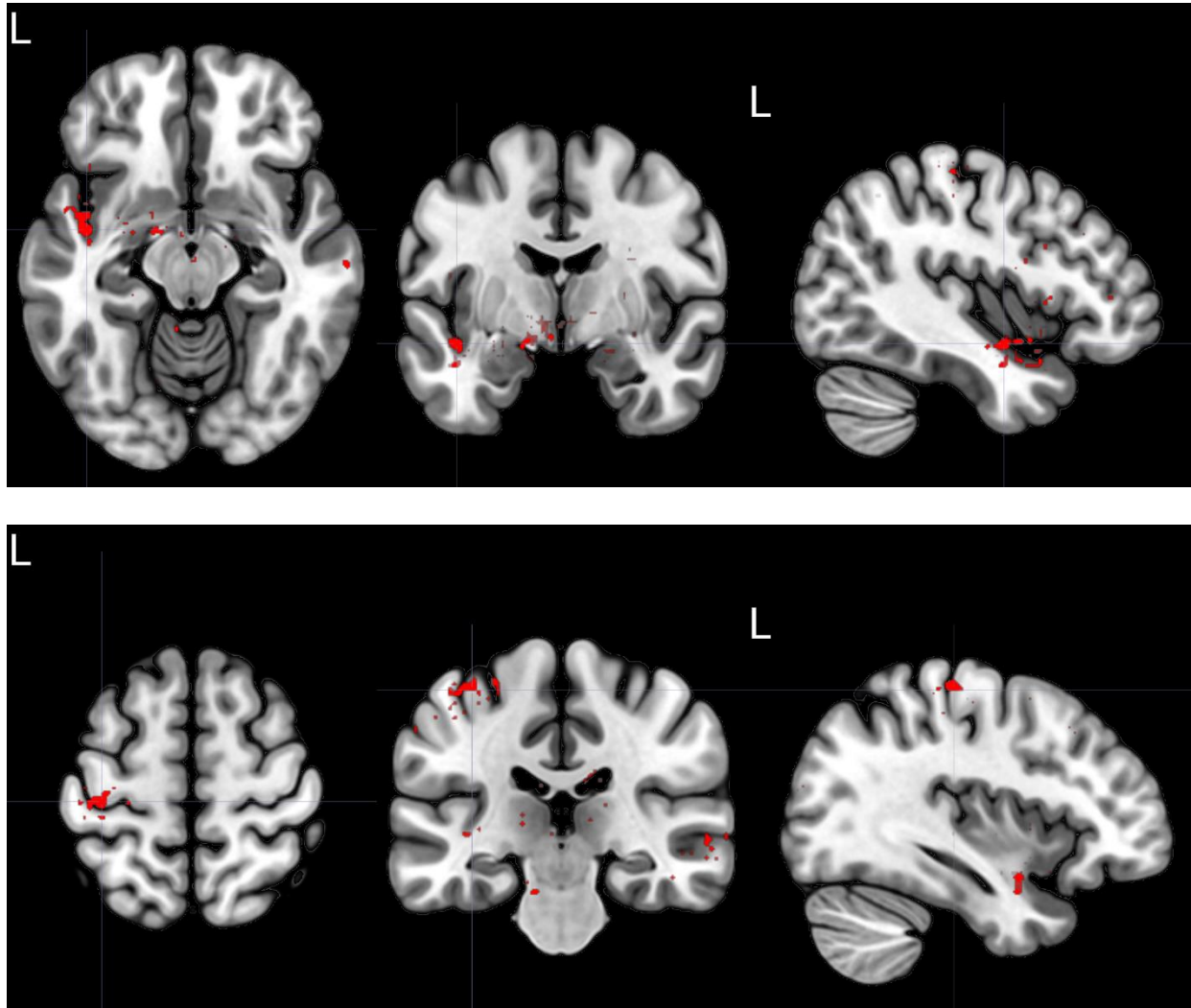


Figure 34. Region of interest. ROI was generated based on the group-level accuracy maps where negative and positive trials could be distinguished. The maps were TFCE corrected, albeit no voxels surpassed the z-score of 1.64. These voxels, 825, mostly located in insular and pre- and post-central regions, were masked as an ROI and used in the latter steps of the classification analysis.

Proof-of-Concept: Reference Run Confusion Matrix

As a proof-of-concept, the SVM classifier was trained and tested (n-fold cross-validation) on the data of the reference run within the ROI, with the expected classification model shown as a confusion matrix on the left of Figure 35. Classification accuracy was found to be poor at 50.12 % (Table 3). The observed values (Figure 35 right) were subjected to a chi-square test for independence, comparing them to chance-level performance (all values of the confusion matrix being 7). The chi-square test yielded a statistic of 0.0289, resulting in a p-value of 0.865. This outcome suggests that there is no significant association between the variables of interest, and, consequently, we fail to reject the null

hypothesis. This finding highlights the absence of an evident relationship between the reference run models.

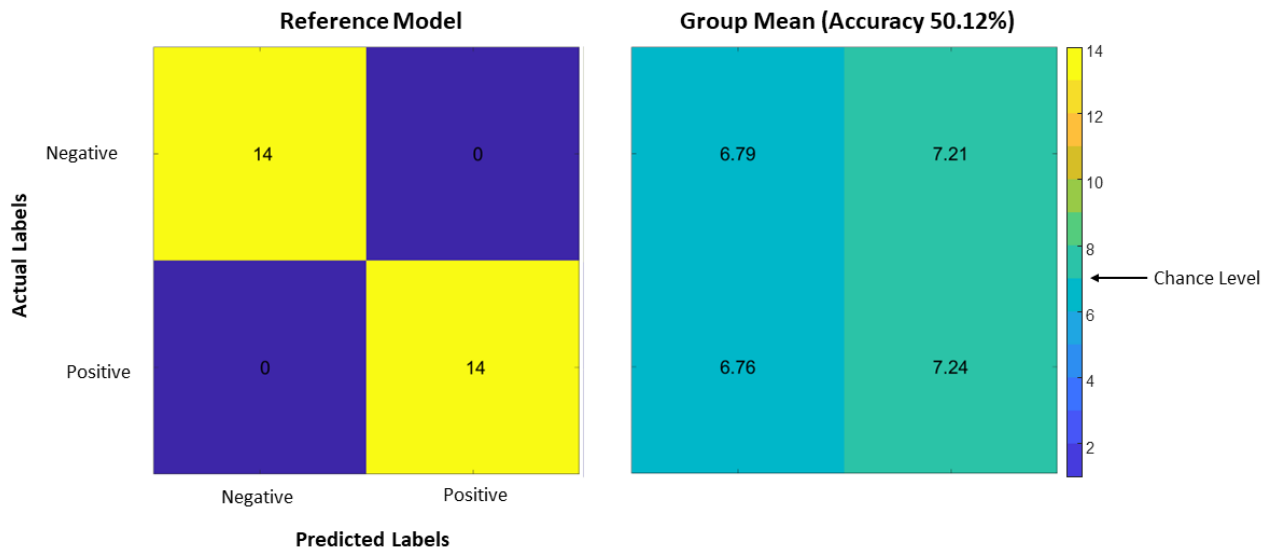


Figure 35. Group mean confusion matrix from reference run. On average, the SVM classifier achieved a modest group mean classification accuracy of 50.12%, barely surpassing the chance level of 50%. Expected results are depicted on the left side reference model. On average, the classifier accurately predicted 6.79 out of 14 negative trials and 7.24 out of 14 positive trials. Actual trial labels are depicted on the vertical axis, while predicted labels are shown along the bottom axis. Warmer colors indicate higher prediction counts. Each label comprises 14 trials, equating to a chance level of 7. The classification was performed within the subject at a trial level using leave-one-trial-out cross-validation, here are the group-level results.

Table 3. Metrics from the classification analysis of reference run. Equations for computing the metrics are shown in the middle column (TP = true positive, TN = true negative, FP = false positive, FN = false negative).

| Metric | Equation | Result |
|--------------------|-------------------------------|---------|
| Accuracy | $TP + TN / TP + TN + FP + FN$ | 50.12 % |
| Misclassification | $FP + FN / TP + TN + FP + FN$ | 49.88 % |
| Precision | $TP / TP + FP$ | 48.52 % |
| Sensitivity/Recall | $TP / TP + FN$ | 50.13 % |
| Specificity | $TN / TN + FP$ | 50.12 % |

Conditioning Run Confusion Matrix

For the conditioning run, the classifier was trained on the data from the reference run and tested on the data from the conditioning run. Expected results are shown in Figure 15 left, assuming the evident effect of conditioning upon the neutral odors. The classification accuracy was poor at 47.66 % (Table 4). The observed values (Figure 36 right) were subjected to a chi-square test for independence, comparing them to chance-level performance (all values of the confusion matrix being 7). The chi-square test yielded a

statistic of 0.3039, resulting in a p-value of 0.859. This suggests no significant difference between the observed results and the chance-level model, where we fail to reject the null hypothesis (no statistically significant difference between observed and chance-level values).

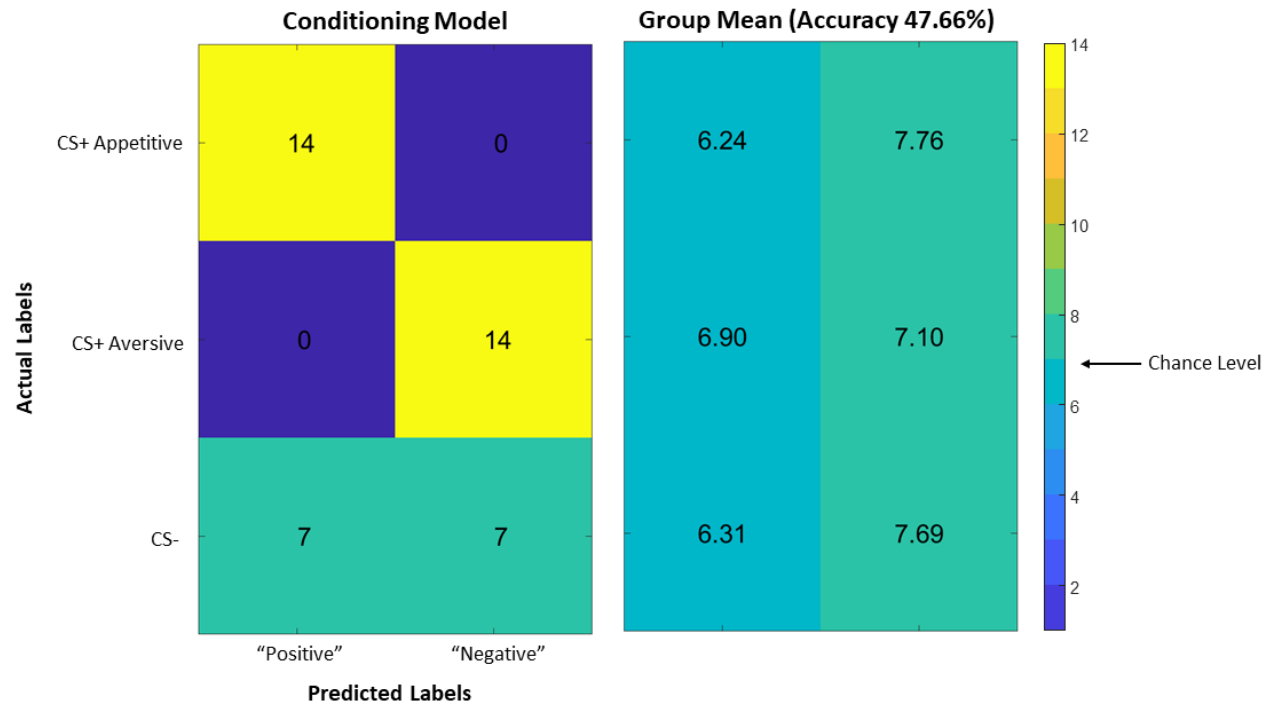


Figure 36. Group mean confusion matrix from conditioning run. On average, the SVM classifier achieved a poor group mean classification accuracy of 47.66%, underperforming the chance level of 50%. Expected results are depicted on the left side conditioning model. On average, the classifier predicted 6.24 out of 14 CS+ appetitive trials as “positive”, 7.1. out of the 14 CS+ aversive trials as “negative”, while 6.31 out of 14 CS- trials were sorted as “positive”. Actual trial labels are depicted on the vertical axis, while predicted labels are shown along the bottom axis. Warmer colors indicate higher prediction counts. Each label comprises 14 trials, equating to a chance level of 7. The classification was performed within the subject at a trial level using leave-one-trial-out cross-validation, here are the group-level results.

Table 4. Metrics from the classification analysis of conditioning run. Note, that on the calculations, only the actual labels CS+ appetitive and CS+ aversive and the predicted labels “negative” and “positive” are considered – i.e., the CS- condition is excluded as a feature of non-interest.

| Metric | Result |
|--------------------|---------|
| Accuracy | 47.66 % |
| Misclassification | 52.36 % |
| Precision | 44.57 % |
| Sensitivity/Recall | 47.49 % |
| Specificity | 47.78 % |

Extinction Run Confusion Matrix

For the extinction run, the classifier was trained on the data from the reference run and tested on the data from the extinction run. We expected results at chance-level (Figure 37 left), assuming that the effect of conditioning had ceased. Surprisingly, the classification accuracy was slightly higher than during the conditioning run, 51.35 % compared to 47.66 % (Table 5). The chi-square test for independence, when comparing the observed results to the chance-level model, yielded a statistic of 0.2724, resulting in a p-value of 0.873. This outcome suggests that there is no significant difference between the observed values and the chance-level model, where we fail to reject the null hypothesis (no statistically significant difference between observed and chance-level values). Contrary to conditioning, the expected results of the chi-square test for independence for extinction is a significant association with the observed results and the chance-level model, as the effect of conditioning should theoretically have ceased.

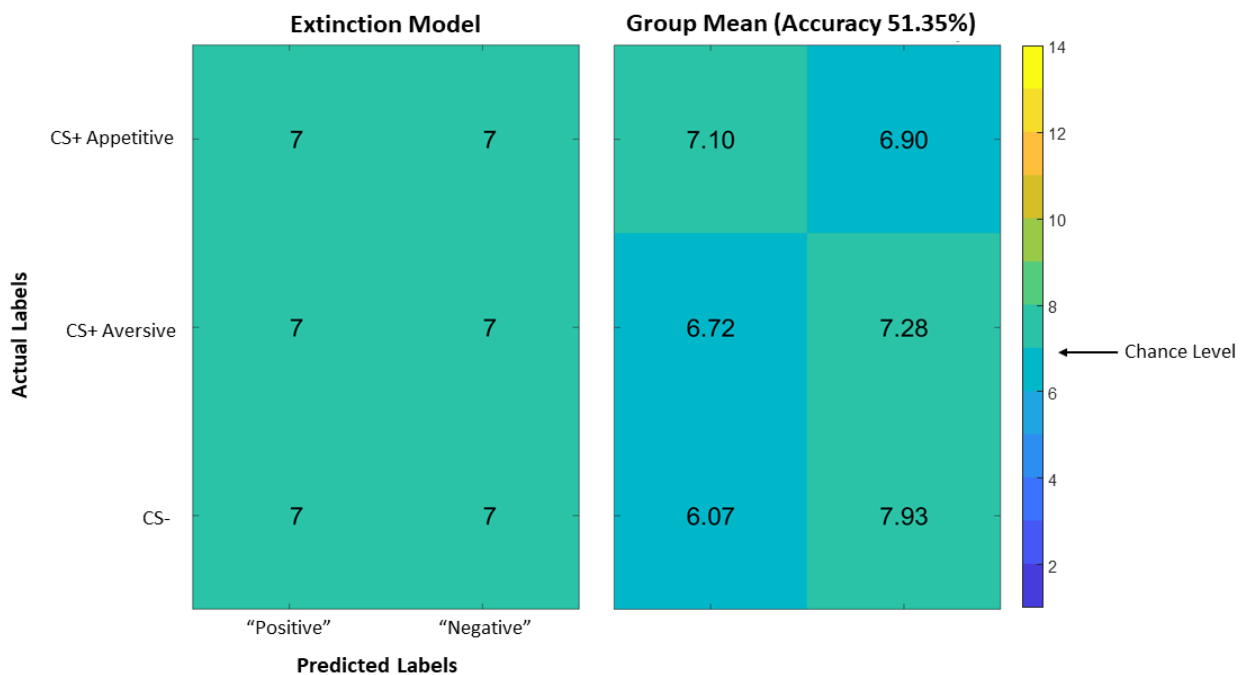


Figure 37. Group mean confusion matrix from extinction run. On average, the SVM classifier achieved a poor group mean classification accuracy of 51.35%, barely surpassing chance level performance. In the extinction run, the classification results were expected to be at chance level, as depicted in the left side model. On average, the classifier predicted 7.1 out of 14 CS+ appetitive trials as “positive”, 7.28 out of the 14 CS+ aversive trials as “negative”, while 6.07 out of 14 CS- trials were sorted as “positive”. Actual trial labels are depicted on the vertical axis, while predicted labels are shown along the bottom axis. Warmer colors indicate higher prediction counts. Each label comprises 14 trials, equating to a chance level of 7. Classification was performed within the subject at a leave-one-trial-out trial level using cross-validation, here are shown the group-level results.

Table 5. Metrics from the classification analysis of extinction run. Note, that on the calculations, only the actual labels CS+ appetitive and CS+ aversive and the predicted labels “negative” and “positive” are considered – i.e., the CS- condition is excluded as a feature of non-interest.

| Metric | Result |
|--------------------|---------|
| Accuracy | 51.35 % |
| Misclassification | 48.64 % |
| Precision | 50.71 % |
| Sensitivity/Recall | 51.37 % |
| Specificity | 51.34 % |

3.2.3.2 Representational Similarity Analysis

3.2.3.2.1 Multiple Model RDM Approach Using Minimal t-Conjunction

Figure 38A illustrates neural RDM derived from the conditioning run, while panel B depicts the theoretical model, with Pearson’s correlation coefficient of -0.48. Hierarchical clustering was applied to both RDMs in panels C and D, while multidimensional scaling (MDS) was used in panels E and F.

The respective results for the extinction run are presented in Figure 39, where Pearson’s correlation coefficient between the theoretical model and neural RDM was found to be 0.36.

Figure 40 displays the minimal t-conjunction results overlaid on a standard brain, adjusted for multiple corrections. Notably, no voxels exceeded the threshold of 1.6449. Hence, the figure presents the two-tailed results with a threshold of 1.96, where only negative activations are present.

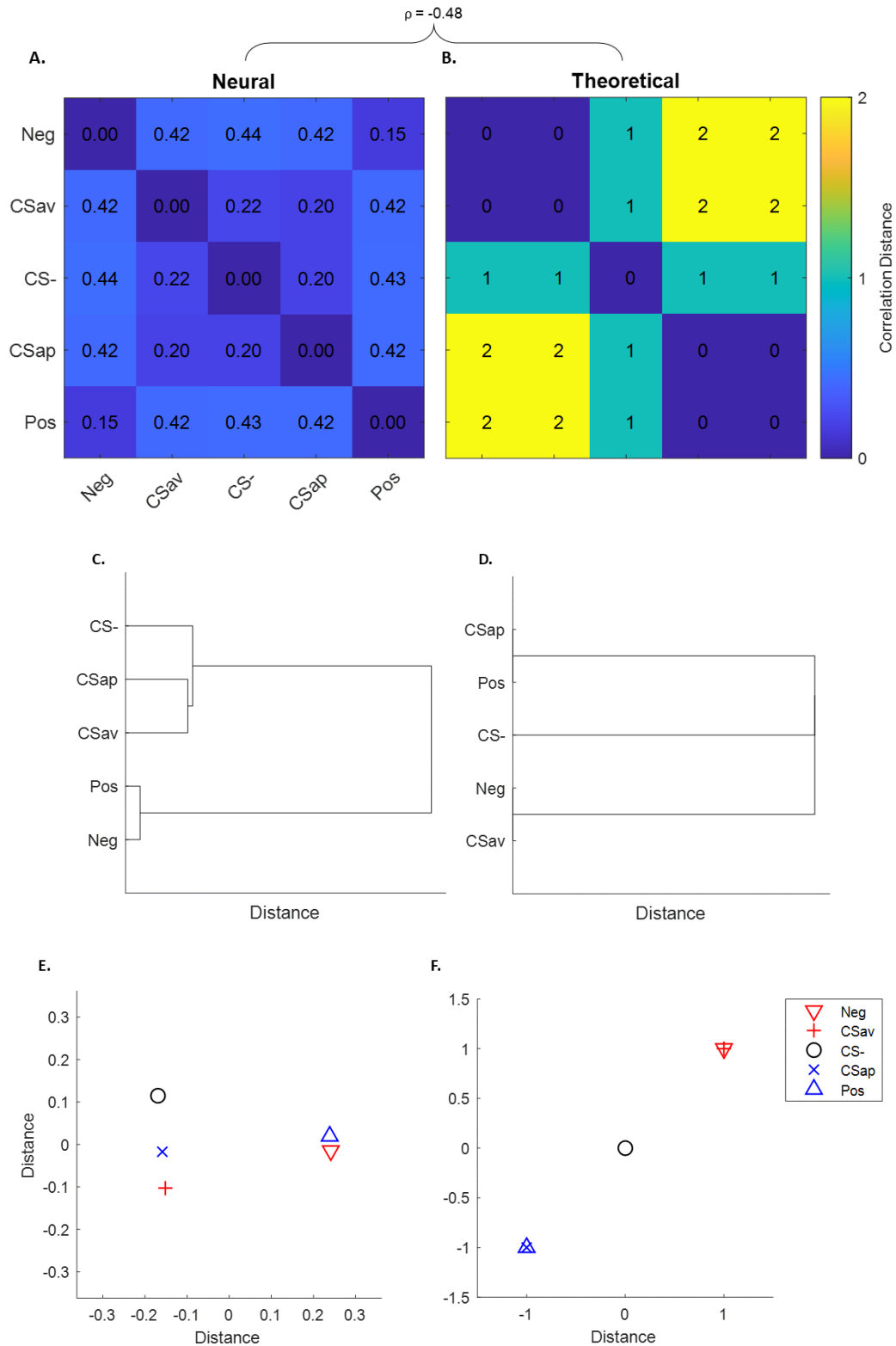


Figure 38. Results from MVPA RSA analysis of conditioning run. On the left panels, neural results are visualized through RDM (A), hierarchical clustering (C), and multidimensional scaling (E). Correspondingly, the theoretically expected model is depicted on the right panels (B, D, F). Spearman's correlation coefficient of the neural and theoretical RDMs is -0.48.

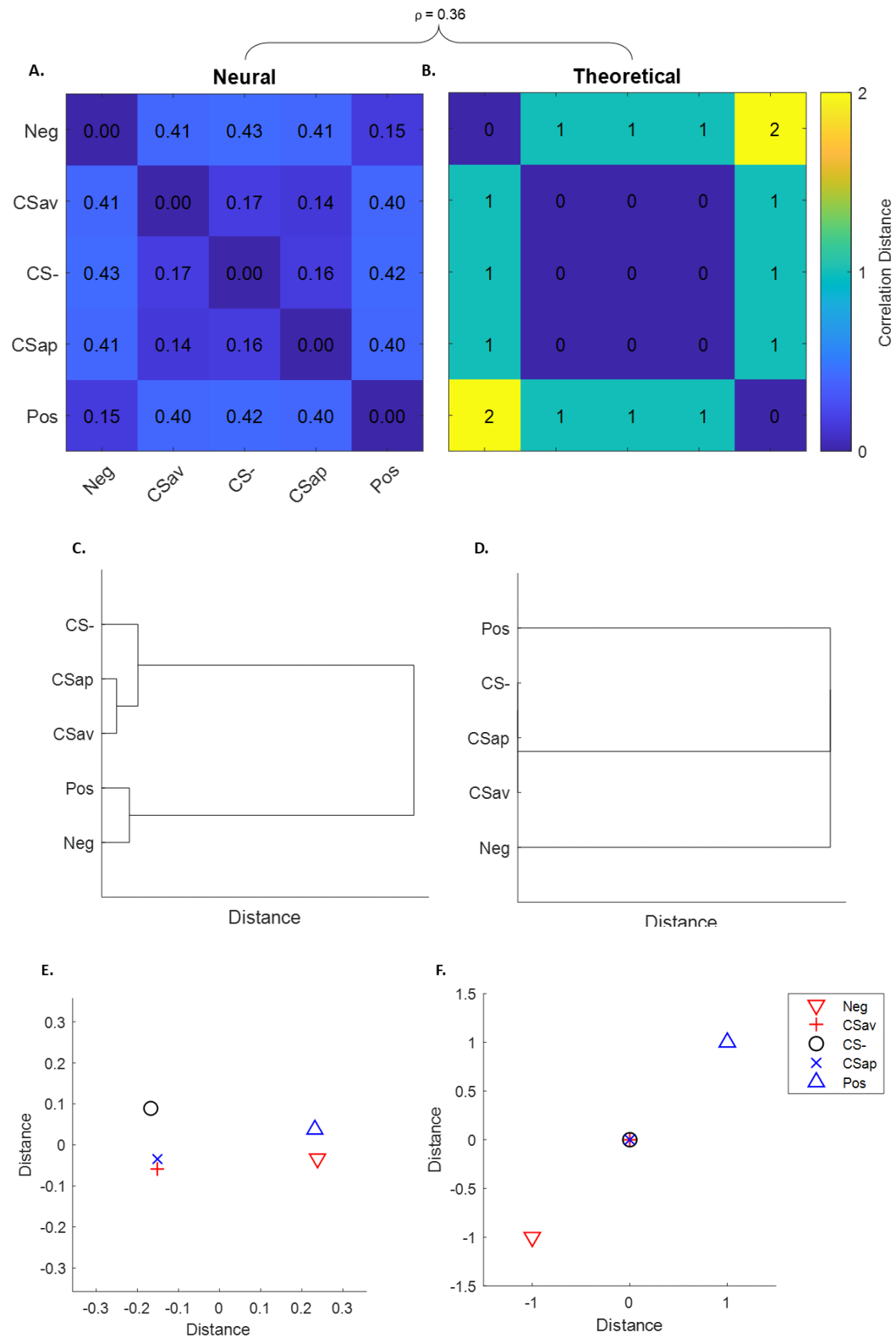


Figure 39. Results from MVPA RSA analysis of extinction run. On the left panels, neural results are visualized through RDM (A), hierarchical clustering (C), and multidimensional scaling (E). Correspondingly, the theoretically expected model is depicted on the right panels (B, D, F). The Spearman's correlation coefficient of the neural and theoretical RDMs is 0.36.

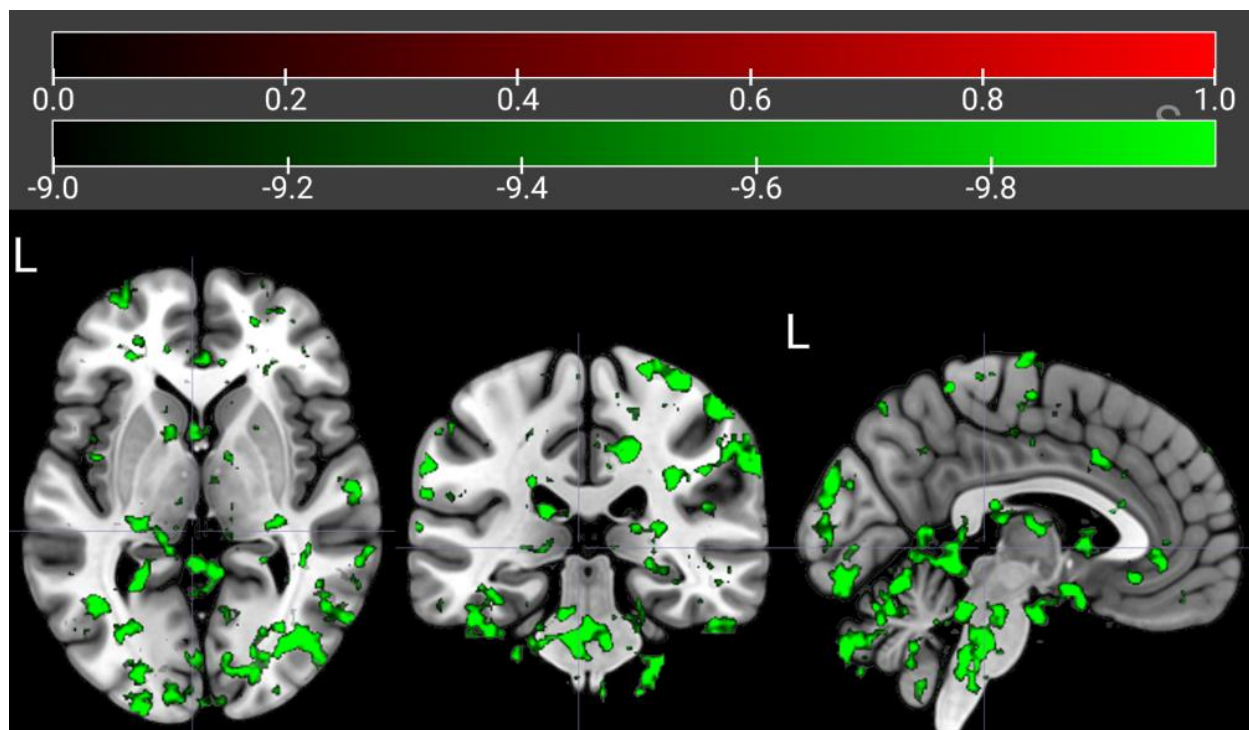


Figure 40. Minimal *t*-conjunction *t*-map overlaid on a standard brain, adjusted for multiple corrections. No voxels exceeded the threshold of 1.6449; hence, the figure presents the two-tailed results with a threshold of 1.96, where only negative activations are present.

3.2.3.2.2 Single Model RDM Approach

Figure 41A presents the neural RDM derived from data across all runs, while panel B illustrates the theoretical model, yielding Pearson's correlation coefficient of 0.21. Hierarchical clustering was applied to both RDMs in panels C and D, while multidimensional scaling was employed in panels E and F.

The *t*-maps are displayed overlaid on a standard brain, with adjustments made for multiple corrections. In Figure 42, one-tailed results are depicted, where voxels exceed the threshold of 1.6449. The same *t*-map is presented as a mosaic in Figure 43. For detailed coordinates of clusters and their respective regions, refer to Appendix G.

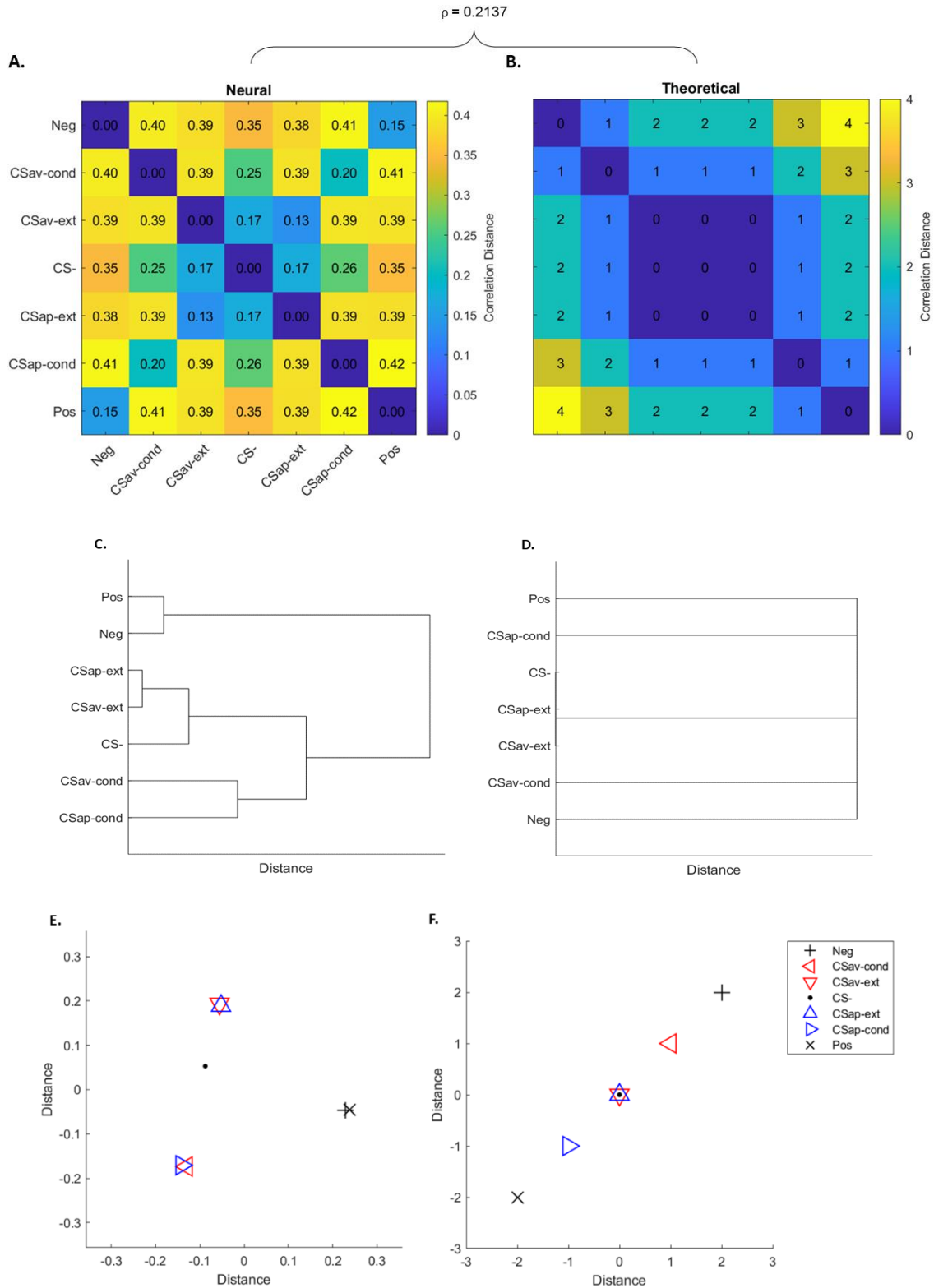


Figure 41. Results from MVPA RSA analysis using a single target matrix. On the left panels, neural results are visualized through RDM (A), hierarchical clustering (C), and multidimensional scaling (E). Correspondingly, the theoretically expected model is depicted on the right panels (B, D, F). The Spearman's correlation coefficient between the neural and theoretical RDMs is 0.2137.



Figure 42. RSA searchlight t-map using a single model RDM approach overlaid on a standard brain, adjusted for multiple corrections. The figure presents one-tailed results of the positive activations exceeding the threshold of 1.6449. A specific slide is taken at coordinates (-17, 12, 4). For detailed coordinates of clusters and their respective regions, please refer to Appendix G.

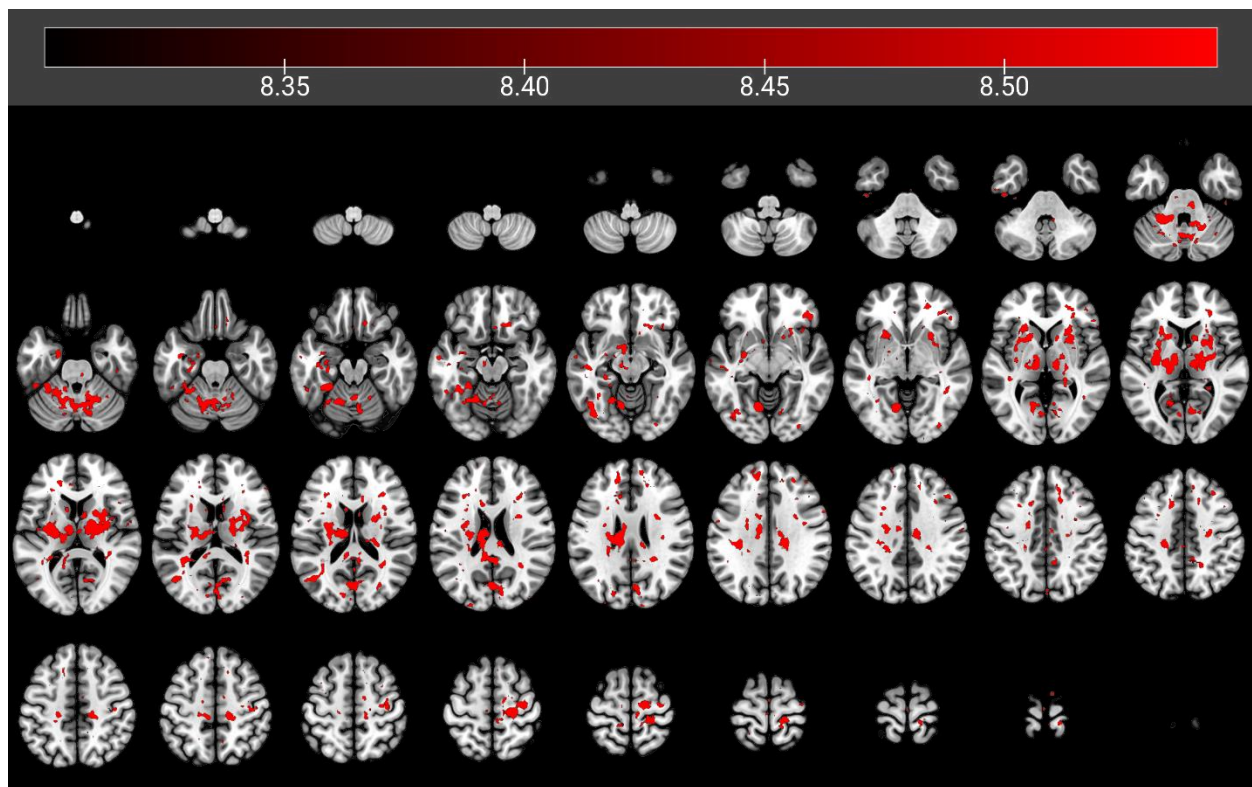


Figure 43. Mosaic of RSA searchlight t-map using a single model RDM approach overlaid on a standard brain, adjusted for multiple corrections. The figure presents one-tailed results of the positive activations exceeding the threshold of 1.6449. Notably, this specific slide presents the left putamen at coordinates (-17, 12, 4). For detailed coordinates of clusters and their respective regions, please refer to Appendix G.

4 DISCUSSION

The present study aimed to investigate how learning alters the representations of odors in the human brain. Specifically, we sought to answer whether appetitive and aversive conditioning renders the representations of neutral olfactory stimuli more stereotypically toward “positive” and “negative”, respectively. This study was inspired by the work of Howard and colleagues, who demonstrated that a classification algorithm could be trained (2016), to decode neural representations of mint and citrus odors from reward-related brain regions (e.g., ventromedial prefrontal cortex) following conditioning. However, an intriguing question, which was not addressed in their study, is how the representations of conditioned and non-conditioned stimuli evolve in relation to each other – specifically, whether they become more similar to one another post-conditioning.

In this thesis, we aim to build upon the work of Howard (2016) by incorporating both aversive and appetitive conditioning within the same paradigm. To ensure comprehensive data collection, we leveraged multiband acceleration methods (Moeller et al., 2010; Seidel et al., 2020) to acquire whole-brain functional images within the MRI scanner while maintaining a higher-resolution voxel size to properly image small structures pertinent to olfaction. By employing this region-naïve approach, we extended the scope of Howard and colleagues’ study, which focused exclusively on known olfactory regions, thereby providing a more holistic view of how learning alters olfactory representations in the brain.

We adopted an event-related fMRI design consisting of three phases. In the first phase, the goal was to establish reference points within the representational space through olfactory stimulation with positive and negative odors. Subsequently, during the second phase, we utilized monetary gain and loss as unconditioned stimuli to condition two neutral odors, designating them as CS+ appetitive and CS+ aversive, while leaving a third neutral odor, CS-, unconditioned. Following conditioning, in the third phase, the neutral odors were presented once more without conditioning outcomes to induce extinction. In each phase, 14 trials for each odor were acquired, with a 2-second stimulation period.

To ensure the generalizability of our findings beyond the specific odors utilized in the study, we incorporated two distinct odor sets, randomly assigned to different participants.

Each set contained the five valence profiles mentioned above (positive, negative, CS+ appetitive, CS+ aversive, CS-), but the specific odors varied between sets. Finally, to provide a comprehensive understanding of the participant's responses, we collected behavioral valence ratings for all five odors both before and after neuroimaging sessions.

The aim was to analyze the data using similarity analysis through the searchlight technique (Kriegeskorte et al., 2006). This method enabled an exploration of the brain for the effect of interest in a less biased manner, without restricting the analysis to a predefined set of brain areas. The analysis pipeline was inspired by the cross-decoding scheme described by Levine et al. (2018). Additionally, as a preliminary validation of data quality, a standard univariate analysis was conducted to examine the effect of conditioning and identify brain regions where negative and positive odors could be distinguished.

The key findings of this thesis are inconclusive, with observed trends indicating that the stimulus material was insufficient, rendering its effectiveness ambiguous. Due to these limitations, the conditioning effect remains uncertain. The detailed findings are discussed below, contextualized within relevant literature, and the implications for the field are considered. Finally, recommendations for future research are provided to guide further studies.

4.1 Interpretation of Findings

We sought to investigate whether certain brain regions exhibit similarity between the aversively conditioned neutral stimulus and negative stimuli, and between the appetitively conditioned stimulus and positive stimuli, while the non-conditioned neutral stimulus does not exhibit a “preference” for either stereotypical valence class. Such brain regions would reflect the outcome of these learning processes. Since these regions do not have to be in or near olfactory brain areas, we opted for whole-brain searchlight-based data-driven analysis.

Our specific hypotheses were:

- 1) For CS+av, the classifier will decode the respective activation patterns as those elicited by negative stimuli (but CS+ ap and CS- will yield chance performance).

- 2) For CS+ap, the classifier will decode the respective activation patterns as those elicited by positive stimuli (but CS+ av and CS- will yield chance performance).
- 3) For both types of CS+, the classifier will decode the respective activation patterns as those elicited by the correspondingly valenced stimuli (but CS- will still yield chance performance).

4.1.1 Behavioral Findings

4.1.1.1 Odor Sets are Comparable in Terms of Their Valence Profiles

As a prerequisite for the neuroimaging study, we conducted three behavioral experiments assessing the participants' perception of the odorants. First, we tested whether the odor sets were comparable in terms of their valence profiles (3.1.2). The motivation for using these sets was to abstract away from the particular odors used in the study, focusing instead on the valence representation of odors rather than their identities. We opted to confirm that the sets were equivalent in terms of their valence profile. The T-test indicated no notable disparities in the sets, allowing us to proceed safely with the planned design.

Few studies have utilized dual or multiple stimulus sets in a single study (e.g. Howard et al., 2016). However, in recent years, the formulation of individualized stimulus sets has gained popularity with the advent of personalized and precision medicine.

4.1.1.2 Participants Score Negative & Positive Odors Inconsistently Across Odor Sets

As a further prerequisite for the subsequent MVPA analyses, we verified participants' perception regarding particularly the “anchors” of the olfactory representational space, i.e., the negative and positive odors. Although the participants consistently rated the positive odors highly in terms of valence across both odor sets, the negative odors did not perform consistently. Notably, the negative odor of set B, ammonium sulfate, did not receive lower ratings than its positive odor pair, jasmin. Five participants out of 14 rated ammonium sulfate as more pleasant than jasmin both *before and after* scanning, while 11 participants rated ammonium sulfate as more pleasant than jasmin *during* the scan.

This inconsistency could be explained by the low concentration of the ammonium sulfate odor, with the dilution ratio was 1:100 (Table 2). Typically, ammonium sulfate is a poorly

tolerated odor due to its rotten egg scent, necessitating careful presentation in an experimental setup. Since the study did not only include behavioral experiments but also a presentation of the odorants during scanning, the concentration had to remain tolerable given the numerous trials for each odor.

Concerning set A, the negative odor of fish sauce was consistently perceived as unpleasant *before and after* the scan, while its positive counterpart, odor orange, was consistently perceived as pleasant. Only two participants out of 15 rated fish sauce more pleasant than orange *during* scanning, although the score difference was minimal.

Previous research has demonstrated that the initially pleasant perception of odors can diminish over time due to repeated exposure (Ferdenzi et al., 2014). This decline in valence can be attributed to a decrease in the novelty of the odor as individuals become more accustomed to it. Conversely, the valence of unpleasant odors tends to remain stable, likely due to their evolutionary role as warning signals that organisms should not habituate to. However, our results regarding this phenomenon are inconsistent. While the reference odors in set A consistently elicited similar responses, the negative odor in set B did not produce the expected results.

4.1.1.3 No Expected Differences for Neutral Odors Before & After Conditioning

Regarding the conditioned neutral odors, we anticipated seeing systematic differences in behavioral ratings: the behavioral ratings of CS+ aversive were expected to decrease after conditioning, while CS+ appetitive ratings were expected to decrease.

However, the anticipated differences were not evident in the group mean ratings. For CS+ aversive, the ratings remained similar (around 5, on a 0-10 scale) for set A, whereas the ratings decreased by about one point for set B (more expectedly). For CS+ appetitive, the group mean ratings in both sets remained almost identical before and after conditioning. For unconditioned CS-, we assumed no changes throughout the experiment, whereas those ratings for set A increased about one score after conditioning, while for set B ratings stayed similar.

One possible explanation for the lack of directionally expected differences in the conditioned odors is the effectiveness of the conditioning paradigm. Monetary gain and

loss were chosen as appetitive and aversive US to ensure that US happens in a single modality, but in a separate modality of the conditioned stimuli (*cross-modal conditioning*). This choice was based on its feasibility and proven effect in many previous studies (e.g. Delgado et al., 2006; Kim et al., 2014; Pessiglione & Delgado, 2015) to ensure the comparability of the results. Per Levine et al., (2018) 50% pairing was chosen with US and CS+ since partial reinforcement has been found effective and pragmatic in fMRI studies to avoid the possible confounding effect of the US presentation in comparison to continuous 100% pairing (Lonsdorf et al., 2017). However, given our weak results, this pairing might have been too low for the number of trials, as studies have shown that partial pairing may lead to delayed learning, as noted by Lonsdorf and colleagues. In addition, we can further speculate on the odorant stimuli reliability, which will be discussed below (4.2.).

4.1.2 Neuroimaging Findings

4.1.2.1 Reaction Time

During the neuroimaging experiment, participants consistently provided valence ratings for both negative and positive odors during the reference run, as well as for the three neutral odors at the extinction run. Notably, there were no significant reaction time differences, indicating consistent processing speed irrespective of the valence profiles or conditioning paradigms associated with the odors.

4.1.2.2 Univariate Analysis

Two univariate analyses were conducted to investigate the simple stimulus-response relationship within the data and to localize effects.

Brain Regions Which Distinguish Negative and Positive Odors

Whole-brain and ROI analyses were conducted to identify brain regions that differentiate between negative and positive odors, but neither approach yielded significant results. After applying a threshold of 95% on multiple corrected data, both approaches revealed bilateral olfactory regions and the left amygdala within the ROI. This aligns with the expected response to unpleasant stimuli, as these regions are associated with olfactory and negative emotion processing, respectively (Zald & Pardo, 2000).

Nonetheless, our whole-brain and ROI analyses reveal a predominance of negative activations in the brain maps (Figures 30 and 31). Our contrast is designed to conceptualize “unpleasantness” by subtracting positive brain activity from negative, thereby identifying neural responses associated with negative valence or unpleasantness. Given the weak behavioral responses to the negative odor in odor set B, this neural response may be attributed to stronger positive stimulation, thus suppressing neural activity in response to unpleasantness – rather than solely reflecting the neural processing of unpleasant odors.

A previous meta-analysis (Costafreda et al., 2008) examining the amygdala’s precise nature discovered that the region’s activity was significantly higher for emotional stimuli over neutral, in particular, the probability for activation was higher for fear-related stimuli than for those associated with happiness. When examining stimuli modalities, gustatory and olfactory stimuli were found to be the strongest predictors of amygdala activation.

Similarly, Winston et al. (2005) conducted a comparative study examining different valence profiles combined with varying intensities. Their findings suggest that the amygdala does not independently encode either valence or intensity. Instead, it represents intensity-by-valence interaction, reflecting the overall emotional value of a stimulus, according to Winston et al (2005).

Anderson and colleagues (2003) offered a different perspective, stating that the amygdala’s neural representations are primarily associated with intensity, while distinct representations in the orbitofrontal cortex independently encode valence. This indicates a more distributed model of olfactory coding, drawn upon separable neural substrates.

Brain Regions Activated by Conditioning

When examining regions related to conditioning, both whole-brain and ROI analyses reveal significant activations when contrasting CS+ aversive and CS+ appetitive against CS- $([-0.5, -0.5, 1])$. This contrast effectively removes the effect of neutrality while preserving the effect of conditioning, whether aversive or appetitive $((CS-) - (CS+aversive + CS+appetitive) = aversive + appetitive)$. The significant regions identified, including the

left inferior occipital area, right middle occipital gyrus, and bilateral fusiform, may play various roles in the learning processes associated with conditioning.

Despite the recent recognition that occipital areas are involved in functions beyond visual processing (Pennartz et al., 2023), it is likely that in this study, the visual cues used as unconditioned stimuli (indicated by the euro symbol to present monetary gain or loss) may have influenced this effect, leading to changes in neural activity based on the conditioned valence. This effect may have extended to odor stimulation due to the time-locking of the visual cue with the odor presentation (fixed 2-second ISI; see limitations below). The bilateral fusiform activation, known for its role in face recognition and object processing (Weiner & Zilles, 2016), can be similarly explained, particularly in the context of complex emotionally salient stimuli.

4.1.2.3 Multivariate Pattern Analysis

Classification Analysis

ROI Analysis: To evaluate the findings from the MVPA classification analysis, an ROI was generated by masking regions where an SVM classifier was trained to discriminate negative and positive odor trials from each other, through a within-subject design and leave-one-trial-out cross-validation. Initially, we experimented with leave-one-subject-out cross-validation design, but the results proved unpromising, leading us to opt for the aforementioned approach. The within-subject results were stacked and submitted to statistical analysis at the group level. The surviving voxels were masked, albeit none of them exceeded a z-score of 1.64. The resulting ROI exhibited a somewhat distributed pattern, with notable activations in the insula, as well as in the pre- and post-central regions.

Reference Run: Although the classifier was retrained within the ROI rather than across the entire brain and despite the data set being balanced, the classification accuracy remained subpar at 50.12%.

Conditioning & Extinction Runs: Given our study's framework, we anticipated a drop in classification from conditioning to extinction. Contrary to expectations, this was not observed; the accuracy rates were 47.66% for conditioning and 51.35% for extinction.

Representational Similarity Analysis

In addition to classification analysis, we employed Kriegeskorte's RSA-based MVPA pattern detection method (2008). While classification analysis inherently tests whether the representations of the neutral odors change after conditioning, RSA evaluates the extent to which these representations change. Consequently, RSA may be a more sensitive method than classification depending on the nature of the data. RSA was implemented using two different methods: the multiple model RDM approach with minimal t-conjunction and the single model RDM approach.

At the outset, we aimed to preserve conditioning and extinction as distinct phases and assess their performance using separate theoretically driven models. However, it became evident that the minimal t-conjunction method (Friston et al., 1999, 2005), which seeks minimum values, is rather stringent. This prompted us to consider the single model RDM as a more liberal alternative. Additionally, one might argue that comparing data collected in different runs is problematic, as the data inherently shows great differences across runs, potentially disrupting the results. Fortunately, since we focused exclusively on the activation patterns rather than amplitude, and because MVPA is not influenced by amplitude variations, we were able to include data from multiple runs within a single model RMD.

Multiple Model RDM Approach Using Minimal t-Conjunction

In the conditioning phase, Pearson's correlation between the neural RDM and the model yielded a surprisingly low value of -0.48 (Figure 38A). Given that Pearson's correlation ranges from -1 to 1, this result indicates an intermediate negative correlation, opposite trend from the hypothesized model. Conversely, during the extinction phase, the correlation increased to 0.36 (Figure 39A).

Visualization produced via MDS in the conditioning phase (Figure 38C) reveals that conditions acquired within the same runs (negative and positive, three neutral conditions) tend to cluster together. However, contrary to expectations, the valence profiles did not exhibit similar clustering (positive with CS+ appetitive; negative with CS+ aversive).

When evaluating the MDS plots from the extinction phase (Figure 39C), one would anticipate the negative and positive reference points to remain fixed while the conditioned odors move further away from them and draw closer to each other. Specifically, one would expect the space between all three neutral odors to contract during extinction, as the effect of conditioning diminishes. Indeed, we observed that CS+ aversive and CS+ appetitive were closer to each other and slightly closer to CS- than during the conditioning phase. Brain activations of the RSA analysis did not produce significant positive activations (Figure 40).

Single Model RDM Approach

The single model RDM approach yielded a Pearson's correlation of 0.21 (Figure 41). The MDS visualizations are ambiguous, as conditions acquired within the same run cluster together. Still, the brain map appeared promising, showing significant activations, notably in the limbic system (Figures 42 and 43).

4.2 Limitations & Methodological Considerations

Given the inconclusive results of this study, this subsection outlines the relevant aspects of the applied methodology that pose potential limitations, along with suggested improvements for future research. Limitations concerning the interpretation of the results as well as their ability to generalize have been incorporated where relevant.

4.2.1 Methodological Limitations

4.2.1.1 Selected Odorants

The first issue concerning the selected stimuli of the study is the weak performance of the odors. An unexpected challenge was the timing of data acquisition during the summer of 2020, which presented obstacles in participant recruitment and limited our possibilities for pretesting the stimuli due to COVID-19 restrictions.

When participants were asked about their general feelings concerning the experiment at the end of the study, 15 out of 29 (8 from odor set A, 7 from odor set B) reported an inability to detect one or more odors during neuroimaging. The most common concern regarded the negative odor from odor set B (ammonium sulfate) and the neutral odors from both odor sets. Positive odors were generally detected well across odor sets. This

weak performance is potentially attributable to a low concentration of the stimulus or issues with odor delivery, particularly during scanning, as the participants exhibited no difficulties in detecting the stimuli during the behavioral experiment. In the behavioral experiment, participants were presented with the odors in glass vials, allowing them to sniff for a moment. In contrast, the stimulus was delivered using an olfactometer during scanning. The differing odor delivery methods likely contributed to variations in participants' odor perception.

The second issue arises with the intended valence profile of the odors. As evident in the valence ratings for odor set B (Figure 24), the negative odor was consistently ranked with relatively high Likert scores, showing no meaningful difference from the positive odor scores. Consequently, it may be that the intended two cornerstones, negative and positive odors, of the olfactory representational space were flawed for about half of the study participants, thereby undermining the study's purpose.

Initially, the use of two sets of odors was considered a significant advantage in this study. However, challenges emerged when participants reported difficulty perceiving the odors during scanning, particularly with the negative odor from set B failing to elicit negative ratings. Thus, MVPA with searchlight did not produce the expected results. This led to us using univariate analysis to especially ensure that conditioning worked, i.e., if regions linked to conditioning would appear. Therefore, what was initially viewed as a strength in the study design ultimately became a notable weakness. Further data acquisition would be beneficial to address this limitation, but it falls beyond the scope of this monograph.

4.2.1.2 Experimental Design

A significant oversight in the experimental design was that the sniffing and required motor response (button press) during runs 1 and 3, as well as sniffing and presentation of the conditioning outcome during run 2, had a fixed 2-second ISI. In neuroimaging studies, where multiple stimulations within a trial are tied in time, concerns arise not only regarding data interpretation but also regarding the reliability of those findings.

In conditioning studies like the current study, fixed ISI designs may lead to temporal confounds in CS+ onset predictability and may lead to participant adaptation (Graner et

al., 2020). For instance, requiring a button press every second irrespective of the stimulus presented can complicate the separation of stimulus-associated neural responses from motor responses. Fixed-time ISI may therefore fail to capture the underlying cognitive processes and dynamic nature of neural mechanisms, confound neural responses, and diminish the reliability or validity of the findings.

A frequently discussed topic in olfaction neuroimaging literature is the aspect of instructions for participants. Often, instructions during stimulation (sniffing) and control conditions differ leading to unmatched attention across conditions (Zald & Pardo, 2000). This is particularly critical when the analysis involves subtraction methods, following Donder's logic (1868). In our study, we employed cued olfactory stimulation which may introduce attentional confounds. However, our analysis primarily compared various olfactory conditions rather than a control condition, thereby mitigating the potential for this confound.

Further design consideration regarding the use of stimuli is the issue of using different stimuli in distinct runs. This approach can lead to some level of autocorrelation and signal drift. Conditions within a single run tend to correlate more with each other than with conditions of different runs, simply due to the autocorrelation of the noise.

4.2.1.3 Conditioning

In this thesis we opted to incorporate both aversive and appetitive conditioning within a singular study design, as only few studies have done before (e.g., Gottfried, 2002). However, as reported by Watanabe and colleagues (2017), it appears that external rewards such as money alone, without accompanying feedback scores, did not yield a substantial impact in simple human instrumental conditioning. Following Howard and colleagues' original study (2016), it might potentially have been beneficial to enhance participants learning process with feedback.

4.2.1.4 Searchlight

Although the searchlight approach with MVPA offers numerous advantages (Popal et al., 2019; Weaverdyck et al., 2020), it may also introduce limitations in capturing neuronal activity (Etzel et al., 2013). The searchlight does not consider brain activity that is

synchronized beyond the span of a given searchlight sphere. Thus, as the search window is limited to a certain sphere size (defined through voxels or radius), one cannot be certain of the ideal searchlight size to catch the regions relevant to our study in such a region-naive approach. Network-based methods or functional connectivity are more suitable to catch inter-regional synchronization and move beyond this local focus.

4.2.1.5 RSA

A meaningful aspect to consider regarding RSA is that it is a correlation-based method and does not make assumptions about the causation underlying the observed correlations. Despite the two models showing perfect correlation, this does not imply equivalence of the underlying causal mechanisms. As noted by Dujmović et al. (2022), “two systems may show similar representational geometries and yet work on very different transformations and features of input stimuli”, emphasizing that similar representational patterns do not necessarily indicate identical underlying processes.

4.2.2 Interpretational, Generalizability, & Conceptual Limitations

4.2.2.1 Interpretational Limitations

Due to the complexity of decoding neural data, some additional interpretational limitations must be mentioned. Although fMRI provides relatively high spatial resolution, its temporal resolution remains insufficient for capturing the temporal dynamics of neuronal activity. Likewise, fMRI signals are inherently noisy, requiring extensive preprocessing of the data. One clear confound in this study is the physiological process related to the effect of interest, particularly breathing. We later developed a protocol to address this issue in the preprocessing pipeline (Alahäivälä et al., 2023). However, the noisiness of the data and the numerous preprocessing steps may introduce potential biases, which can distort our understanding of the underlying effects and neural mechanisms of the brain. Despite these limitations that all fMRI studies are subject to, it remains one of the few non-invasive methods for human brain research, and these disadvantages are relatively minor.

4.2.2.2 Generalizability Limitations

Several factors constrain the ability to generalize our findings. Individual variability in brain function can result in significant differences in neural responses to conditioning and

odorants across participants, limiting the extent of our results to a broader population. Additionally, while fMRI studies aim to recreate real-world scenarios, the results often have reduced ecological validity. Finally, cultural differences regarding the use of odors as stimuli constrain the applicability of our conclusions to diverse populations. For instance, it has been found that although the perception of pleasantness can be shared across cultures, the odor labels from the cultural background and related semantic information greatly influence the perception (Arshamian et al., 2022; Ferdenzi et al., 2017).

4.2.2.3 Conceptual Limitations

Conceptually, this study addresses the fundamental challenge of understanding neural representations. The exact nature of how neural patterns encode specific stimuli remains elusive, despite extensive research in the field. The concept of representation itself is debated, with no consensus on how abstract neural codes translate into concrete perceptual experiences (Vilarroya, 2017). As Dietrich (2007) notes, “though there is a vast quantity of ongoing research dependent on representations, and though there is a vast quantity of ongoing research *on* representation, no scientist knows how representations represent” (p. 1.). This knowledge gap persists even in this decade (Baker et al., 2022), hindering our ability to draw definitive conclusions about the neural correlations of conditioned responses and odor perception.

4.3 Future Outlook

Despite the intriguing questions about the nature of olfactory representations that motivated our explorative journey, the inconclusive findings of our analysis did not yield definite answers. Considering the interpretation of results and limitations discussed earlier, this subsection explores the implications of the study and its relevance in the field. Further, this subsection offers prospects for future research with tangible suggestions that were beyond the scope of this thesis.

4.3.1 *Garbage In, Garbage Out...*

In data science, the principle “garbage in, garbage out” dictates that the quality of the output is directly dependent on the quality of the input; skewed, flawed, or low-quality input

data inevitably results in similarly compromised output. Given that the quality of the stimulus material was a clear limitation of this study, it is highly recommended to conduct a preliminary study to explore the compatibility of the odorants before fMRI, ensuring alignment with the specific research question.

When the interest of the study focuses on valence profiles rather than the particular odorants themselves, an individualized approach, as employed in many contemporary studies, strengthens participant responses. Instead of assuming “negative odor” is universally perceived as negative, using personalized stimuli tailored to each participant’s preferences could provide more robust data. We opted out of the subjective approach due to the feasibility constraints of our experimental setup. This personalized approach is based on the idea that although individual preferences and brain structures may vary, our brains may be different, but they are in similar ways (Weaverdyck et al., 2020). We can assume that the underlying representational space has a similar structure, spanning from one extreme to another, regardless of the specific stimulus identities. For instance, one individual's preference for milk chocolate and another's preference for dark chocolate both fit within a similar valence framework. Future studies could adopt a personalized approach by creating a set of odors with varying valences, having participants rate all of them, and selecting the odors with the greatest differences as the final stimuli.

Expanding upon the individualized approach, incorporating personality questionnaires such as approach-avoidance or hypersensitivity tests may allow a better understanding of individual learning processes. Lissek (2012) highlighted the association between anxiety disorders and aberrant learning processes, whereas individuals commonly either overgeneralize the learning effect or lack affective regulation. Building on this rationale, Graner et al. (2020) demonstrated that highly anxious individuals exhibit enduring threat representations, with extinction-related changes to the CS+ pattern notably attenuated, particularly in the amygdala. This approach may serve as an effective means of preselecting participants for conditioning studies.

Furthermore, future studies may aim to evaluate the conditioning effect in greater detail. One potential approach is to split the conditioning run into two sets, comparing the first 50% of the first trials with the latter 50%. Similarly, dividing the extinction run trials into the

first and latter 50% may reveal the progression of extinction in the latter portion of the trial set.

Regarding the analysis, particularly MVPA, it may be beneficial to explore alternative approaches, such as MVPA at multiple spatial scales (Bulthé, De Smedt, et al., 2014; Bulthé, van den Hurk, et al., 2014). As mentioned in the limitations, the searchlight method is restrictive in capturing synchronized brain activity across regions and only considers local activation patterns. Utilizing multi-spatial scale MVPA, including whole-brain MVPA, ROI-based MVPA, and a small radius searchlight, allows for a more structured analysis of neural representations, whether centralized, clustered, or distributed across the brain.

Furthermore, optimization techniques are recommended when using machine learning models. For instance, ridge and lasso regression are types of regularization for linear regression models aimed at reducing overfitting training data (for further details see Chang et al., 2020).

Finally, an intriguing proposition with RSA is to construct several model RDMS representing different aspects of the stimuli beyond sole valence, such as intensity or molecular structure (e.g., Yang et al., 2023). This approach of multiple regression-based RSA, with data- and hypothesis-driven model matrices, would allow us to bridge the gap from chemical compounds and the makeup of an odor to the higher-order associative olfactory areas, cognition, and behavior.

4.3.2 Particularities of Olfaction

Certain particulars pertain to the olfaction, necessitating careful experimental design and analysis for future research.

The influence of vision on olfactory perception appears intuitive, as our instinct often leads us to close our eyes when smelling something pleasant. Yet, comprehensive investigations into this effect are lacking, and there are no clear recommendations on whether olfaction is enhanced with eyes closed versus open while ensuring participants' engagement throughout experiments.

Similarly, the comparative recommendation of cued versus uncued sniffing has not been exhaustively researched. Contrasting normal breathing with cued sniffing may pose

methodological challenges concerning attention to the stimuli. Furthermore, Seubert et al. (2013) observed that cued versus uncued sniffing may involve different brain regions. In turn, Croy et al., (2015) observed that planned and conscious smelling may actually reduce detection of an odor compared to spontaneous exposure.

Determining the duration of the odor stimulation should be based on the research question; short stimulation is likely insufficient for emotion elicitation. Still, a key factor is to determine whether the interest lies in emotion or simply preferences, where short stimulation may suffice.

Methodological considerations extend to experimental design paradigms. Olfactory neuroscience has traditionally favored simple block designs (Sobel et al., 1997; Yang et al., 1997; Yousem et al., 1997). Event-related designs are conventionally considered better for precise hemodynamic response function characterization, while block designs aim to push the action to the maximum over longer time periods, potentially leading to habituation effects.

In contrast, visual studies seeking to elicit activation for an object do not benefit from showing a photo for an extended duration. Instead, these studies often use flickering images to maintain continuous detection of the image. The optimal experimental design depends thus highly on the research modality. In a follow-up study to this project, we showed that the optimal design in olfaction involves breathing modulated block design, with long stimulation, despite their lower design efficiency (Alahäivälä et al., 2023).

Lastly, related to the above, the incorporation of a breathing belt is infrequently utilized in olfaction research, except when the focus is especially on measuring inhalation (Johnson et al., 2006). Using breathing belts could offer valuable insights into how respiratory patterns influence olfactory processing, enabling the development of breathing-modulated experimental designs (Alahäivälä et al., 2023; Wang et al., 2014).

4.3.3 Sampling the Odor Space

The multidimensional nature of the olfactory sensory space can be effectively represented in a low-dimensional plot, such as one with valence (x-axis) and intensity (y-axis). Unlike other sensory systems, where valence tends to correlate with high intensity or arousal,

olfaction uniquely allows for various combinations of these features: low valence/low intensity, low valence/high intensity, high valence/low intensity, and high valence/high intensity. This distinction of olfaction means that when selecting stimuli for experimental purposes, especially those diluted for low intensity to prevent discomfort over repeated exposure in a scanner, the multidimensional representation of the odor space is inherently undersampled.

Considerably, when designing future multivariate experiments, the stimuli selection strategy can be tailored according to the research question. Specifically, one must determine whether the emphasis is on (1) individualized representations, where participants' responses disagree and exhibit variability, or (2) invariant representations, where participants' responses agree and remain consistent.

For (1) individualized representations of valence and intensity, the balanced ratings for valence and intensity (with zero mean) become less significant. Instead, the focus shifts towards mitigating high correlations between valence and intensity, as these correlations complicate regression-based MVPA methods like regression-RSA. One way to control these correlations is to measure the variance inflation factor, which estimates multicollinearity among variables in the model.

For (2) invariant representations, the goal is to balance the ratings for valence and intensity to achieve zero mean and minimize their correlation, which is challenging. Nonetheless, this approach ensures the robustness of univariate analysis when comparing it with multivariate methods.

4.3.4 Synthesis & Perspectives: Asking Better Questions

The exact nature of representational space of olfactory information, encoding, and processing of odors in the human brain is still an open question in the scientific community and remains an active area of research (Dikeçligil & Gottfried, 2024; Purves et al., 2020, p. 325). Compared to other senses, olfaction presents unique challenges. Regarding vision and hearing, for example, research has successfully depicted the brain processes underlying color and sound based on clear physical properties they possess, whereas

odors are often complex mixtures of molecules, lacking such clear mapping (Meister, 2015).

Olfaction remains an often overlooked sensory system, but many scientists have started to recognize its peculiarity. The early evolutionary development of olfaction, in comparison to other sensory systems, ties it to many cognitive functions like memory, emotion, and decision-making (Purves et al., 2020, p. 325). The link to these functions roots the rich interconnections of the olfactory system to other cognitively involved regions, like the limbic system and higher-order processing of the orbitofrontal cortex and insula.

In light of the above-mentioned limitations, it is challenging to interpret the findings of this study, in relation to the field. Yet, this thesis provides relevant insight into the current methods used to study neural representations as the aim of this study redirected itself to explore various analysis methods and how they work with this particular data set. For example, although the results of the MVPA searchlight were not promising, this method has been shown very effective in decoding with e.g. the seminal study of faces and objects (Haxby et al., 2001), spatial information of somatosensory stimulation across the body (Lee et al., 2020), or pairings of audio-visual stimuli (Emberson et al., 2017).

Olfactory neuroscience has remained a relatively subdued field, with most studies conducted with animal models and the research of human olfaction primarily relying on standard univariate analyses. More sophisticated techniques, like RSA, which are slowly becoming standard tools in cognitive neuroscience, offer intriguing possibilities for the field. In line with Maslow's law of the instrument, relying solely on familiar tools may limit our perspectives, potentially hindering progress in olfaction research. Similarly, in affective neuroscience, focusing exclusively on established brain regions like the amygdala may oversimplify the complex nature of emotions.

Recent research emphasizes higher-order processing as our gateway toward understanding olfactory representation in the human brain, despite many aspects of olfaction remaining poorly understood (Brann & Datta, 2020; Dikeçligil & Gottfried, 2024; Fournel et al., 2016). Fournel et al. (2016) refer to the olfactory experience as an "odor object", which is an integrated representation constructed from perceptual attributes and physical features within the olfactory system. This neural signature comprises multiple

traces, extending from the piriform cortex to the amygdala, with RSA proving useful in describing how odor characteristics are distinctly encoded in various olfactory areas. Other research has also shown that different features composed of the complete neural signature of the odor can be found in a distributed manner across the olfactory system (Stevenson & Wilson, 2007). Therefore, instead of focusing solely on bottom-up processes, from the discovery of receptors (Buck & Axel, 1991) to the organization of olfactory bulb, the past decade has shifted towards a top-down perspective, emphasizing the centrality of higher-order processing in our understanding of olfactory representation (Stevenson & Wilson, 2007).

Concluding this study of olfactory representations in the human brain, it is essential to acknowledge the essence of scientific pursuit: asking better questions. Despite rapid advancements in neuroscience, our understanding of the brain's complexities remains fragmented, with different models providing varying explanations. As the brain continues to be vastly unknown, the process of continuous questioning and refining our understanding remains paramount.

As stated by Poldrack (2019, p. 295):

“The goal of research is not to find a significant result; rather, it is to ask and answer questions about nature in the most truthful way possible. Most of our hypotheses will be wrong, and we should be comfortable with that so that when we find one that's right, we will be even more confident in its truth.”

5 CONCLUSION

This thesis set out to investigate whether appetitive and aversive conditioning modulates the neural representations of neutral olfactory stimuli, rendering them more toward conventionally positive or negative, respectively. While previous studies have demonstrated the impact of fear conditioning on visual stimuli (Visser et al., 2011; Dunsmoor et al., 2014; Levine et al., 2018), research on conditioning processes in other sensory systems, particularly olfaction, remains limited.

Using a sample of 29 healthy individuals, olfactory stimuli consisting of five odorants were presented, with three perceived as neutral and one each as stereotypically positive and negative. Appetitive and aversive conditioning was induced using visual stimuli indicating monetary gain (CS+ appetitive) or loss (CS+ aversive) paired with two neutral odors, while a third neutral odor remained unconditioned (CS-). Neuroimaging data were acquired via a 3T Siemens Prisma MRI scanner and the Riech-O-Mat olfactometer, delivering odorants in a birhinal manner.

Data preprocessing followed a standardized pipeline, and analysis comprised both univariate and more sophisticated multivariate pattern analysis (MVPA). MVPA included two approaches: (1) classification analysis, training a support vector machine classifier on neural representations of positive and negative odors and testing it on conditioned neutral odors (CS+ aversive, CS+ appetitive, CS-), and (2) representational similarity analysis, employing theoretically driven representational dissimilarity matrices to explore olfactory representational spaces.

Pertaining to the methodological limitations, particularly concerning stimuli quality, the findings of this thesis remained inconclusive. Despite the suboptimal results, this study contributes to our understanding of olfactory neuroscience by shedding light on the challenges inherent in studying olfactory representational spaces and conditioning effects.

Future research should focus on robust stimulus quality and tailoring the stimuli selection strategy according to the research question while ensuring the robustness of the experimental paradigms. Leveraging sophisticated multivariate pattern analysis methods, such as machine learning-based classification and representational similarity analysis,

may broaden insights into the organization of representational spaces of olfaction. Enhanced methodological approaches could provide clearer insights into how conditioning influences neural representations of olfactory stimuli, contributing to a deeper understanding of sensory processing and associative learning in the olfactory domain.

6 APPENDIX

A. Riech-O-Mat Olfactometer

The custom-build Riech-O-Mat olfactometer (Figure 12; Sommer et al., 2012) is controlled via a designated Linux-based computer program, which allows for different channels to open, one at a time, and pass air from the air source to designated valves. These valves are connected to glass vials containing liquid odorant. Valve opening causes clean air to be mixed with an odor, creating airborne odorant, that is then delivered via further tubing to the scanner room and the participant's noses. When the stimulation is off, the air is passed through the machine without contact with odorants.

Simple text files, called punchcards, are inputted to the Riech-O-Mat computer program, which dictates the odor stimulation – namely, when are the individual odor valve positions opened and closed and for how long. The punchcards are organized as shown in Table 6 below. Constant (air) flow is on (indicated by 1) throughout the experiment. Meanwhile, either an air valve (no stimulation) or one of the odor values (1-2) is open (indicated by 1), one at a time. Time progresses along the number of rows, i.e., each new line has a timing of e.g., 1000 milliseconds. Here, during the first 1000ms, there is no odor stimulation (air valve open) and on the next 1000ms, valve 1 with odor 1 stimulation is on.

Figure 44 depicts the interphase of the Riech-O-Mat program, including a punchcard file on the right used in this study. Note that the timing for a specific sequence must be the same throughout the experiment, as the “step length” is entered into the Riech-O-Mat software manually at the beginning of the given experiment (left on the figure). Airflow remains constant throughout the experiment e.g., 2.5 L/min as in this study or 3.20 L/min as in Howard et al. (2016).

Table 6. Example of a Riech-O-Mat punchcard file. A simple text file controls the functioning of the Riecht-O-Mat olfactometer – a table is shown here to clarify, whereas, in the experimental text files, columns are separated by spaces.

| Flow | Air | Valve 1 (Odor 1) | Valve 2 (Odor 2) |
|------|-----|---------------------|---------------------|
| 1 | 1 | 0 | 0 |
| 1 | 0 | 1 | 0 |
| ... | | | |

Figure 44 depicts the interface of the Riech-O-Mat program; on the right, the step length of the experiment is set in milliseconds, and on the left, a punchcard file can be seen, with two odor valves and a constant airflow throughout.

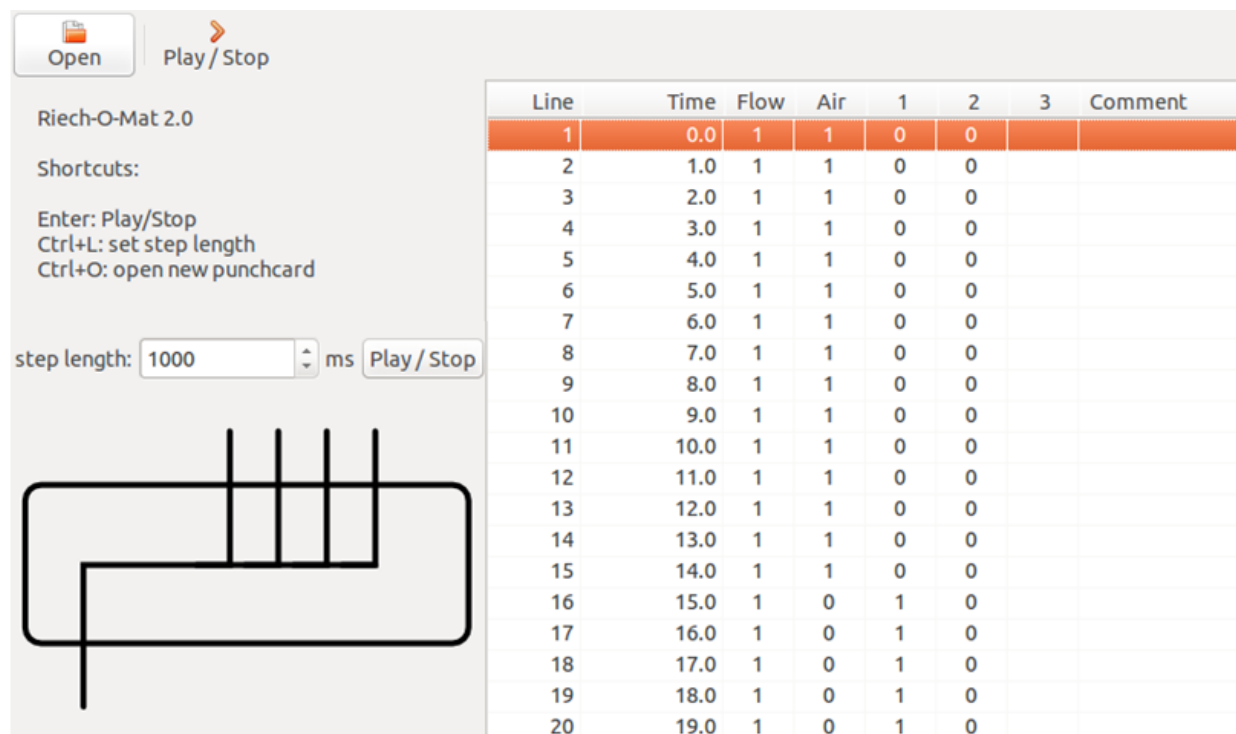


Figure 44. The interface of the Riech-O-Mat 2.0 computer program (Sommer et al., 2012). Photo by Aino-Lotta Alahäivälä.

B. Division of Odor Sets Among Participants

To centralize the study on odor valence, instead of focusing on specific odors themselves, two odor sets (A and B) were created and randomly assigned to different participants.

Each set encompassed one odor typically perceived as negative, one as positive, and three as neutral, although the specific odors varied. 15 participants received odor stimuli from odor set A, while 14 participants received stimuli from odor set B. Table 7 below lists the participants grouped according to their assigned odor set.

Consecutively assigning participants the same odor set (e.g., participants 1-4 and 5-9) was necessitated by the requirement for separate tubing for each odor within a set. Given the time-consuming setup of tubing in the scanner room, switching between participants on the same day was not feasible.

Table 7. Division of odor sets among participants. 15 participants received stimuli from odor set A, while 14 participants received stimuli from odor set B.

| Participant Number | Participant ID | Odor Set |
|--------------------|----------------|----------|
| 1 | SMELLS_SUB001 | A |
| 2 | SMELLS_SUB002 | A |
| 3 | SMELLS_SUB003 | A |
| 4 | SMELLS_SUB004 | A |
| 5 | SMELLS_SUB006 | B |
| 6 | SMELLS_SUB007 | B |
| 7 | SMELLS_SUB008 | B |
| 8 | SMELLS_SUB009 | B |
| 9 | SMELLS_SUB010 | B |
| 10 | SMELLS_SUB013 | A |
| 11 | SMELLS_SUB012 | A |
| 12 | SMELLS_SUB014 | A |
| 13 | SMELLS_SUB015 | B |
| 14 | SMELLS_SUB016 | B |
| 15 | SMELLS_SUB017 | B |
| 16 | SMELLS_SUB018 | B |
| 17 | SMELLS_SUB019 | B |
| 18 | SMELLS_SUB020 | B |
| 19 | SMELLS_SUB021 | B |
| 20 | SMELLS_SUB022 | B |
| 21 | SMELLS_SUB023 | B |
| 22 | SMELLS_SUB024 | A |
| 23 | SMELLS_SUB025 | A |
| 24 | SMELLS_SUB026 | A |
| 25 | SMELLS_SUB027 | A |

| | | |
|-----------|---------------|---|
| 26 | SMELLS_SUB028 | A |
| 27 | SMELLS_SUB029 | A |
| 28 | SMELLS_SUB030 | A |
| 29 | SMELLS_SUB031 | A |

C. Sniffin' Sticks: 16-Item Test for Odor Identification

The Sniffin' Sticks odor "Identification Test 16, Blue" (Burghardt®, Wedel, Germany; Hummel *et al.*, 1997) is a forced-choice assessment of olfactory function. The examination comprises 16 odors, each embedded in markers. Participants are instructed to sniff the odors in a birhinal manner and select the correct odor from four alternatives (as shown in Table 8). A score below 10 indicates a diminished ability to identify odors, while a score above indicates normal olfactory function (MediSense®, 2019).

The alternative options for odor identification were provided in German, based on the specific test kit used in this study. For 10 out of 29 participants who were not German speakers, the options were translated into English if needed.

Table 8. Sniffin' Sticks 16-item test for odor identification. Correct items are marked in **bold**. Choices for odor identification were provided in German, based on the specific test kit used in the study. For the participants who were not German speakers (10 out of 29 participants), the choices were translated if necessary.

| Marker Number | Alternatives Choices for Odor Identification | | | |
|---------------|--|--------------------|-------------------|------------------|
| 1 | Orange | Brombeere | Erdbeere | Ananas |
| 2 | Rauch | Klebstoff | Schuhleder | Gras |
| 3 | Honig | Vanille | Schokolade | Zimt |
| 4 | Schnittlauch | Pfefferminz | Fichte | Zwiebel |
| 5 | Kokos | Banane | Walnuß | Kirsche |
| 6 | Pfisch | Apfel | Zitrone | Grapefruit |
| 7 | Lakritz | Gummi-bärchen | Kaugummi | Kekse |
| 8 | Senf | Gummi | Menthol | Terpentin |
| 9 | Zwiebel | Sauerkraut | Knoblauch | Möhren |
| 10 | Zigarette | Kaffee | Wein | Kerzenrauch |
| 11 | Melone | Pfirsicht | Orange | Apfel |
| 12 | Gewürznelke | Pfeffer | Zimt | Senf |
| 13 | Birne | Plfaume | Pfirsich | Ananas |
| 14 | Kamille | Himbeere | Rose | Kirsche |
| 15 | Anis | Rum | Honig | Fichte |

| | | | | |
|----|------|-------|------|----------|
| 16 | Brot | Fisch | Käse | Schinken |
|----|------|-------|------|----------|

D. fMRIPrep Preprocessing Boilerplate

Results included in this manuscript come from preprocessing performed using **fMRIPrep** 20.2.1 (@fmrip1; @fmrip2; RRID:SCR_016216), which is based on **Nipype** 1.5.1 (@nipype1; @nipype2; RRID:SCR_002502).

Anatomical data preprocessing

: A total of 1 T1-weighted (T1w) images were found within the input BIDS dataset. The T1-weighted (T1w) image was corrected for intensity non-uniformity (INU) with ``N4BiasFieldCorrection`` [n4], distributed with ANTs 2.3.3 [ants, RRID:SCR_004757], and used as T1w-reference throughout the workflow. The T1w-reference was then skull-stripped with a **Nipype** implementation of the ``antsBrainExtraction.sh`` workflow (from ANTs), using OASIS30ANTs as target template. Brain tissue segmentation of cerebrospinal fluid (CSF), white-matter (WM) and gray-matter (GM) was performed on the brain-extracted T1w using ``fast`` [FSL 5.0.9, RRID:SCR_002823, @fsl_fast].

Brain surfaces were reconstructed using ``recon-all`` [FreeSurfer 6.0.1, RRID:SCR_001847, @fs_reconall], and the brain mask estimated previously was refined with a custom variation of the method to reconcile ANTs-derived and FreeSurfer-derived segmentations of the cortical gray-matter of Mindboggle [RRID:SCR_002438, @mindboggle]. Volume-based spatial normalization to one standard space (MNI152NLin2009cAsym) was performed through nonlinear registration with ``antsRegistration`` (ANTs 2.3.3), using brain-extracted versions of both T1w reference and the T1w template. The following template was selected for spatial normalization: **ICBM 152 Nonlinear Asymmetrical template version 2009c** [mni152nlin2009casym, RRID:SCR_008796; TemplateFlow ID: MNI152NLin2009cAsym],

Functional data preprocessing

: For each of the 3 BOLD runs found per subject (across all tasks and sessions), the following preprocessing was performed. First, a reference volume and its skull-stripped version were generated using a custom methodology of **fMRIPrep**. A B0-nonuniformity

map (or **fieldmap**) was estimated based on a phase-difference map calculated with a dual-echo GRE (gradient-recall echo) sequence, processed with a custom workflow of **SDCFlows** inspired by the [*epidewarp.fsl`script`*](<http://www.nmr.mgh.harvard.edu/~greve/fbirn/b0/epidewarp.fsl>) and further improvements in HCP Pipelines [*@hcpipelines*]. The **fieldmap** was then co-registered to the target EPI (echo-planar imaging) reference run and converted to a displacements field map (amenable to registration tools such as ANTs) with FSL's *`fugue`* and other **SDCflows** tools. Based on the estimated susceptibility distortion, a corrected EPI (echo-planar imaging) reference was calculated for a more accurate co-registration with the anatomical reference. The BOLD reference was then co-registered to the T1w reference using *`bbregister`* (FreeSurfer) which implements boundary-based registration [*@bbr*]. Co-registration was configured with six degrees of freedom. Head-motion parameters with respect to the BOLD reference (transformation matrices, and six corresponding rotation and translation parameters) are estimated before any spatiotemporal filtering using *`mcflirt`* [FSL 5.0.9, *@mcflirt*]. BOLD runs were slice-time corrected using *`3dTshift`* from AFNI 20160207 [*@afni*, RRID:SCR_005927]. The BOLD time-series (including slice-timing correction when applied) were resampled onto their original, native space by applying a single, composite transform to correct for head-motion and susceptibility distortions. These resampled BOLD time-series will be referred to as **preprocessed BOLD in original space**, or just **preprocessed BOLD**.

The BOLD time-series (including slice-timing correction when applied) were resampled onto their original, native space by applying a single, composite transform to correct for head-motion and susceptibility distortions. These resampled BOLD time-series will be referred to as **preprocessed BOLD in original space**, or just **preprocessed BOLD**. The BOLD time-series were resampled into standard space, generating a **preprocessed BOLD run in MNI152NLin2009cAsym space**. First, a reference volume and its skull-stripped version were generated using a custom methodology of **fMRIPrep**.

Several confounding time-series were calculated based on the **preprocessed BOLD**: framewise displacement (FD), DVARS and three region-wise global signals. FD was computed using two formulations following Power (absolute sum of relative motions,

@power_fd_dvars) and Jenkinson (relative root mean square displacement between affines, @mcflirt). FD and DVARS are calculated for each functional run, both using their implementations in *Nipype* [following the definitions by @power_fd_dvars]. The three global signals are extracted within the CSF, the WM, and the whole-brain masks. Additionally, a set of physiological regressors were extracted to allow for component-based noise correction [*CompCor*, @compcor]. Principal components are estimated after high-pass filtering the *preprocessed BOLD* time-series (using a discrete cosine filter with 128s cut-off) for the two *CompCor* variants: temporal (tCompCor) and anatomical (aCompCor). tCompCor components are then calculated from the top 2% variable voxels within the brain mask. For aCompCor, three probabilistic masks (CSF, WM and combined CSF+WM) are generated in anatomical space. The implementation differs from that of Behzadi et al. in that instead of eroding the masks by 2 pixels on BOLD space, the aCompCor masks are subtracted a mask of pixels that likely contain a volume fraction of GM. This mask is obtained by dilating a GM mask extracted from the FreeSurfer's *aseg* segmentation, and it ensures components are not extracted from voxels containing a minimal fraction of GM. Finally, these masks are resampled into BOLD space and binarized by thresholding at 0.99 (as in the original implementation). Components are also calculated separately within the WM and CSF masks. For each CompCor decomposition, the *k* components with the largest singular values are retained, such that the retained components' time series are sufficient to explain 50 percent of variance across the nuisance mask (CSF, WM, combined, or temporal). The remaining components are dropped from consideration.

The head-motion estimates calculated in the correction step were also placed within the corresponding confounds file. The confound time series derived from head motion estimates and global signals were expanded with the inclusion of temporal derivatives and quadratic terms for each [@confounds_satterthwaite_2013]. Frames that exceeded a threshold of 0.5 mm FD or 1.5 standardised DVARS were annotated as motion outliers.

All resamplings can be performed with *a single interpolation step* by composing all the pertinent transformations (i.e. head-motion transform matrices, susceptibility distortion correction when available, and co-registrations to anatomical and output spaces). Gridded

(volumetric) resamplings were performed using ``antsApplyTransforms`` (ANTs), configured with Lanczos interpolation to minimize the smoothing effects of other kernels [[@lanczos](#)]. Non-gridded (surface) resamplings were performed using ``mri_vol2surf`` (FreeSurfer).

Many internal operations of `*fMRIPrep*` use `*Nilearn*` 0.6.2 [[@nilearn](#), RRID:SCR_001362], mostly within the functional processing workflow. For more details of the pipeline, see [the section corresponding to workflows in `*fMRIPrep*`'s documentation](<https://fmriprep.readthedocs.io/en/latest/workflows.html> "fMRIPrep's documentation").

Copyright Waiver

The above boilerplate text was automatically generated by fMRIPrep with the express intention that users should copy and paste this text into their manuscripts **unchanged**. It is released under the [CC0](<https://creativecommons.org/publicdomain/zero/1.0/>) license.

E. Behavioral Results – Odor Rating Scores

Figures 45-49 below depict the odor valence ratings acquired in the behavioral experiment, both *before* and *after* the neuroimaging, as well as during the neuroimaging experiment at the scanner. Participants were instructed to rate odors (negative, positive, CS+ appetitive, CS+ aversive, and CS-) using a 10-point Likert scale. The left panels represent the results from odor set A, right panels from odor set B. The top panels show the ratings obtained before and after the neuroimaging experiment, while the bottom panels show the ratings obtained during the neuroimaging experiment.



Figure 45. Valence results from the behavioral experiment involving negative odor rating. The top panels display the results obtained before (blue bars) and after (red bars) the neuroimaging experiment, while the bottom panels show the results obtained during the neuroimaging experiment (average rating of 14 trials, indicated using button press). The left panels present the results from odor set A (fish sauce), while the right panels show the results from odor set B (rotten egg). The y-axes indicate odor valence, which was rated on a 10-point Likert scale ranging from 0 (most disliked sensation imaginable) to 10 (most liked sensation imaginable). The x-axes indicate participant IDs. Dotted lines express the group means.

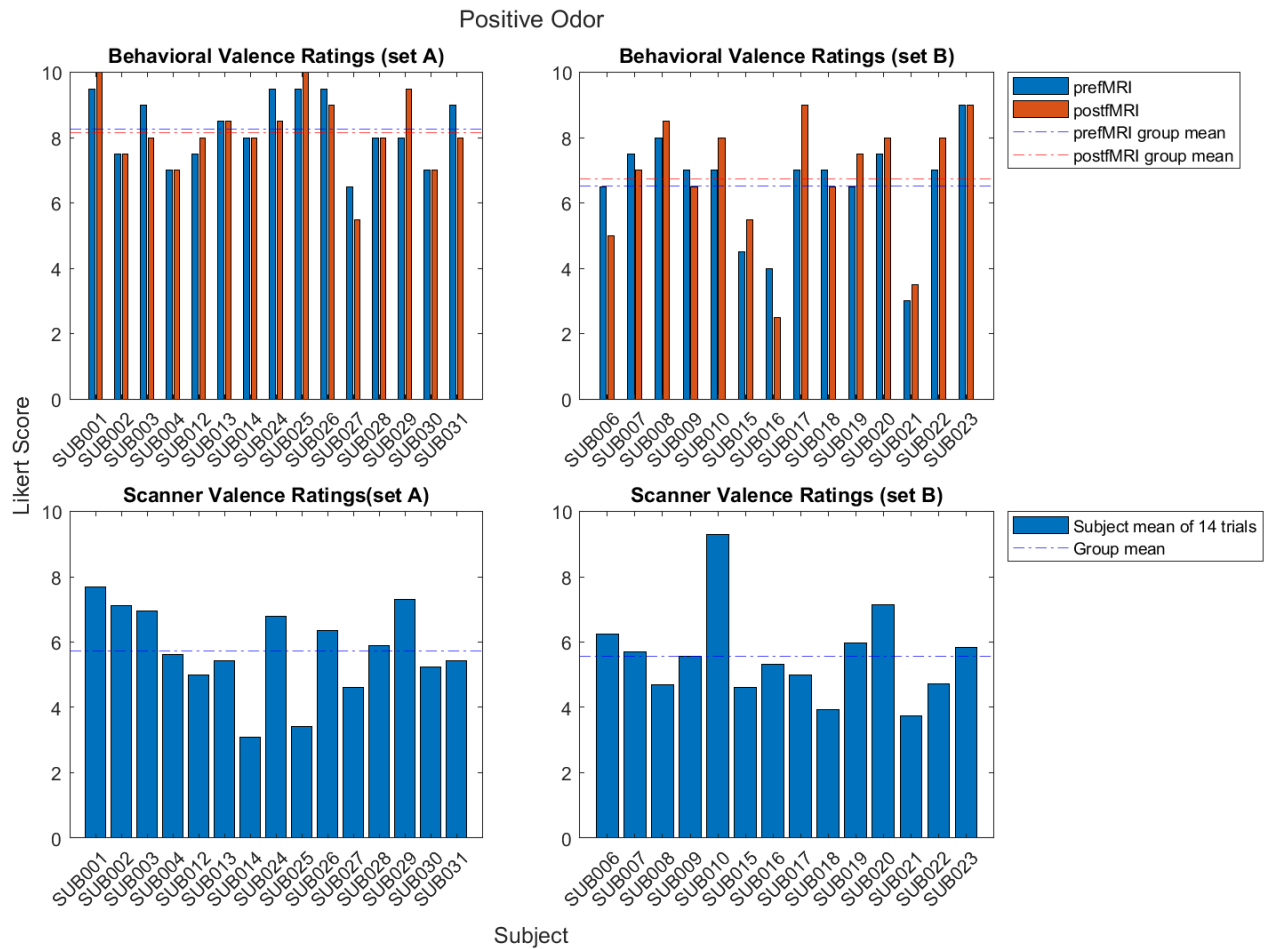


Figure 46. Valence results from the behavioral experiment involving positive odor rating. The top panels display the results obtained before (blue bars) and after (red bars) the neuroimaging experiment, while the bottom panels show the results obtained during the neuroimaging experiment (average rating of 14 trials, indicated using button press). The left panels present the results from odor set A (orange), while the right panels show the results from odor set B (jasmin). The y-axes indicate odor valence, which was rated on a 10-point Likert scale ranging from 0 (most disliked sensation imaginable) to 10 (most liked sensation imaginable). The x-axes indicate participant IDs. Dotted lines express the group means.



Figure 47. Valence results from the behavioral experiment involving CS+ appetitive odor rating. The top panels display the results obtained before (blue bars) and after (red bars) the neuroimaging experiment, while the bottom panels show the results obtained during the neuroimaging experiment (average rating of 14 trials, indicated using a button press). The left panels present the results from odor set A (musk), while the right panels show the results from odor set B (potato chips). The y-axes indicate odor valence, which was rated on a 10-point Likert scale ranging from 0 (most disliked sensation imaginable) to 10 (most liked sensation imaginable). The x-axes indicate participant IDs. Dotted lines express the group means.



Figure 48. Valence results from the behavioral experiment involving CS+ aversive odor rating. The top panels display the results obtained before (blue bars) and after (red bars) the neuroimaging experiment, while the bottom panels show the results obtained during the neuroimaging experiment (average rating of 14 trials, indicated using a button press). The left panels present the results from odor set A (benzoyl), while the right panels show the results from odor set B (karmaflor). The y-axes indicate odor valence, which was rated on a 10-point Likert scale ranging from 0 (most disliked sensation imaginable) to 10 (most liked sensation imaginable). The x-axes indicate participant IDs. Dotted lines express the group means.

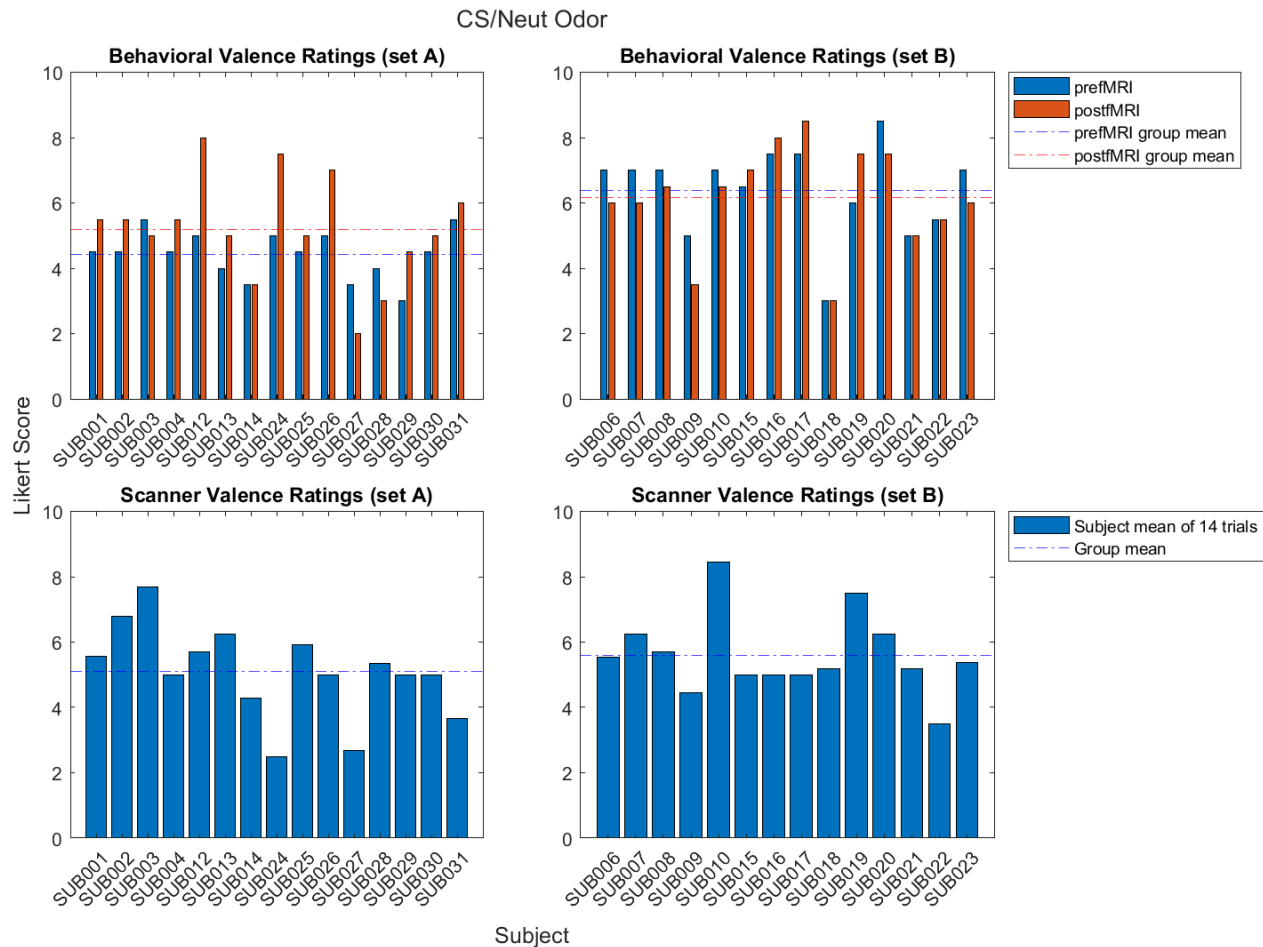


Figure 49. Valence results from the behavioral experiment involving CS- odor rating (i.e., the neutral odor that was not conditioned). The top panels display the results obtained before (blue bars) and after (red bars) the neuroimaging experiment, while the bottom panels show the results obtained during the neuroimaging experiment (average rating of 14 trials, indicated using a button press). The left panels present the results from odor set A (basil), while the right panels show the results from odor set B (vanillin). The y-axes indicate odor valence, which was rated on a 10-point Likert scale ranging from 0 (most disliked sensation imaginable) to 10 (most liked sensation imaginable). The x-axes indicate participant IDs. Dotted lines express the group means.

F. Neuroimaging Experiment– Reaction Time

Figures 50-51 below illustrate the reaction times collected during the neuroimaging experiment. During runs 1 (reference) and 3 (extinction), participants were asked to rate odor valence using a Likert score. The scores were collected using a bottom box. Their reaction times to the rating were collected, as shown below. Each odor was presented 14 times (trials), wherefrom the average reaction time is depicted below.

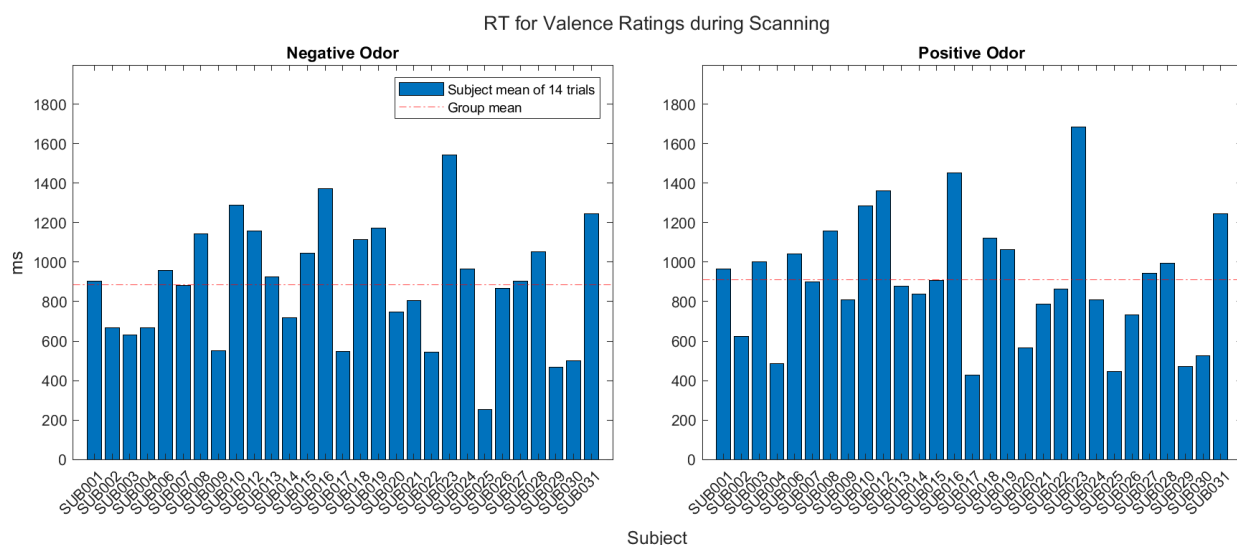


Figure 50. Reaction times were collected during the first run (reference), where participants were asked to rate the valence of negative and positive odors. Figures depict the average reaction times from the 14 trials.

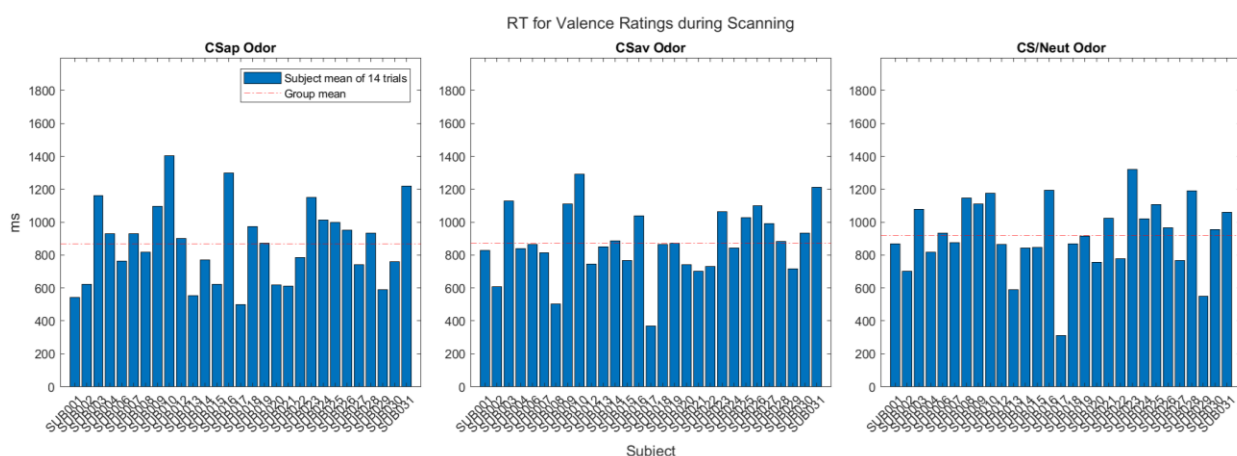


Figure 51. Reaction times were collected during the third run (extinction), where participants were asked to rate the valence of CS appetitive (CSap), CS aversive (CSav), and CS- neutral odor. Figures depict the average reaction times from the 14 trials.

G. Neuroimaging Experiment – RSA Clusters

Table 9 below illustrates the clusters identified through MVPA RSA using a single target matrix approach, which encompasses both conditioning and extinction phases in one RDM. Results are adjusted for multiple corrections with TFCE (Smith & Nichols, 2009) and a total of 10'000 Monte Carlo iterations with a corrected cluster threshold of $p = 0.05$. The table displays positive activations (one-tailed) that surpassed the threshold of 1.6449. Clusters were automatically identified using AtlasReader (cluster_extent = 0, voxel_tresh = 0; version 0.1.2.; Notter *et al.*, 2019).

Table 9. Positive activations (one-tailed) identified through MVPA RSA using a single target matrix approach, exceeding the threshold of 1.6449.

| cluster_id | peak_x | peak_y | peak_z | cluster_mean | volume_mm | aal | desikan_killiany | harvard_oxford |
|-------------------|---------------|---------------|---------------|---------------------|------------------|---------------------------|-------------------------|-----------------------|
| 1 | -12 | -64 | -8 | 5.72343 | 1.8994e+06 | 25.39% no_label | 25.87% Unknown | |
| 2 | 20 | -44 | -58 | 2.11871 | 24 | 100.00% Cerebellum_8_R | 66.67% Unknown | |
| 3 | -18 | -32 | -60 | 2.06554 | 16 | 100.00% no_label | 100.00% Unknown | 100.00% no_label |
| 4 | 4 | -28 | -62 | 2.03035 | 16 | 100.00% no_label | 100.00% Unknown | 100.00% no_label |
| 5 | 10 | -22 | -60 | 2.02793 | 16 | 100.00% no_label | 100.00% Unknown | 100.00% no_label |
| 6 | -20 | -34 | -60 | 2.01923 | 8 | 100.00% no_label | 100.00% Unknown | 100.00% no_label |
| 7 | -16 | -32 | -56 | 2.14359 | 8 | 100.00% no_label | 100.00% Unknown | 100.00% no_label |
| 8 | -14 | -32 | -58 | 1.99246 | 8 | 100.00% no_label | 100.00% Unknown | 100.00% no_label |
| 9 | 2 | -30 | -56 | 2.00348 | 8 | 100.00% no_label | 100.00% Unknown | 100.00% Brain-Stem |
| 10 | 6 | -30 | -60 | 2.35224 | 8 | 100.00% no_label | 100.00% Unknown | 100.00% no_label |
| 11 | 12 | -42 | -56 | 2.01963 | 8 | 100.00% Cerebellum_9_R | 100.00% Unknown | 100.00% no_label |

7 REFERENCES

- Alahäivälä, A. L. I., Thaploo, D., Wein, S., Seidel, P., Riebel, M., Hummel, T., & Schwarzbach, J. V. (2023). Inhalation-Modulated Detection of Olfactory BOLD Responses in The Human Brain. In Preparation.
- Anderson, A. K., Christoff, K., Stappen, I., Panitz, D., Ghahremani, D. G., Glover, G., Gabrieli, J. D. E., & Sobel, N. (2003). Dissociated neural representations of intensity and valence in human olfaction. *Nature Neuroscience*, 6(2), 196–202.
- Andreatta, M., & Pauli, P. (2015). Appetitive vs. aversive conditioning in humans. *Frontiers in Behavioral Neuroscience*, 9, 128.
- Andreatta, M., Fendt, M., Mühlberger, A., Wieser, M. J., Imobersteg, S., Yarali, A., Gerber, B., & Pauli, P. (2012). Onset and offset of aversive events establish distinct memories requiring fear and reward networks. *Learning & Memory*, 19(11), 518–526.
- Anonymous. (1970). No Title. *Chem Rundschau*, 37(821).
- Arbabshirani, M. R., Plis, S., Sui, J., & Calhoun, V. D. (2017). Single subject prediction of brain disorders in neuroimaging: Promises and pitfalls. *Neuroimage*, 145, 137–165.
- Arshamian, A., Gerkin, R. C., Kruspe, N., Whuk, E., Floyd, S., O'Meara, C., Rodriguez, G. G., Lundström, J. N., Mainland, J. D., & Majid, A. (2022). The perception of odor pleasantness is shared across cultures. *Current Biology*, 32(9), 2061–2066.
- Asogwa, C. (2019). Quantum Biology: Can we explain olfaction using quantum phenomenon? *ArXiv Preprint ArXiv:1911.02529*.
- Auffarth, B. (2013). Understanding smell—The olfactory stimulus problem. *Neuroscience & Biobehavioral Reviews*, 37(8), 1667–1679.
- Austin, A. J., & Duka, T. (2010). Mechanisms of attention for appetitive and aversive outcomes in Pavlovian conditioning. *Behavioural Brain Research*, 213(1), 19–26.

- Bach, D. R., Weiskopf, N., & Dolan, R. J. (2011). A stable sparse fear memory trace in human amygdala. *Journal of Neuroscience*, 31(25), 9383–9389.
- Baker, B., Lansdell, B., & Kording, K. P. (2022). Three aspects of representation in neuroscience. *Trends in Cognitive Sciences*, 26(11), 942–958.
- Barbas, H., Saha, S., Rempel-Clower, N., & Ghashghaei, T. (2003). Serial pathways from primate prefrontal cortex to autonomic areas may influence emotional expression. *BMC Neuroscience*, 4(1), 1–12.
- Bennett, C. M., Miller, M. B., & Wolford, G. L. (2009). Neural correlates of interspecies perspective taking in the post-mortem Atlantic Salmon: An argument for multiple comparisons correction. *Neuroimage*, 47(Suppl 1), S125.
- Bensafi, M. (2012). The role of the piriform cortex in human olfactory perception: insights from functional neuroimaging studies. *Chemosensory Perception*, 5(1), 4–10.
- Bensafi, M., Rouby, C., Farget, V., Bertrand, B., Vigouroux, M., & Holley, A. (2003). Perceptual, affective, and cognitive judgments of odors: pleasantness and handedness effects. *Brain and Cognition*, 51(3), 270–275. [https://doi.org/10.1016/S0278-2626\(03\)00019-8](https://doi.org/10.1016/S0278-2626(03)00019-8)
- Bissonette, G. B., Gentry, R. N., Padmala, S., Pessoa, L., & Roesch, M. R. (2014). Impact of appetitive and aversive outcomes on brain responses: linking the animal and human literatures. *Frontiers in Systems Neuroscience*, 8, 24.
- Boesveldt, S., Frasnelli, J., Gordon, A. R., & Lundström, J. N. (2010). The fish is bad: negative food odors elicit faster and more accurate reactions than other odors. *Biological Psychology*, 84(2), 313–317.
- Brainard, D. H. (1997). The Psychophysics Toolbox. *Spatial Vision*, 10(4), 433–436.
- Brann, D. H., & Datta, S. R. (2020). Finding the brain in the nose. *Annual Review of Neuroscience*, 43, 277–295.
- Bregman, A. (1990). *Auditory Scene Analysis: The Perceptual Organization of Sound*. Massachusetts Institute of Technology. Cambridge, Mass: MIT Press.

- Büchel, C, Holmes, A. P., Rees, G., & Friston, K. J. (1998). Characterizing stimulus–response functions using nonlinear regressors in parametric fMRI experiments. *Neuroimage*, 8(2), 140–148.
- Büchel, Christian, Morris, J., Dolan, R. J., & Friston, K. J. (1998). Brain systems mediating aversive conditioning: an event-related fMRI study. *Neuron*, 20(5), 947–957.
- Buck, L., & Axel, R. (1991). A novel multigene family may encode odorant receptors: a molecular basis for odor recognition. *Cell*, 65(1), 175–187.
- Bulthé, J., De Smedt, B., & de Beeck, H. P. O. (2014). Format-dependent representations of symbolic and non-symbolic numbers in the human cortex as revealed by multi-voxel pattern analyses. *NeuroImage*, 87, 311–322.
- Bulthé, J., van den Hurk, J., Daniels, N., De Smedt, B., & de Beeck, H. P. O. (2014). A validation of a multi-spatial-scale method for multivariate pattern analysis. 2014 International Workshop on Pattern Recognition in Neuroimaging, 1–4.
- Caffier, P. P., Erdmann, U., & Ullsperger, P. (2003). Experimental evaluation of eye-blink parameters as a drowsiness measure. *European Journal of Applied Physiology*, 89(3), 319–325.
- Cain, W. S. (1976). Olfaction and the common chemical sense: some psychophysical contrasts. *Sensory Processes*, 1(1), 57–67.
- Carrie, S., Scannell, J. W., & Dawes, P. J. D. (1999). The smell map: is there a commonality of odour perception? *Clinical Otolaryngology & Allied Sciences*, 24(3), 184–189.
- Chang, L. (2021). Modeling Single Subject Data. DartBrains. https://dartbrains.org/content/GLM_Single_Subject_Model.html#noise-covariates
- Chang, L. J., Huckins, J., Cheong, J. H., Brietzke, S., Lindquist, M. A., & Wager, T. D. (2020). *ljchang/dartbrains*: An online open access resource for learning functional neuroimaging analysis methods in Python. Zenodo.
- Connor, C. E. (2005). Friends and grandmothers. *Nature*, 435(7045), 1036–1037.

- Costafreda, S. G., Brammer, M. J., David, A. S., & Fu, C. H. Y. (2008). Predictors of amygdala activation during the processing of emotional stimuli: a meta-analysis of 385 PET and fMRI studies. *Brain Research Reviews*, 58(1), 57–70.
- Croy, I., & Hummel, T. (2017). Olfaction as a marker for depression. *Journal of Neurology*, 264(4), 631–638.
- Croy, I., Krone, F., Walker, S., & Hummel, T. (2015). Olfactory processing: Detection of rapid changes. *Chemical Senses*, 40(5), 351–355.
- Damadian, R., Goldsmith, M., & Minkoff, L. (1977). Nmr in cancer: Xvi. fonar image of the live human body. *Physiol. Chem*, 9, 97–100.
- Dawes, P. J. D., Dawes, M. T., & Williams, S. M. (2004). The smell map: commonality of odour perception confirmed 1. *Clinical Otolaryngology & Allied Sciences*, 29(6), 648–654.
- Delgado, M. R., Jou, R. L., & Phelps, E. A. (2011). Neural systems underlying aversive conditioning in humans with primary and secondary reinforcers. *Frontiers in Neuroscience*, 5(MAY), 1–10. <https://doi.org/10.3389/fnins.2011.00071>
- Delgado, M. R., Labouliere, C. D., & Phelps, E. A. (2006). Fear of losing money? Aversive conditioning with secondary reinforcers. *Social Cognitive and Affective Neuroscience*, 1(3), 250–259. <https://doi.org/10.1093/scan/nsi025>
- Descartes, R. (2013). *Meditations on first philosophy*. Broadview Press.
- Diedrichsen, J., & Kriegeskorte, N. (2017). Representational models: A common framework for understanding encoding, pattern-component, and representational-similarity analysis. *PLoS Computational Biology*, 13(4), e1005508.
- Dietrich, E. (2007). Representation. In P. Thagard (Ed.), *Philosophy of Psychology and Cognitive Science* (pp. 1–29). Amsterdam: Elsevier.
- Dikeçligil, G. N., & Gottfried, J. A. (2024). What Does the Human Olfactory System Do, and How Does It Do It? *Annual Review of Psychology*, 75, 155–181.

- Donders, F. C. (1868). Over de snelheid van psychische processen [On the speed of mental processes]. *Onderzoekingen Gedaan in Het Physiologisch Laboratorium Der Utrechtsche Hoogeschool*, Transl. by W. G. Koster (1969), *Atten. Perform.* 2, Tweeds ree(||), 92–120.
- Doty, R. L. (2015). *Handbook of olfaction and gustation*. John Wiley & Sons.
- Doty, R. L., Brugger, W. E., Jurs, P. C., Orndorff, M. A., Snyder, P. J., & Lowry, L. D. (1978). Intranasal trigeminal stimulation from odorous volatiles: psychometric responses from anosmic and normal humans. *Physiology & Behavior*, 20(2), 175–185.
- Doty, R. L., Shaman, P., & Dann, M. (1984). Development of the University of Pennsylvania Smell Identification Test: a standardized microencapsulated test of olfactory function. *Physiology & Behavior*, 32(3), 489–502.
- Dufossé, L., Latrasse, A., & Spinnler, H.-E. (1994). Importance des lactones dans les arômes alimentaires: structure, distribution, propriétés sensorielles et biosynthèse. *Sciences Des Aliments*.
- Dujmović, M., Bowers, J. S., Adolphi, F., & Malhotra, G. (2022). The pitfalls of measuring representational similarity using representational similarity analysis. *BioRxiv*, 2022.04.05.487135. <https://doi.org/10.1101/2022.04.05.487135>
- Dunsmoor, J. E., Kragel, P. A., Martin, A., La Bar, K. S., LaBar, K. S., & La Bar, K. S. (2014). Aversive learning modulates cortical representations of object categories. *Cerebral Cortex*, 24(11), 2859–2872. <https://doi.org/10.1093/cercor/bht138>
- Ecker, A. (1857). Ueber die Geruchsschleimhaut des Menschen. *Z Wiss Zool*, 8, 303–306.
- Eisenbarth, H., Chang, L. J., & Wager, T. D. (2016). Multivariate brain prediction of heart rate and skin conductance responses to social threat. *Journal of Neuroscience*, 36(47), 11987–11998.
- Ekman, P. (1992). An argument for basic emotions. *Cognition & Emotion*, 6(3), 169–200. <https://doi.org/10.1080/02699939208411068>

- Elsaesser, R., & Paysan, J. (2007). The sense of smell, its signalling pathways, and the dichotomy of cilia and microvilli in olfactory sensory cells. *BMC Neuroscience*, 8(3), 1–13.
- Emberson, L. L., Zinszer, B. D., Raizada, R. D. S., & Aslin, R. N. (2017). Decoding the infant mind: Multivariate pattern analysis (MVPA) using fNIRS. *PloS One*, 12(4), e0172500.
- Eskenazi, B., Cain, W. S., Novelly, R. A., & Friend, K. B. (1983). Olfactory functioning in temporal lobectomy patients. *Neuropsychologia*, 21(4), 365–374.
- Eskenazi, B., Cain, W. S., Novelly, R. A., & Mattson, R. (1986). Odor perception in temporal lobe epilepsy patients with and without temporal lobectomy. *Neuropsychologia*, 24(4), 553–562.
- Esteban, O., Markiewicz, C. J., Blair, R. W., Moodie, C. A., Isik, A. I., Erramuzpe, A., Kent, J. D., Goncalves, M., DuPre, E., & Snyder, M. (2019). fMRIPrep: a robust preprocessing pipeline for functional MRI. *Nature Methods*, 16(1), 111–116.
- Etzel, J. A., Zacks, J. M., & Braver, T. S. (2013). Searchlight analysis: promise, pitfalls, and potential. *Neuroimage*, 78, 261–269.
- Ferdenzi, C., Joussain, P., Digard, B., Luneau, L., Djordjevic, J., & Bensafi, M. (2017). Individual differences in verbal and non-verbal affective responses to smells: influence of odor label across cultures. *Chemical Senses*, 42(1), 37–46.
- Ferdenzi, C., Poncelet, J., Rouby, C., & Bensafi, M. (2014). Repeated exposure to odors induces affective habituation of perception and sniffing. *Frontiers in Behavioral Neuroscience*, 8, 119. <https://doi.org/10.3389/fnbeh.2014.00119>
- Flenady, T., Dwyer, T., & Applegarth, J. (2017). Accurate respiratory rates count: So should you! *Australasian Emergency Nursing Journal*, 20(1), 45–47.
- Fournel, A., Ferdenzi, C., Sezille, C., Rouby, C., & Bensafi, M. (2016). Multidimensional representation of odors in the human olfactory cortex. *Human Brain Mapping*, 37(6), 2161–2172. <https://doi.org/10.1002/hbm.23164>

- Frasnelli, J., Schuster, B., & Hummel, T. (2007). Interactions between olfaction and the trigeminal system: what can be learned from olfactory loss. *Cerebral Cortex*, 17(10), 2268–2275.
- Freiherr, J. (2017). Cortical olfactory processing. In *Springer handbook of odor* (pp. 97–98). Springer.
- Friston, K. J., Holmes, A. P., Price, C. J., Büchel, C., & Worsley, K. J. (1999). Multisubject fMRI studies and conjunction analyses. *Neuroimage*, 10(4), 385–396.
- Friston, K. J., Penny, W. D., & Glaser, D. E. (2005). Conjunction revisited. *Neuroimage*, 25(3), 661–667.
- Fullana, M. A., Harrison, B. J., Soriano-Mas, C., Vervliet, B., Cardoner, N., Àvila-Parcet, A., & Radua, J. (2016). Neural signatures of human fear conditioning: An updated and extended meta-analysis of fMRI studies. *Molecular Psychiatry*, 21(4), 500–508. <https://doi.org/10.1038/mp.2015.88>
- Gabbott, P., Warner, T., Brown, J., Salway, P., Gabbott, T., & Busby, S. (2012). Amygdala afferents monosynaptically innervate corticospinal neurons in rat medial prefrontal cortex. *Journal of Comparative Neurology*, 520(11), 2440–2458.
- Gagnon, L., & Peretz, I. (2000). Laterality effects in processing tonal and atonal melodies with affective and nonaffective task instructions. *Brain and Cognition*.
- Galvin, R. J., Regan, D., & Heron, J. R. (1976). Impaired temporal resolution of vision after acute retrobulbar neuritis. *Brain: A Journal of Neurology*, 99(2), 255–268.
- Genva, M., Kenne Kemene, T., Deleu, M., Lins, L., & Fauconnier, M.-L. (2019). Is It Possible to Predict the Odor of a Molecule on the Basis of its Structure? *International Journal of Molecular Sciences*, 20(12), 3018.
- Glover, G. H., & Lee, A. T. (1995). Motion artifacts in fMRI: comparison of 2DFT with PR and spiral scan methods. *Magnetic Resonance in Medicine*, 33(5), 624–635.
- Goldstein, N. (2002). Getting to know the odor compounds. *Biocycle*, 43(7), 42.

- Gorgolewski, K. J., Auer, T., Calhoun, V. D., Craddock, R. C., Das, S., Duff, E. P., Flandin, G., Ghosh, S. S., Glatard, T., & Halchenko, Y. O. (2016). The brain imaging data structure, a format for organizing and describing outputs of neuroimaging experiments. *Scientific Data*, 3(1), 1–9.
- Gorgolewski, K., Burns, C. D., Madison, C., Clark, D., Halchenko, Y. O., Waskom, M. L., & Ghosh, S. S. (2011). Nipype: a flexible, lightweight and extensible neuroimaging data processing framework in python. *Frontiers in Neuroinformatics*, 13.
- Gottfried, J. A. (2006). Smell: central nervous processing. *Taste and Smell*, 63, 44–69.
- Gottfried, J. A. (2015). Structural and functional imaging of the human olfactory system. *Handbook of Olfaction and Gustation*, 279–304.
- Gottfried, J. A., Deichmann, R., Winston, J. S., & Dolan, R. J. (2002). Functional heterogeneity in human olfactory cortex: an event-related functional magnetic resonance imaging study. *Journal of Neuroscience*, 22(24), 10819–10828.
- Gottfried, J. A., O'Doherty, J., & Dolan, R. J. (2002). Appetitive and aversive olfactory learning in humans studied using event-related functional magnetic resonance imaging. *Journal of Neuroscience*, 22(24), 10829–10837.
- Graner, J. L., Stjepanović, D., & LaBar, K. S. (2020). Extinction learning alters the neural representation of conditioned fear. *Cognitive, Affective, & Behavioral Neuroscience*, 20(5), 983–997.
- Gross, C. G. (2002). Genealogy of the “grandmother cell.” *The Neuroscientist*, 8(5), 512–518.
- Gross, C. T., & Canteras, N. S. (2012). The many paths to fear. *Nature Reviews Neuroscience*, 13(9), 651–658. <https://doi.org/10.1038/nrn3301>
- Haehner, A., Hummel, T., Hummel, C., Sommer, U., Junghanns, S., & Reichmann, H. (2007). Olfactory loss may be a first sign of idiopathic Parkinson's disease. *Movement Disorders*, 22(6), 839–842.

- Hampton, A. N., & O'Doherty, J. P. (2007). Decoding the neural substrates of reward-related decision making with functional MRI. *Proceedings of the National Academy of Sciences*, 104(4), 1377–1382.
- Han, P., Zang, Y., Akshita, J., & Hummel, T. (2019). Magnetic Resonance Imaging of Human Olfactory Dysfunction. *Brain Topography*, 32(6), 987–997. <https://doi.org/10.1007/s10548-019-00729-5>
- Handjaras, G., Ricciardi, E., Leo, A., Lenci, A., Cecchetti, L., Cosottini, M., Marotta, G., & Pietrini, P. (2016). How concepts are encoded in the human brain: a modality independent, category-based cortical organization of semantic knowledge. *Neuroimage*, 135, 232–242.
- Haruno, M., & Kawato, M. (2006). Different neural correlates of reward expectation and reward expectation error in the putamen and caudate nucleus during stimulus-action-reward association learning. *Journal of Neurophysiology*, 95(2), 948–959.
- Haruno, M., Kuroda, T., Doya, K., Toyama, K., Kimura, M., Samejima, K., Imamizu, H., & Kawato, M. (2004). A neural correlate of reward-based behavioral learning in caudate nucleus: a functional magnetic resonance imaging study of a stochastic decision task. *Journal of Neuroscience*, 24(7), 1660–1665.
- Hawkes, C. H., Shephard, B. C., & Daniel, S. E. (1997). Olfactory dysfunction in Parkinson's disease. *Journal of Neurology, Neurosurgery & Psychiatry*, 62(5), 436–446.
- Haxby, J. V, Gobbini, M. I., Furey, M. L., Ishai, A., Schouten, J. L., & Pietrini, P. (2001). Distributed and overlapping representations of faces and objects in ventral temporal cortex. *Science*, 293(5539), 2425–2430.
- Haxby, J. V, Guntupalli, J. S., Connolly, A. C., Halchenko, Y. O., Conroy, B. R., Gobbini, M. I., Hanke, M., & Ramadge, P. J. (2011). A common, high-dimensional model of the representational space in human ventral temporal cortex. *Neuron*, 72(2), 404–416.

- Hayes, D. J., Duncan, N. W., Xu, J., & Northoff, G. (2014). A comparison of neural responses to appetitive and aversive stimuli in humans and other mammals. *Neuroscience & Biobehavioral Reviews*, 45, 350–368.
- Hebart, M. N., & Baker, C. I. (2018). Deconstructing multivariate decoding for the study of brain function. *Neuroimage*, 180, 4–18.
- Henkin, R. I. (1977). Defects in taste and smell recognition following temporal lobectomy. *Trans. Am. Neurol. Assoc.*, 102, 146–150.
- Holland, P. C., & Bouton, M. E. (1999). Hippocampus and context in classical conditioning. *Current Opinion in Neurobiology*, 9(2), 195–202.
- Hornuss, D., Lange, B., Schroeter, N., Rieg, S., Kern, W. V., & Wagner, D. (2020). Anosmia in COVID-19 patients. *Clinical Microbiology and Infection*, 26(10), 1426–1427.
- Howard, J. D., Kahnt, T., & Gottfried, J. A. (2016). Converging prefrontal pathways support associative and perceptual features of conditioned stimuli. *Nature Communications*, 7(1), 1–11. <https://doi.org/10.1038/ncomms11546>
- Howard, J. D., Plailly, J., Grueschow, M., Haynes, J.-D., & Gottfried, J. A. (2009). Odor quality coding and categorization in human posterior piriform cortex. *Nature Neuroscience*, 12(7), 932–938.
- Howell, J., Costanzo, R. M., & Reiter, E. R. (2018). Head trauma and olfactory function. *World Journal of Otorhinolaryngology-Head and Neck Surgery*, 4(1), 39–45.
- Huettel, S. A., Song, A. W., & McCarthy, G. (2004). *Functional magnetic resonance imaging* (Vol. 1). Sinauer Associates Sunderland, MA.
- Hummel, T., & Kobal, G. (2001). Olfactory event-related potentials. In S. Simon & M. Nicolelis (Eds.), *Methods and frontiers in chemosensory research* (pp. 429–464).
- Hummel, T., Sekinger, B., Wolf, S. R., Pauli, E., & Kobal, G. (1997). ‘Sniffin’sticks’: olfactory performance assessed by the combined testing of odor identification, odor discrimination and olfactory threshold.’ *Chemical Senses*, 22(1), 39–52.

- Hummel, T., Sekinger, B., Wolf, S. R., Pauli, E., & Kobal, G. (1997). 'Sniffin'sticks': olfactory performance assessed by the combined testing of odor identification, odor discrimination and olfactory threshold.' *Chemical Senses*, 22(1), 39–52.
- Huth, A. G., de Heer, W. A., Griffiths, T. L., Theunissen, F. E., & Gallant, J. L. (2016). Natural speech reveals the semantic maps that tile human cerebral cortex. *Nature*, 532(7600), 453–458. <https://doi.org/10.1038/nature17637>
- Johnson, B. N., Russell, C., Khan, R. M., & Sobel, N. (2006). A comparison of methods for sniff measurement concurrent with olfactory tasks in humans. *Chemical Senses*, 31(9), 795–806.
- Johnson, B., & Leon, M. (2009). Glomerular Map. In M. D. Binder, N. Hirokawa, & U. Windhorst (Eds.), *Encyclopedia of Neuroscience* (pp. 1745–1748). Springer Berlin Heidelberg. https://doi.org/10.1007/978-3-540-29678-2_2024
- Johnson, D. M. G., Illig, K. R., Behan, M., & Haberly, L. B. (2000). New features of connectivity in piriform cortex visualized by intracellular injection of pyramidal cells suggest that “primary” olfactory cortex functions like “association” cortex in other sensory systems. *Journal of Neuroscience*, 20(18), 6974–6982.
- Johnson, R. A., & Bhattacharyya, G. K. (2019). *Statistics: principles and methods*. John Wiley & Sons.
- Jones-Gotman, M., & Zatorre, R. J. (1988). Olfactory identification deficits in patients with focal cerebral excision. *Neuropsychologia*, 26(3), 387–400.
- Jones-Gotman, M., & Zatorre, R. J. (1993). Odor recognition memory in humans: role of right temporal and orbitofrontal regions. *Brain and Cognition*, 22(2), 182–198.
- Kadohisa, M. (2013). Effects of odor on emotion, with implications. *Frontiers in Systems Neuroscience*, 7, 66.
- Kahnt, T., Heinzle, J., Park, S. Q., & Haynes, J.-D. (2011). Decoding different roles for vmPFC and dlPFC in multi-attribute decision making. *Neuroimage*, 56(2), 709–715.

- Keefe, J. O., & Nadel, L. (1978). *The hippocampus as a cognitive map*. Clarendon Press.
- Kesner, R. P., & Rolls, E. T. (2015). A computational theory of hippocampal function, and tests of the theory: new developments. *Neuroscience & Biobehavioral Reviews*, 48, 92–147.
- Kesner, R. P., Gilbert, P. E., & Barua, L. A. (2002). The role of the hippocampus in memory for the temporal order of a sequence of odors. *Behavioral Neuroscience*, 116(2), 286.
- Keverne, E. B., Murphy, C. L., Silver, W. L., Wysocki, C. J., & Meredith, M. (1986). Non-olfactory chemoreceptors of the nose: recent advances in understanding the vomeronasal and trigeminal systems. *Chemical Senses*, 11(1), 119–133.
- Kim, S. H., Yoon, H. S., Kim, H., & Hamann, S. (2014). Individual differences in sensitivity to reward and punishment and neural activity during reward and avoidance learning. *Social Cognitive and Affective Neuroscience*, 10(9), 1219–1227. <https://doi.org/10.1093/scan/nsv007>
- Klucken, T., Schweckendiek, J., Merz, C. J., Tabbert, K., Walter, B., Kagerer, S., Vaitl, D., & Stark, R. (2009). Neural activations of the acquisition of conditioned sexual arousal: Effects of contingency awareness and sex. *The Journal of Sexual Medicine*, 6(11), 3071–3085.
- Klucken, T., Wehrum, S., Schweckendiek, J., Merz, C. J., Hennig, J., Vaitl, D., & Stark, R. (2013). The 5-HTTLPR polymorphism is associated with altered hemodynamic responses during appetitive conditioning. *Human Brain Mapping*, 34(10), 2549–2560.
- Kobal, G., Hummel, T. H., Sekinger, B., Barz, S., Roscher, S., & Wolf, S. (1996). “Sniffin’sticks”: screening of olfactory performance. *Rhinology*, 34(4), 222–226.
- Kragel, P. A., & LaBar, K. S. (2015). Multivariate neural biomarkers of emotional states are categorically distinct. *Social Cognitive and Affective Neuroscience*, 10(11), 1437–1448.

- Kragel, P. A., Koban, L., Barrett, L. F., & Wager, T. D. (2018). Representation, pattern information, and brain signatures: from neurons to neuroimaging. *Neuron*, 99(2), 257–273.
- Kriegeskorte, N. (2008). Representational similarity analysis – connecting the branches of systems neuroscience. *Frontiers in Systems Neuroscience*, 2(November), 1–28. <https://doi.org/10.3389/neuro.06.004.2008>
- Kriegeskorte, N., Goebel, R., & Bandettini, P. (2006). Information-based functional brain mapping. *Proceedings of the National Academy of Sciences of the United States of America*, 103(10), 3863–3868.
- LaBar, K. S., Gatenby, J. C., Gore, J. C., LeDoux, J. E., & Phelps, E. A. (1998). Human amygdala activation during conditioned fear acquisition and extinction: a mixed-trial fMRI study. *Neuron*, 20(5), 937–945.
- Larsson, M., & Willander, J. (2009). Autobiographical odor memory. *Annals of the New York Academy of Sciences*, 1170(1), 318–323.
- Laska, M., & Ringh, A. (2010). How big is the gap between olfactory detection and recognition of aliphatic aldehydes? *Attention, Perception, & Psychophysics*, 72(3), 806–812.
- Lee, I.-S., Jung, W., Park, H.-J., & Chae, Y. (2020). Spatial information of somatosensory stimuli in the brain: multivariate pattern analysis of functional magnetic resonance imaging data. *Neural Plasticity*, 2020.
- Levine, C., & Marcillo, A. (2008). Origin and endpoint of the olfactory nerve fibers: as described by Santiago Ramon y Cajal. *The Anatomical Record: Advances in Integrative Anatomy and Evolutionary Biology: Advances in Integrative Anatomy and Evolutionary Biology*, 291(7), 741–750.
- Levine, S. M., Pfaller, M., Reichenberger, J., Shiban, Y., Mühlberger, A., Rupperecht, R., & Schwarzbach, J. V. (2018). Relating experimentally-induced fear to pre-existing phobic fear in the human brain. *Social Cognitive and Affective Neuroscience*, 13(2), 164–172. <https://doi.org/10.1093/scan/nsx147>

- Levy, D. J., & Glimcher, P. W. (2011). Comparing apples and oranges: using reward-specific and reward-general subjective value representation in the brain. *Journal of Neuroscience*, 31(41), 14693–14707.
- Levy, L. M., Henkin, R. I., Lin, C. S., Hutter, A., & Schellinger, D. (1999). Odor memory induces brain activation as measured by functional MRI. *Journal of Computer Assisted Tomography*, 23(4), 487–498.
- Lissek, S. (2012). Toward an Account of Clinical Anxiety Predicted on Basic, Neurally Mapped Mechanisms of Pavlovian Fear-Learning: The Case for Conditioned Overgeneralization. *Depression and Anxiety*, 29(4), 257–263.
- Lonsdorf, T. B., Menz, M. M., Andreatta, M., Fullana, M. A., Golkar, A., Haaker, J., Heitland, I., Hermann, A., Kuhn, M., Kruse, O., Meir Drexler, S., Meulders, A., Nees, F., Pittig, A., Richter, J., Römer, S., Shibani, Y., Schmitz, A., Straube, B., ... Merz, C. J. (2017). Don't fear 'fear conditioning': Methodological considerations for the design and analysis of studies on human fear acquisition, extinction, and return of fear. *Neuroscience & Biobehavioral Reviews*, 77, 247–285. <https://doi.org/10.1016/j.neubiorev.2017.02.026>
- Lundström, J. N., Seven, S., Olsson, M. J., Schaal, B., & Hummel, T. (2006). Olfactory event-related potentials reflect individual differences in odor valence perception. *Chemical Senses*, 31(8), 705–711.
- Lyon, L. (2017). Dead salmon and voodoo correlations: should we be sceptical about functional MRI? *Brain*, 140(8), e53–e53.
- Magritte, R. (1929). *La Trahison des images (Ceci n'est pas une pipe)*. [Oil on canvas]. Los Angeles County Museum of Art, United States. <https://collections.lacma.org/node/239578>
- Malnic, B., Godfrey, P. A., & Buck, L. B. (2004). The human olfactory receptor gene family. *Proceedings of the National Academy of Sciences*, 101(8), 2584–2589.

- Martin-Soelch, C., Linthicum, J., & Ernst, M. (2007). Appetitive conditioning: Neural bases and implications for psychopathology. *Neuroscience and Biobehavioral Reviews*, 31(3), 426–440. <https://doi.org/10.1016/j.neubiorev.2006.11.002>
- McGann, J. P. (2017). Poor human olfaction is a 19th-century myth. *Science*, 356(6338), eaam7263.
- MediSense®. (2019). User Manual Sniffin' Sticks. <https://www.smelltest.eu/en/smell-and-taste/how-to-use-the-sniffin-sticks/>
- Meister, M. (2015). On the dimensionality of odor space. *Elife*, 4(JULY 2015), e07865. <https://doi.org/10.7554/eLife.07865>
- Metereau, E., & Dreher, J.-C. C. (2015). The medial orbitofrontal cortex encodes a general unsigned value signal during anticipation of both appetitive and aversive events. *Cortex*, 63, 42–54. <https://doi.org/10.1016/j.cortex.2014.08.012>
- Misaki, M., Kim, Y., Bandettini, P. A., & Kriegeskorte, N. (2010). Comparison of multivariate classifiers and response normalizations for pattern-information fMRI. *Neuroimage*, 53(1), 103–118.
- Mitchell, T. M., Shinkareva, S. V, Carlson, A., Chang, K.-M., Malave, V. L., Mason, R. A., & Just, M. A. (2008). Predicting human brain activity associated with the meanings of nouns. *Science*, 320(5880), 1191–1195.
- Moberg, P. J., Agrin, R., Gur, R. E., Gur, R. C., Turetsky, B. I., & Doty, R. L. (1999). Olfactory dysfunction in schizophrenia: a qualitative and quantitative review. *Neuropsychopharmacology*, 21(3), 325–340.
- Moeller, S., Yacoub, E., Olfman, C. A., Auerbach, E., Strupp, J., Harel, N., & Uğurbil, K. (2010). Multiband multislice GE-EPI at 7 tesla, with 16-fold acceleration using partial parallel imaging with application to high spatial and temporal whole-brain fMRI. *Magnetic Resonance in Medicine*, 63(5), 1144–1153.
- Morrell, G., & Spielman, D. (1997). Dynamic shimming for multi-slice magnetic resonance imaging. *Magnetic Resonance in Medicine*, 38(3), 477–483.

- Nara, K., Saraiva, L. R., Ye, X., & Buck, L. B. (2011). A large-scale analysis of odor coding in the olfactory epithelium. *Journal of Neuroscience*, 31(25), 9179–9191.
- Nicolas, S., & Bensafi, M. (2021). A historical review of olfactometry. *L'Année Psychologique*, 121(3), 311–351.
- Nikonov, A. A., Finger, T. E., & Caprio, J. (2005). Beyond the olfactory bulb: an odotopic map in the forebrain. *Proceedings of the National Academy of Sciences*, 102(51), 18688–18693.
- Notter, M. P. et al. (2019) 'AtlasReader: A Python package to generate coordinate tables, region labels, and informative figures from statistical MRI images', *Journal of Open Source Software*, 4(34), p. 1257.
- O'Keefe, J., & Dostrovsky, J. (1971). The hippocampus as a spatial map: Preliminary evidence from unit activity in the freely-moving rat. *Brain Research*.
- Onat, S., & Büchel, C. (2015). The neuronal basis of fear generalization in humans. *Nature Neuroscience*, 18(12), 1811–1818.
- Oosterhof, N. N., & Connolly, A. C. (2013). Multivariate Pattern Analysis. CoSMoMvPA. https://www.cosmomvpa.org/mvpa_concepts.html
- Oosterhof, N. N., Connolly, A. C., & Haxby, J. V. (2016). CoSMoMvPA: multi-modal multivariate pattern analysis of neuroimaging data in Matlab/GNU Octave. *Frontiers in Neuroinformatics*, 10, 27.
- Pause, B. M., Hellmann, G., Göder, R., Aldenhoff, J. B., & Ferstl, R. (2008). Increased processing speed for emotionally negative odors in schizophrenia. *International Journal of Psychophysiology*, 70(1), 16–22.
- Pavlov, I. P. (1927). *Conditioned Reflexes: An Investigation of the Physiological Activity of the Cerebral Cortex*. Translated and Edited by G. V. Anrep. Oxford University Press, London, 142.
- Pennartz, C. M. A., Oude Lohuis, M. N., & Olcese, U. (2023). How 'visual' is the visual cortex? The interactions between the visual cortex and other sensory, motivational

- and motor systems as enabling factors for visual perception. *Philosophical Transactions of the Royal Society B*, 378(1886), 20220336.
- Pessiglione, M., & Delgado, M. R. (2015). The good, the bad and the brain: Neural correlates of appetitive and aversive values underlying decision making. *Current Opinion in Behavioral Sciences*, 5, 78–84. <https://doi.org/10.1016/j.cobeha.2015.08.006>
- Philpott, C. M., Bennett, A., & Murty, G. E. (2008). A brief history of olfaction and olfactometry. *The Journal of Laryngology & Otology*, 122(7), 657–662.
- Pickenhagen, W. (2017). History of odor and odorants. In *Springer handbook of odor* (pp. 1–6). Springer.
- Pitkänen, A., Pikkarainen, M., Nurminen, N., & Ylinen, A. (2000). Reciprocal connections between the amygdala and the hippocampal formation, perirhinal cortex, and postrhinal cortex in rat: a review. *Annals of the New York Academy of Sciences*, 911(1), 369–391.
- Poldrack, R. A. (2019). *Statistical Thinking for the 21st Century*. Russell Poldrack. https://books.google.fi/books?id=o_NDzQEACAAJ
- Poldrack, R. A., Halchenko, Y. O., & Hanson, S. J. (2009). Decoding the large-scale structure of brain function by classifying mental states across individuals. *Psychological Science*, 20(11), 1364–1372.
- Poldrack, R. A., Mumford, J. A., & Nichols, T. E. (2011). *Handbook of Functional MRI Data Analysis* (1st ed.). <http://www.google.co.in/search?hl=en&client=firefox-a&hs=kVI&rls=org.mozilla%3Aen-US%3Aofficial&channel=s&q=www.cambridge.org%2F9780521517669&aq=f&aqi=&aql=&oq=>
- Pollatos, O., Kopietz, R., Linn, J., Albrecht, J., Sakar, V., Anzinger, A., Schandry, R., & Wiesmann, M. (2007). Emotional stimulation alters olfactory sensitivity and odor judgment. *Chemical Senses*, 32(6), 583–589.

- Polyn, S. M., Natu, V. S., Cohen, J. D., & Norman, K. A. (2005). Category-specific cortical activity precedes retrieval during memory search. *Science*, 310(5756), 1963–1966.
- Popal, H., Wang, Y., & Olson, I. R. (2019). A Guide to Representational Similarity Analysis for Social Neuroscience. *Social Cognitive and Affective Neuroscience*, 14(11), 1243–1253. <https://doi.org/10.1093/scan/nsz099>
- Posner, M. I., & Cohen, Y. (1984). Components of visual orienting. *Attention and Performance X: Control of Language Processes*, 32, 531–556.
- Purves, D., Augustine, G. J., Fitzpatrick, D., Hall, W. C., LaMantia, A.-S., McNamara, J. O., & Williams, S. M. (2004). *Neuroscience* (3rd ed.). Sinauer Associates.
- Purves, D., Augustine, G. J., Fitzpatrick, D., Hall, W. C., LaMantia, A.-S., Mooney, R. D., Platt, M. L., & While, L. E. (2018). *Neuroscience*. In Oxford University Press (6th ed.). Sinauer Associates Sunderland, MA.
- Purves, D., Augustine, G. J., Fitzpatrick, D., Hall, W. C., LaMantia, A.-S., Mooney, R. D., Platt, M. L., & While, L. E. (2020). *Neuroscience* (6th ed.). Oxford University Press.
- Quian Quiroga, R., & Kreiman, G. (2010). Postscript: About grandmother cells and Jennifer Aniston neurons.
- Quian Quiroga, R., Reddy, L., Kreiman, G., Koch, C., & Fried, I. (2005). Invariant visual representation by single neurons in the human brain. *Nature*, 435(7045), 1102–1107.
- Rausch, R., & Serafetinides, E. A. (1975). Specific alterations of olfactory function in humans with temporal lobe lesions. *Nature*, 255(5509), 557–558.
- Rausch, R., Serafetinides, E. A., & Crandall, P. H. (1977). Olfactory memory in patients with anterior temporal lobectomy. *Cortex*, 13(4), 445–452.
- Rolls, E. T., Kringelbach, M. L., & De Araujo, I. E. T. (2003). Different representations of pleasant and unpleasant odours in the human brain. *European Journal of Neuroscience*, 18(3), 695–703.

- Ross, G. W., Petrovitch, H., Abbott, R. D., Tanner, C. M., Popper, J., Masaki, K., Launer, L., & White, L. R. (2008). Association of olfactory dysfunction with risk for future Parkinson's disease. *Annals of Neurology*, 63(2), 167–173.
- Royet, J.-P., Plailly, J., Delon-Martin, C., Kareken, D. A., & Segebarth, C. (2003). fMRI of emotional responses to odors:: influence of hedonic valence and judgment, handedness, and gender. *Neuroimage*, 20(2), 713–728.
- Rumeau, C., Nguyen, D. T., & Jankowski, R. (2016). How to assess olfactory performance with the Sniffin'Sticks test®. *European Annals of Otorhinolaryngology, Head and Neck Diseases*, 133(3), 203–206.
- Saarimäki, H., Gotsopoulos, A., Jääskeläinen, I. P., Lampinen, J., Vuilleumier, P., Hari, R., Sams, M., & Nummenmaa, L. (2016). Discrete Neural Signatures of Basic Emotions. *Cerebral Cortex*, 26(6). <https://doi.org/10.1093/cercor/bhv086>
- Sarafoleanu, C., Mella, C., Georgescu, M., & Perederco, C. (2009). The importance of the olfactory sense in the human behavior and evolution. *Journal of Medicine and Life*, 2(2), 196.
- Savic, I. (2002). Imaging of brain activation by odorants in humans. *Current Opinion in Neurobiology*, 12(4), 455–461.
- Savic, I. (2005). Brain imaging studies of the functional organization of human olfaction. *Chemical Senses*, 30(suppl_1), i222–i223.
- Schneider, F., Habel, U., Reske, M., Toni, I., Falkai, P., & Shah, N. J. (2007). Neural substrates of olfactory processing in schizophrenia patients and their healthy relatives. *Psychiatry Research: Neuroimaging*, 155(2), 103–112.
- Schriever, V. A., Frenzel, C., Wernecke, S., Croy, I., Valder, C., & Hummel, T. (2015). Olfactory speed–Temporal odor processing of paired stimuli. *Neuroscience*, 295, 72–79.
- Schwarzbach, J. (2011). A Simple Framework (ASF) for Behavioral and Neuroimaging Experiments Based on the Psychophysics Toolbox for MATLAB. 3, 1194–1201. <https://doi.org/10.3758/s13428-011-0106-8>

- Seidel, P., Levine, S. M., Tahedl, M., & Schwarzbach, J. V. (2020). Temporal Signal-to-Noise Changes in Combined Multislice- and In-Plane-Accelerated Echo-Planar Imaging with a 20- and 64-Channel Coil. *Scientific Reports*, 10(1), 5536. <https://doi.org/10.1038/s41598-020-62590-y>
- Sela, L., & Sobel, N. (2010). Human olfaction: a constant state of change-blindness. *Experimental Brain Research*, 205(1), 13–29.
- Setsompop, K., Gagoski, B. A., Polimeni, J. R., Witzel, T., Wedeen, V. J., & Wald, L. L. (2012). Blipped-controlled aliasing in parallel imaging for simultaneous multislice echo planar imaging with reduced g-factor penalty. *Magnetic Resonance in Medicine*, 67(5), 1210–1224.
- Seubert, J., Freiherr, J., Djordjevic, J., & Lundström, J. N. (2013). Statistical localization of human olfactory cortex. *Neuroimage*, 66, 333–342.
- Seubert, J., Rea, A. F., Loughhead, J., & Habel, U. (2009). Mood induction with olfactory stimuli reveals differential affective responses in males and females. *Chemical Senses*, 34(1), 77–84.
- Smith, S. M., & Nichols, T. E. (2009). Threshold-free cluster enhancement: addressing problems of smoothing, threshold dependence and localisation in cluster inference. *Neuroimage*, 44(1), 83–98.
- Sobel, N., Prabhakaran, V., Desmond, J. E., Glover, G. H., Sullivan, E. V., & Gabrieli, J. D. E. (1997). A method for functional magnetic resonance imaging of olfaction. *Journal of Neuroscience Methods*, 78(1–2), 115–123.
- Sommer, J. U. (2012). Riech-O-Mat Version 1.12.1b. <https://usermanual.wiki/Document/RiechOMat20Manual.1148068301/html>
- Sommer, J. U., Maboche, W., Griebel, M., Heiser, C., Hörmann, K., Stuck, B. A., & Hummel, T. (2012). A mobile olfactometer for fMRI-studies. *Journal of Neuroscience Methods*, 209(1), 189–194.

- Son, G., Jahanshahi, A., Yoo, S.-J., Boonstra, J. T., Hopkins, D. A., Steinbusch, H. W. M., & Moon, C. (2021). Olfactory neuropathology in Alzheimer's disease: a sign of ongoing neurodegeneration. *BMB Reports*, 54(6), 295.
- Soudry, Y., Lemogne, C., Malinvaud, D., Consoli, S.-M., & Bonfils, P. (2011). Olfactory system and emotion: common substrates. *European Annals of Otorhinolaryngology, Head and Neck Diseases*, 128(1), 18–23.
- Spielberger, C. (1983). *Manual for the State-Trait Anxiety Inventory (STAI)*. Consulting Psychologists Press, 4–26. https://doi.org/10.1007/978-0-387-78665-0_6709
- Splavski, B., Rotim, K., Lakičević, G., Gienapp, A. J., Boop, F. A., & Arnautović, K. I. (2019). Andreas vesalius, the predecessor of neurosurgery: How his progressive scientific achievements affected his professional life and destiny. *World Neurosurgery*, 129, 202–209.
- Stevenson, R. J., & Wilson, D. A. (2007). Odour perception: an object-recognition approach. *Perception*, 36(12), 1821–1833.
- Tagliazucchi, E., & Laufs, H. (2014). Decoding wakefulness levels from typical fMRI resting-state data reveals reliable drifts between wakefulness and sleep. *Neuron*, 82(3), 695–708.
- Temmel, A. F. P., Quint, C., Schickinger-Fischer, B., Klimek, L., Stoller, E., & Hummel, T. (2002). Characteristics of olfactory disorders in relation to major causes of olfactory loss. *Archives of Otolaryngology–Head & Neck Surgery*, 128(6), 635–641.
- Tzourio-Mazoyer, N., Landeau, B., Papathanassiou, D., Crivello, F., Etard, O., Delcroix, N., Mazoyer, B., & Joliot, M. (2002). Automated anatomical labeling of activations in SPM using a macroscopic anatomical parcellation of the MNI MRI single-subject brain. *Neuroimage*, 15(1), 273–289.
- Viana, F. (2011). Chemosensory properties of the trigeminal system. *ACS Chemical Neuroscience*, 2(1), 38–50.

- Vilarroya, O. (2017). Neural representation. A survey-based analysis of the notion. *Frontiers in Psychology*, 8, 1458.
- Visser, R. M., Scholte, H. S., & Kindt, M. (2011). Associative learning increases trial-by-trial similarity of BOLD-MRI patterns. *Journal of Neuroscience*, 31(33), 12021–12028. <https://doi.org/10.1523/JNEUROSCI.2178-11.2011>
- Walla, P. (2008). Olfaction and its dynamic influence on word and face processing: Cross-modal integration. *Progress in Neurobiology*, 84(2), 192–209.
- Walla, P., Hufnagl, B., Lehrner, J., Mayer, D., Lindinger, G., Deecke, L., & Lang, W. (2002). Evidence of conscious and subconscious olfactory information processing during word encoding: a magnetoencephalographic (MEG) study. *Cognitive Brain Research*, 14(3), 309–316.
- Wang, J., Rupprecht, S., Sun, X., Freiberg, D., Crowell, C., Cartisano, E., Vasavada, M., & Yang, Q. X. (2017). A free-breathing fMRI method to study human olfactory function. *JoVE (Journal of Visualized Experiments)*, 125, e54898.
- Wang, J., Sun, X., & Yang, Q. X. (2014). Methods for olfactory fMRI studies: implication of respiration. *Human Brain Mapping*, 35(8), 3616–3624.
- Wang, Q., Cagna, B., Chaminade, T., & Takerkart, S. (2020). Inter-subject pattern analysis: A straightforward and powerful scheme for group-level MVPA. *NeuroImage*, 204, 116205.
- Watanabe, T., Sasaki, Y., Shibata, K., & Kawato, M. (2017). Advances in fMRI real-time neurofeedback. *Trends in Cognitive Sciences*.
- Weaverdyck, M. E., Lieberman, M. D., & Parkinson, C. (2020). Tools of the Trade Multivoxel pattern analysis in fMRI: a practical introduction for social and affective neuroscientists. *Social Cognitive and Affective Neuroscience*, 15(4), 487–509.
- Weber, S. T., & Heuberger, E. (2008). The impact of natural odors on affective states in humans. *Chemical Senses*, 33(5), 441–447.

- Weiner, K. S., & Zilles, K. (2016). The anatomical and functional specialization of the fusiform gyrus. *Neuropsychologia*, 83, 48–62.
- Weiss, T., Snitz, K., Yablonka, A., Khan, R. M., Gafsou, D., Schneidman, E., & Sobel, N. (2012). Perceptual convergence of multi-component mixtures in olfaction implies an olfactory white. *Proceedings of the National Academy of Sciences*, 109(49), 19959–19964. <https://doi.org/10.1073/pnas.1208110109>
- Wiesmann, M., Yousry, I., Heuberger, E., Nolte, A., Ilmberger, J., Kobal, G., Yousry, T. A., Kettenmann, B., & Naidich, T. P. (2001). Functional magnetic resonance imaging of human olfaction. *Neuroimaging Clinics of North America*, 11(2), 237–250. <https://doi.org/10.1002/9780470995716.ch7>
- Wilson, D. A., Chapuis, J., & Sullivan, R. M. (2015). Cortical Olfactory Anatomy and Physiology. In R. L. Doty (Ed.), *Handbook of olfaction and gustation* (pp. 209–223). John Wiley & Sons.
- Wilson, D. A., Donald, A., Stevenson, R. J., Stevenson, R. J., & Stevenson, R. J. (2006). *Learning to smell: olfactory perception from neurobiology to behavior*. JHU Press.
- Winston, J. S., Gottfried, J. A., Kilner, J. M., & Dolan, R. J. (2005). Integrated neural representations of odor intensity and affective valence in human amygdala. *Journal of Neuroscience*, 25(39), 8903–8907.
- Woo, C.-W., Chang, L. J., Lindquist, M. A., & Wager, T. D. (2017). Building better biomarkers: brain models in translational neuroimaging. *Nature Neuroscience*, 20(3), 365–377.
- Wysocki, C. J., & Gilbert, A. N. (1989). National Geographic Smell Survey: effects of age are heterogenous. *Annals of the New York Academy of Sciences*.
- Wysocki, C. J., Cowart, B. J., & Radil, T. (2003). Nasal trigeminal chemosensitivity across the adult life span. *Perception & Psychophysics*, 65(1), 115–122.
- Yang, J.-Y., O'Connell, T. F., Hsu, W.-M. M., Bauer, M. S., Dylla, K. V, Sharpee, T. O., & Hong, E. J. (2023). Restructuring of olfactory representations in the fly brain around odor relationships in natural sources. *BioRxiv*.

- Yang, Q. X., Dardzinski, B. J., Li, S., Eslinger, P. J., & Smith, M. B. (1997). Multi-gradient echo with susceptibility inhomogeneity compensation (MGESIC): demonstration of fMRI in the olfactory cortex at 3.0 T. *Magnetic Resonance in Medicine*, 37(3), 331–335.
- Yarkoni, T., Poldrack, R. A., Nichols, T. E., Van Essen, D. C., & Wager, T. D. (2011). Large-scale automated synthesis of human functional neuroimaging data. *Nature Methods*, 8(8), 665–670.
- Yeretzian, C. (2017). Coffee. In *Springer handbook of odor* (pp. 21–22). Springer.
- Yousem, D. M., Williams, S. C., Howard, R. O., Andrew, C., Simmons, A., Allin, M., Geckle, R. J., Suskind, D., Bullmore, E. T., & Brammer, M. J. (1997). Functional MR imaging during odor stimulation: preliminary data. *Radiology*, 204(3), 833–838.
- Zald, D. H., & Pardo, J. V. (1997). Emotion, olfaction, and the human amygdala: amygdala activation during aversive olfactory stimulation. *Proceedings of the National Academy of Sciences*, 94(8), 4119–4124.
- Zald, D. H., & Pardo, J. V. (2000). Functional neuroimaging of the olfactory system in humans. *International Journal of Psychophysiology*, 36(2), 165–181.
- Zald, D. H., Mattson, D. L., & Pardo, J. V. (2002). Brain activity in ventromedial prefrontal cortex correlates with individual differences in negative affect. *Proceedings of the National Academy of Sciences*, 99(4), 2450–2454.
- Zatorre, R. J., & Jones-Gotman, M. (1991). Human olfactory discrimination after unilateral frontal or temporal lobectomy. *Brain*, 114(1), 71–84.
- Zatorre, R. J., Jones-Gotman, M., Evans, A. C., & Meyer, E. (1992). Functional localization and lateralization of human olfactory cortex. *Nature*, 360(6402), 339–340.
- Zhou, G., Lane, G., Cooper, S. L., Kahnt, T., & Zelano, C. (2019). Characterizing functional pathways of the human olfactory system. *Elife*, 8, e47177.

Zippel, H. P. (1993). Historical aspects of research on the vertebrate olfactory system.
Die Naturwissenschaften, 80(2), 65–76.

SELBSTÄNDIGKEITSERKLÄRUNG

Ich, Aino-Lotta Ilona Alahäivälä geboren am 18.06.1993 in Kemi, Finnland erkläre hiermit, dass ich die vorliegende Arbeit ohne unzulässige Hilfe Dritter und ohne Benutzung anderer als der angegebenen Hilfsmittel angefertigt habe. Die aus anderen Quellen direkt oder indirekt übernommenen Daten und Konzepte sind unter Angabe der Quelle gekennzeichnet. Insbesondere habe ich nicht die entgeltliche Hilfe von Vermittlungs- bzw. Beratungsdiensten (Promotionsberater oder andere Personen) in Anspruch genommen. Die Arbeit wurde bisher weder im In- noch im Ausland in gleicher oder ähnlicher Form einer anderen Prüfungsbehörde vorgelegt.

Regensburg, 29. Januar 2025



Ort, Datum, eigenhändige Unterschrift des Promovierenden

